Wigner negativity on the sphere

by

Jack Davis

A thesis
presented to the University of Waterloo
in fulfillment of the
thesis requirement for the degree of
Doctor of Philosophy
in
Physics (Quantum Information)

Waterloo, Ontario, Canada, 2023

Examining Committee Membership

The following served on the Examining Committee for this thesis. The decision of the Examining Committee is by majority vote.

External Examiner:	Daniel James Professor, Dept. of Physics, University of Toronto
Supervisor(s):	Robert Mann Professor, Dept. Physics & Astronomy, University of Waterloo Shohini Ghose Professor, Dept. Physics & Computer Sci., Wilfrid Laurier University
Internal Member:	Niayesh Afshordi Professor, Dept. Physics & Astronomy, University of Waterloo
Internal-External Member:	Eduardo Martin-Martinez Assoc. Professor, Dept. of Applied Mathematics, University of Waterloo
Other Member(s):	Lucien Hardy Research Faculty, Perimeter Institute for Theoretical Physics

Author's Declaration

This thesis consists of material all of which I authored or co-authored: see Statement of Contributions included in the thesis. This is a true copy of the thesis, including any required final revisions, as accepted by my examiners.

I understand that my thesis may be made electronically available to the public.

Statement of Contributions

Chapters 3 and 4 are largely based on the respective works [1] and [2]. In both of these Jack Davis was the principal investigator and drafted the majority of the manuscripts under the supervision of Profs. Shohini Ghose and Robert Mann, together with significant results and drafting from respective co-authors Dr. Meenu Kumari and Dr. Robie Hennigar. Chapter 5 is based on [3], where Jack Davis was a co-principal investigator and drafted approximately half of the manuscript under the supervision of Prof. Robert Mann, together with significant results and drafting from co-principal investigator Jérôme Denis under the supervision of Prof. John Martin.

Abstract

The rise of quantum information theory has largely vindicated the long-held belief that Wigner negativity is an indicator of genuine nonclassicality in quantum systems. This thesis explores its manifestation in spin-j systems using the spherical Wigner function. Common symmetric multi-qubit states are studied and compared. Spin coherent states are shown to never have vanishing Wigner negativity. Pure states that maximize negativity are determined and analyzed using the Majorana stellar representation. The relationship between negativity and state mixedness is discussed, and polytopes characterizing unitary orbits of lower-bounded Wigner functions are studied. Results throughout are contrasted with similar works on symmetric state entanglement and other forms of phase-space nonclassicality.

Acknowledgements

I would like to thank my supervisors Robert Mann and Shohini Ghose for their willingness and openness in pursuing this work, together with their unwavering support and guidance.

I would also like to thank my co-authors Jérôme Denis, Robie Hennigar, Meenu Kumari, and John Martin.

I would additionally like to thank a handful of the many colleagues who played a role in my life during this time: Amit Anand, Archishna Bhattacharyya, Ulysse Chabaud, Tomáš Gonda, Finnian Gray, Daniel Grimmer, Laura Henderson, Aditya Jain, Kieran Mastel, Fiona McCarthy, Prof. Ruxandra Moraru, Arsalan Motamedi, Shlok Nahar, Pablo Palacios, Arthur Pesah, Nachiket Sherlekar, Fil Simovic, Alexander Smith, Sanchit Srivastava, Esha Swaroop, Ramy Tannous, Erickson Tjoa, Michael Vasmer, Lei Gioia Yang, many many others at the Institute for Quantum Computing and beyond, and a special thanks to Thomas "TC" Fraser. I would not like to thank covid-19 for its contribution to this work.

This thesis was supported in part by the Natural Sciences and Engineering Research Council of Canada. This work was also conducted on the traditional territory of the Neutral, Anishnaabeg, and Haudenosaunee Peoples. The University of Waterloo and the Institute for Quantum Computing are situated on the Haldimand Tract, land that was promised to Six Nations, which includes six miles on each side of the Grand River.

Table of Contents

List of Figures

List of Tables

Epigraph

"From the physical point of view, the prevalence of the Heisenberg groups in quantization is an artifact...schemes based on other groups may look anomalous to the Heisenberg-trained mind."

José M. Gracia-Bondía

Chapter 1

Introduction

Quantum physics, our most successful yet most puzzling physical theory of nature, is currently experiencing a paradigm shift. This was brought about by a relatively recent fusion of information theory and quantum mechanics as they were previously understood. Their marriage, which forms the now vastly encompassing subject of *quantum information theory*, has promised to yield the advent of technology capable of completing tasks otherwise thought to be practically impossible. And as the industry of quantum technology grows this revolution simultaneously informs our philosophical outlook, particularly so with the stubborn conceptual problems of quantum theory. This intertwined progression has placed us at a peculiar crossroads where the task of understanding exactly why quantum technologies are so powerful is intricately connected to the task of understanding why quantum mechanics is so puzzling in the first place. And while the history of the word "nonclassicality" has been nebulous and dynamic, this new information-theoretic re-interpretation of quantum physics continues to inform us on how to move forward.

One aspect of quantum physics that has benefited particularly well from this new perspective is the phase space formulation, the origins of which can largely be attributed to the work of Wigner, Weyl, Moyal, and Groenewold [4, 5, 6, 7]. This formulation is autonomous in its construction yet equivalent to the original formulation of Heisenberg [8] and its subsequent development in terms of density matrices, quantum channels, and fuzzy measurements. The principal advantage of this picture is the ability to simultaneously describe quantum and classical physics on the common stage of phase space. This facilitates a direct comparison between the two theories in terms of both kinematics (i.e. probability distributions vs. quasiprobability distributions) and dynamics (i.e. Poisson brackets vs.

Moyal brackets). See [9] for a recent review with an information-theoretic perspective.

One loosely chronological wave of generalizations to this picture may broadly be grouped into two directions. The first is the introduction of additional quasiprobability distributions based on the coherent states associated to the Heisenberg-Weyl group. This may be attributed to the works of Husimi [10], Sudarshan [11], Glauber [12], and Kano [13], which brought about the Husimi(-Kano) Q function and the Glauber-Sudarshan P function. These two, together with the originating Wigner function, were then found to be intimately related [14, 15, 16, 17, 18], and the unified product is a one-parameter family of functions now referred to as the *s-ordered class* in reference to the different ways of constructing a Hilbert space operator from a given phase space function. In this setting the Wigner function plays a special role as it may be thought of as sitting directly "in between" the Husimi Q function and the Sudarshan-Glauber P function. An important structural aspect was then revealed by Grossman [19] and Royer [20], who showed the deep connection to phase space inversion symmetry. In particular, the Wigner function in its most modern form is best thought of as a collection of expectation values of an operator-valued distribution over phase space, collectively referred to as the *kernel*. The phase-point operator at $(x, p) \in \mathbb{R}^2$ is furthermore to be interpreted as the *displaced parity operator* that inverts phase space about that point. This perspective naturally integrates with the entire s-ordered class, with different quasiprobability distributions being generated by different kernels [21].

The second direction within this first wave is the switch to finite dimensional quantum systems, the first step into which was done by Hannay and Berry in 1980 [22] based on earlier insights by Schwinger and Weyl [23]. Important subsequent works include those by Wootters *et al.* [24, 25] together with contributions from Cohendet *et al.* [26], Leonhardt [27, 28], and Klimov *et al.* [29, 30] (see [31] for an overview). This effort culminated in the discrete Wigner function identified by Gross [32], hereafter referred to as the Gross-Wigner function[1]. In an odd prime Hilbert space dimension d, the phase space that this Wigner function lives on is a $d \times d$ toroidal lattice, where the two constituent "rings" of the torus may be thought of as discretized versions of position and momentum [33, 34]. The Gross-Wigner function is also best thought of as emerging from a canonical set of displaced parity operators, analogous to the original Wigner function.

These two directions, from the modern information-theoretic lens, may be respectively

[1]While Gross did not define this function he argued for its information-theoretic canonicality in the context of quantum error correction; as a result the quantum information community seems to have adopted the title *Gross-Wigner function*.

placed into two broader research programs: continuous-variable quantum information [35, 36, 37] and discrete-variable quantum information [38, 39]. It is here where negativity in the Wigner function has blossomed, particularly so in the context of quantum computation. Central to both cases is Hudson's theorem, which determines exactly the subset of pure states that are Wigner-positive [40, 41, 32]. In the continuous-variable regime these are the Gaussian states and in the discrete-variable regime they are the stabilizer states, which are central to the stabilizer formalism of quantum error correction and universal fault-tolerance quantum computation [42]. A running theme is that states with a positive Wigner function — together with negativity-preserving transformations (Gaussian operations / Clifford group operations) and Wigner-positive measurements (quadrature measurement / Pauli measurement) — are consistently found to be efficiently simulable on a classical computer; see [43, 44, 45, 46, 47] for continuous-variable and [48, 49, 50, 51, 52] for discrete-variable. These results may collectively be thought of as various extensions and reformulations of the celebrated Gottesman-Knill theorem [42, 53]. Related to this "indirect" approach, i.e. characterizing the non-classicality of Wigner negativity by means of showing its absence is classical, is a "direct" approach that seeks to relate Wigner negativity to quantum contextuality [54, 55] and magic states [56] – two related notions that constitute essential computational resources [57, 58, 59]. Indeed there is a growing body of work that directly relates Wigner negativity to such notions [58, 60, 61, 62, 63, 64]. Wigner negativity furthermore acts as a magic monotone with respect to Gaussian / Clifford group operations, which offers some credence to the idea that more negativity implies more non-classicality [65, 66, 67, 68]. To summarize, an important and ongoing lesson of the quantum information revolution is that, at least in the context of quantum computation,

Wigner negativity is a foundational and practical physical resource that can achieve a quantum advantage.

In light of the above it is natural to wonder if there are other physical circumstances where Wigner negativity is well-defined. This becomes particularly interesting after noticing that both the continuous-variable and discrete-variable regimes are fundamentally based on the same position-momentum duality (i.e. a Heisenberg-Weyl-like conjugacy)[2]. And while these are highly important types of systems they are not the only ones within

[2]Not to mention the substantial body of related work on cylindrical-like phase spaces; see for example the Pegg-Barnett research programme [69] and [70, 71, 72, 73, 74, 75, 76]. These important and interesting Heisenberg-Weyl-like systems are not emphasized here due to their (as of yet) relatively smaller presence in the quantum information and quantum computation literature.

the purview of non-relativistic quantum physics or even quantum information theory. The simplest examples of such a non-Heisenberg-Weyl-like object are perhaps the spin-j systems, which are instead based on the commutation relations of angular momentum, $[J_i, J_j] = i\epsilon_{ijk}J_k$. Can we define a canonical Wigner function and Wigner negativity for such systems and others like it? If so, will it also give insight to their fundamental nature or perhaps offer a quantum advantage when this object is applied or contained within some operational task/protocol?

These questions may be probed within a (related, but pedagogically speaking) second wave of generalizations to the original Wigner function that is more concerned with changing the *shape* of phase space while retaining as many of the original properties as possible [77, 78, 79, 80]. In the additional presence of a dynamical symmetry group more structure is afforded and the phase space may often be thought of as essentially[3] the group manifold itself [81, 82]. In this setting *different phase space manifolds correspond to different physical systems and are classified by their dynamical symmetry* [83, 84, 85]. For example, the original phase space being $\mathbb{R}^2$ should be thought of as a *consequence* of working with the Heisenberg-Weyl group. Spin-j systems, which come from SU(2) [86, 87], by contrast are associated to a spherical phase space with radius indexed by j. Similar to the planar case, spherical quasiprobability distributions may furthermore be thought of as arising from a collection of displaced (i.e. rotated) parity operators.

The requirements of a well-defined Wigner function over such a symmetry-derived phase space are known as the Stratonovich axioms, which were first described in 1956 and incidentally in the present context of SU(2) [88]. As will be discussed later, the two most important axioms are *covariance* (i.e. translations of phase space must be in compatible correspondence with translation operators over Hilbert space) and *traciality* (i.e. the Born rule is mapped to an L^2 inner product). The Stratonovich axioms were forgotten for several decades but were resurrected in a seminal paper by Joseph C. Várilly and José M. Gracia-Bondía, who went on to derive the set of all spherical Wigner functions satisfying the Stratonovich axioms [89]. There has since been much work done on spherical quasiprobability distributions [90, 91, 92, 93, 94, 95, 96, 97]; see [98] and references therein for a recent overview. Despite the just implied non-uniqueness of the SU(2)-covariant Wigner function, the vast majority of these works focus, as does this thesis, on the same particular one that was independently discovered by Agarwal in 1981, presumably without knowledge of the Stratonovich axioms [99]. Like many others, implicitly or explicitly, I consider it

[3]More precisely a quotient group with respect to the stabilizer group of some fiducial state, often chosen to have physical significance such as the bosonic vacuum in the case of Heisenberg-Weyl symmetry.

to be the canonical Wigner function for spin systems because it is the only such spherical Wigner function to satisfy, in addition to the Stratonovich axioms, *either* of the following two properties:

- Compatibility with the SU(2) s-ordered class of functions: it is exactly "in between" the Husimi Q function and the Glauber-Sudarshan P function (as generated by the standard spin-coherent state $|j, j\rangle$) [89].[4]
- Compatibility with Heisenberg-Weyl symmetry: its infinite-spin limit is the original Wigner function on $\mathbb{R}^2$ [92, 97].

So equipped with a canonical Wigner function on the sphere and a reputable history of Wigner negativity, this thesis represents the first focused approach to the question of Wigner negativity in spin-j systems. This work complements an increasingly large research programme on the nonclassicality of spin-j systems in general. Indeed the past two decades (even the past decade) have seen an explosion of progress in the understanding and characterization of quantum spin despite its first physical observation in the famous Stern-Gerlach experiment being just over 100 years ago [100] and its mathematical roots planted even earlier in the 19th century [101]; see for example [102, 103, 104, 105, 106, 107, 108, 109, 110, 111, 112]. Fueled by the quantum information revolution, this explosion comes largely from studying the entanglement and nonlocality properties of spin-j systems through their equivalent representation as the symmetric subspace of a collection of $2j$ qubits[5]. In lieu of a (yet) established connection to, say, quantum contextuality, here we gain insight on spherical Wigner negativity largely through its contrast with the above mentioned body of work on symmetric state entanglement.

[4] Note that in [83, 84] for example, one may naturally modify the traciality axiom to accommodate the spherical s-ordered class and so bypass the non-uniqueness issue altogether.

[5] This equivalence has been known in one way or another for a long time (arguably since at least 1932 from a physics perspective [113, 114]), but see [115] for a modern take with applications in information science.

Chapter 1 is an introduction, Chapter 2 is background, and Chapter 6 concludes and comments on future directions. The results of Chapters 3, 4 and 5, which are based on completed works and presented in chronological order, are summarized as follows:

- Chapter 3. Commonly used symmetric states from various fields of quantum information theory are analyzed, in particular the spin coherent states (i.e. computational basis states and their simultaneous rotations), the n-qubit Greenberger–Horne–Zeilinger (GHZ) states and the Dicke (generalized W) states. Spin coherent states are shown to always have a non-vanishing amount of Wigner negativity in all dimensions. An approximation formula for GHZ negativity is obtained, and it is shown that such states have a relatively low amount of negativity as compared to the Dicke states. Dicke state negativity is furthermore found to behave differently than entanglement entropy, with the relative ranking of the Dicke basis via their nonclassicality being highly spin-dependent.

- Chapter 4. The Majorana stellar representation is used to characterize pure spin states that maximize Wigner negativity. Such states are found to generally exhibit a partial but not maximal degree of symmetry within their constellations. In particular, for spin $j > 2$, maximal constellations do not correspond to an embedded Platonic solid when available and do not follow an obvious geometric pattern as dimension increases. They also do not maximize various other measures of phase space nonclassicality such as anticoherence, geometric entanglement, or Glauber-Sudarshan negativity. Random states display on average a relatively high amount of negativity, but the extremal states and those with similar negativity are statistically rare in Hilbert space.

- Chapter 5. This chapter studies the relationship between Wigner negativity and state mixedness, in particular the unitary orbits of spin Wigner functions lower-bounded by a specified value. To this end, my collaborators and I extended a characterization of the set of absolutely Wigner positive states as a set of linear eigenvalue constraints, which together define a polytope in the simplex of spin-j mixed states centred on the maximally mixed state. The lower bound determines the relative size of such absolutely Wigner bounded (AWB) polytopes and we study their geometric properties. In particular, in each dimension a Hilbert-Schmidt ball representing a tight AWB sufficiency criterion based on the purity is exactly determined, while another ball representing AWB necessity is conjectured. Special attention is given to the case

where the polytope separates orbits containing only positive Wigner functions from other orbits because of the use of Wigner negativity as a witness of non-classicality of spin states. Comparisons are made to absolute symmetric state separability and Glauber-Sudarshan positivity, with additional details given for low spin quantum numbers.

Chapter 2

Background

Here some of the building blocks of quantum spin are recalled, its various representations are reviewed, and the spherical Wigner function is presented. The convention used is the "quantum information" style where the state $|0\rangle$ lives at the North pole of the Bloch sphere and an arbitrary qubit state is given by $\cos(\theta/2)|0\rangle + e^{i\phi}\sin(\theta/2)|1\rangle$. This is in line with the "physicist's" spherical coordinates where θ denotes colatitude. The reduced Planck constant $\hbar$ is set to 1 throughout.

2.1 Structure theory of quantum spin

2.1.1 SU(2) fundamentals

Many of these results may be found the textbooks [101, 116, 117, 118] and the review article [98]. The special unitary group SU(2) is the set of 2×2 unitary matrices with determinant one together with matrix multiplication. The generators of this group are the Pauli matrices divided by 2:

$$J_x = \frac{1}{2}\begin{pmatrix} 0 & 1 \\ 1 & 0 \end{pmatrix} \qquad J_y = \frac{1}{2}\begin{pmatrix} 0 & -i \\ i & 0 \end{pmatrix} \qquad J_z = \frac{1}{2}\begin{pmatrix} 1 & 0 \\ 0 & -1 \end{pmatrix}. \tag{2.1}$$

These generators satisfy the *canonical commutation relations for angular momentum*

$$[J_i, J_j] = i\epsilon_{ijk}J_k, \tag{2.2}$$

(i.e. the $\mathfrak{su}(2)$ Lie bracket) which are the defining relations for spin systems. The subscripts x, y, z come from SU(2) being the double cover of SO(3), which is the group of rotations in Euclidean space $\mathbb{R}^3$, meaning that J_k may be thought to generate rotations about the k-th axis in standard Cartesian coordinates.

The algebraic structures of Eqs. (2.1) and (2.2) may be unitarily and irreducibly represented on any finite dimensional Hilbert space $\mathcal{H} \simeq \mathbb{C}^{2j+1}$ where j, called the *spin* of the system, is indexed through the eigenvalues of the Casimir element $J^2 = J_x^2 + J_y^2 + J_z^2$. The spin j is either a positive integer or half-integer, leading to one instance of SU(2) per finite Hilbert space. Indeed such a representation on $\mathbb{C}^{2j+1}$ is unique up to unitary equivalence, a property not always satisfied by groups found in physics.

The *standard Dicke states* of spin j, denoted $|j, m\rangle$, are the eigenvectors of the spin-j representation of the J_z generator:

$$J_z|j, m\rangle = m|j, m\rangle, \tag{2.3}$$

where m, the magnetic quantum number, runs in integer steps from $-j$ to j. The spin ladder operators, $J_\pm = J_1 \pm iJ_2$, walk up and down the standard *Dicke basis* as

$$J_\pm|j, m\rangle = \sqrt{(j \mp m)(j \pm m + 1)}|j, m \pm 1\rangle, \qquad J_\pm|j, \pm j\rangle = \mathbf{0}, \tag{2.4}$$

and form part of another basis for the spin algebra: $\{J_+, J_-, J_z\}$. The ladder operators will not be explicitly needed but are included to emphasize the central role of J_z as a *quantization axis*.

The group SU(2) as a manifold may be parameterized by the Euler angles (θ, ϕ, φ) with respect to the z-y-z convention, meaning that any abstract *rotation operator* U_g where $g \in$ SU(2) can be written in the form

$$U_g \simeq U(\theta, \phi, \varphi) = e^{-i\theta J_z} e^{-i\phi J_y} e^{-i\varphi J_z} \tag{2.5}$$

where $\theta \in [0, \pi]$, $\phi \in \mathbb{R} \mod 2\pi$ and $\varphi \in \mathbb{R} \mod 2\pi$. That is, the ϕ and φ variables are periodic while θ is not. The *Wigner D-matrix (of spin j)* is the arbitrary rotation operator expressed in the standard Dicke basis

$$D^{(j)}_{mn}(\theta, \phi, \varphi) = \langle j, m|U(\theta, \phi, \varphi)|j, n\rangle. \tag{2.6}$$

Hence the fully coordinatised version of the abstract action $U_g|\psi\rangle$ is the matrix-vector multiplication

$$|\phi\rangle = U_g|\psi\rangle \qquad \Longleftrightarrow \qquad \phi_m = \sum_n D^{(j)}_{mn}(\theta, \phi, \varphi)\psi_n, \tag{2.7}$$

where $\psi_m = \langle j, m|\psi\rangle$ are the *Dicke coefficients* of $|\psi\rangle$. The Wigner D-matrix satisfies many properties, one of which that will be used is

$$D^{(j)}_{mp}(g)D^{*(j)}_{m'q}(g) = \sum_{\ell=0}^{2j} \frac{2\ell+1}{2j+1} \left\langle \begin{matrix} j & \ell \\ m & m'-m \end{matrix} \middle| \begin{matrix} j \\ m' \end{matrix} \right\rangle \left\langle \begin{matrix} j & \ell \\ p & q-p \end{matrix} \middle| \begin{matrix} j \\ q \end{matrix} \right\rangle D^{*(\ell)}_{m'-m,q-p}(g), \tag{2.8}$$

where $*$ denotes complex conjugation and

$$\left\langle \begin{matrix} j_1 & j_2 \\ m_1 & m_2 \end{matrix} \middle| \begin{matrix} J \\ M \end{matrix} \right\rangle \equiv C^{J,M}_{j_1,m_1;j_2,m_2} \tag{2.9}$$

denotes the Clebsch-Gordan coefficient associated to rotating the global Dicke state $|J, M\rangle$ into the local Dicke state $|j_1, m_1\rangle \otimes |j_2, m_2\rangle$.

In the setting of square-integrable functions on the sphere, $L^2(S^2)$, the spherical harmonics $Y_{\ell,m}(\theta, \phi)$ play an important role as they are the Dicke states for that space. When the sphere is transformed via a rigid rotation $R(\theta, \phi)$ (i.e. with the φ Euler angle dropped; see (2.17) later) the spherical harmonics satisfy the transformation relation

$$Y_{\ell,m'}(R(\theta, \phi)) = \sum_m D^{*(\ell)}_{m'm}(R)Y_{\ell,m}(\theta, \phi). \tag{2.10}$$

The important thing is that the Wigner D-matrix preserves the degree ℓ. A closely related concept is that of the *spherical tensor operators*, also known as the Fano multipole operators [119]. If we have a spin-j irrep on the Hilbert space $\mathbb{C}^{2j+1}$ then the spherical tensor operators $T^{(j)}_{\ell,m}$ are an incarnation of the spherical harmonics of degree ℓ but in the operator space $L(\mathbb{C}^{2j+1})$ where now the action of R is by matrix conjugation:

$$U(R)T^{(j)}_{\ell,m'}U^\dagger(R) = \sum_m D^{*(\ell)}_{m'm}(R)T^{(j)}_{\ell,m}. \tag{2.11}$$

The set of operators $\{T^{(j)}_{\ell,m}\}$ where $m \in \{-\ell, ..., \ell\}$ and $\ell \in \{0, ..., 2j\}$, both in integer steps, forms a orthogonal basis for $L(\mathbb{C}^{2j+1})$. And because the Wigner D-matrix preserves the degree ℓ each span of the subsets $\{T^{(j)}_{\ell,m}\}^{\ell}_{m=-\ell}$, one for each ℓ, is invariant under the SU(2) action on $L(\mathbb{C}^{2j+1})$ via matrix conjugation.

The key takeaway is that the space of operators $L(\mathbb{C}^{2j+1})$ may be decomposed into a direct sum of *multipoles*, one for each $\ell \in \{0, ..., 2j\}$, similar to how spherical functions may be decomposed into spherical harmonics. The critical difference however is that we

are forever linked to the original spin-j irrep on $\mathbb{C}^{2j+1}$ and the multipole operators depend on this. This can be explicitly seen when expressing them in terms of Clebsch-Gordan coefficients and Dicke states:

$$T^{(j)}_{\ell,m} = \sqrt{\frac{2\ell+1}{2j+1}} \sum_{n,n'=-j}^{j} \left\langle \begin{matrix} j & \ell \\ n & m \end{matrix} \middle| \begin{matrix} j \\ n' \end{matrix} \right\rangle |j,n'\rangle\langle j,m|. \tag{2.12}$$

2.1.2 Spin coherent states, SU(2) phase space, the Husimi function, and the Glauber-Sudarshan function

Within the Dicke basis, the state $|j,j\rangle$ plays an exceedingly important role for much of what follows[1]. Perhaps its most immediately motivating property is that it saturates the Heisenberg uncertainty relations associated to any orthonormal basis of $\mathfrak{su}(2)$:

$$\Delta(\mathbf{J}\cdot\mathbf{u})\Delta(\mathbf{J}\cdot\mathbf{v}) = \frac{1}{2}|\langle \mathbf{J}\cdot\mathbf{w}\rangle|, \tag{2.13}$$

meaning that the *relative* uncertainty (i.e. of J_i/j) is minimal at $\frac{1}{2j}$ [87][2]. The state $|j,j\rangle$ is therefore directly analogous, at least in the sense of (2.13), to the bosonic vacuum state, which minimizes the regular Heisenberg uncertainty relations. It is for this reason (among many others, some of which will be discussed in subsequent chapters) that the $|j,j\rangle$ state is considered to be the "most classical" Dicke state. Indeed as $j\to\infty$ the relative uncertainty goes to zero, which would effectively imply that it is possible to know the outcomes of all $\mathfrak{su}(2)$ measurements simultaneously.

If the state $|j,j\rangle$ is acted upon by a spin-j rotation operator (2.5) then the resulting state will minimize a similar uncertainty relation but instead with respect to a different set of perpendicular generator axes. An important observation however is that the rotation operator (2.5) is slightly redundant from the perspective of quantum physics where global phases are immaterial. This can easily be seen for example by direct application

$$e^{-i\theta J_z}e^{-i\phi J_y}e^{-i\varphi J_z}|j,j\rangle = e^{-i\varphi j}e^{-i\theta J_z}e^{-i\phi J_y}|j,j\rangle. \tag{2.14}$$

[1]Other works may instead focus on the bottom Dicke state $|j,-j\rangle$ in an attempt to mimic the idea of a bosonic vacuum waiting to be acted upon by J_+. That convention is not used here because it sacrifices the intuition behind the "top" of the quantization axis matching up with the highest m value.

[2]Interestingly, despite this common presentation, spin coherent states are in fact not the only pure spin states to satisfy Eq. (2.13) for a given orthonormal basis. One resolution is to instead consider the *uncertainty solid angle*, which does uniquely single out the spin coherent states [120]. See also [121, 122] and references therein for a broader discussion.

Hence there is a set of vectors in $\mathbb{C}^{2j+1}$ parameterized by a phase $e^{-i\varphi j} \in \mathrm{U}(1)$ that are physically identical. One can furthermore imagine the same thing occurring for all rotated versions of $|j,j\rangle$. In other words, the *stabilizer subgroup* of $|j,j\rangle$ in SU(2) is U(1).

With this in mind, the set of *spin coherent states* is defined as the unitary orbit of the SU(2) irrep acting on $|j,j\rangle$ up to global phase:

$$\text{spin coherent states: } \{|\psi\rangle \in \mathbb{C}^{2j+1} : |\psi\rangle = e^{i\vartheta_\psi} U_g |j,j\rangle \text{ for some } e^{i\vartheta_\psi} \in U(1)\}. \tag{2.15}$$

Had we let SU(2) act on a different state then a different unitary orbit of states within Hilbert space would have been produced [123, 124]. Eq. (2.15) is a special case of the *Perelomov system* of SU(2) with respect to the fiducial state $|j,j\rangle$ [81]. But since we chose $|j,j\rangle$ (2.15) represents the set of all SU(2) minimum uncertainty states, which again are the most classical states possible in terms of the joint measurability of $\mathfrak{su}(2)$ observables. Spin coherent states and many of their properties were first discovered in the two seminal papers [86, 87].

This construction is of critical importance because now we have a set of the most classical spin states possible. And since the stabilizer subgroup for the spin coherent states is U(1), the orbit-stabilizer theorem implies that this set is topologically equivalent to the sphere via the quotient

$$SU(2)/U(1) \simeq S^2. \tag{2.16}$$

This is the phase space for SU(2) systems. The sphere is a symplectic manifold with a Poisson bracket and so is a *bona fide* classical phase space [95, 98]. The classical states of this phase space (i.e. the individual points $(\theta,\phi) \in S^2$) are furthermore in bijective correspondence with spin coherent states. This is also exactly how the original phase space arises from a quantum mechanical setting: the stabilizer subgroup of the bosonic vacuum is U(1) and the quotient of H_1, the Heisenberg-Weyl group (i.e. the group generated by $\{x,p,\mathbb{I}\}$), is $H_1/U(1) \simeq \mathbb{R}^2$. Again we have a symplectic manifold with a Poisson bracket whose classical points (x,p) are in bijective correspondence with coherent states. See [83, 84, 85] and references therein for more detail on these examples and a general theory for other Lie groups.

In practice (2.16) also effectively means the φ Euler angle may be dropped and the spin coherent states are obtained by the action of

$$R(\theta,\phi) \equiv e^{-i\theta \boldsymbol{k}\cdot\boldsymbol{J}} = e^{\xi J_- - \xi^* J_+} \tag{2.17}$$

on $|j,j\rangle$, where $\boldsymbol{k} = (-\sin\phi, \cos\phi, 0)$ and $\xi = \frac{\theta}{2}e^{i\phi}$. The operator $R(\theta,\phi)$, expressed in the middle using axis-angle variables and on the right using ladder operators, enacts in Hilbert space the spherical rotation that takes the North pole $(0,0)$ to the point (θ,ϕ), which may also be denoted $\Omega \equiv (\theta,\phi)$. The resulting spin coherent state is denoted $|\theta,\phi\rangle$ and its Dicke coefficients $\langle j,m|\theta,\phi\rangle$ may be obtained as follows. Begin by using the so-called Gilmore-Feynman disentangling formulas for SU(2), which relate different sets of exponential parameters that produce the same group element:

$$e^{a_+J_+ + a_zJ_z + a_-J_-} = e^{b_+J_+}e^{b_zJ_z}e^{b_-J_-} = e^{c_-J_-}e^{c_zJ_z}e^{c_+J_+}, \tag{2.18}$$

where each parameter is a function of the others [87, 125]. These relations constitute a Baker-Campbell-Hausdorff-like generalization of the Glauber-Cahill operator orderings [14] to other Lie groups [126]; see also [127]. In short, they allow us to express the rotation operator in a sort of "spherical anti-normal" order:

$$e^{\xi J_- - \xi^* J_+} = e^{\gamma J_-}e^{\ln(\frac{1}{1+|\gamma|^2})J_z}e^{-\gamma^* J_+} \qquad \text{where } \gamma = e^{i\phi}\tan\frac{\theta}{2}. \tag{2.19}$$

This form of the rotation operator allows us to compute its action as

$$\begin{aligned}
|\theta,\phi\rangle &= R(\theta,\phi)|j,j\rangle \\
&= e^{\gamma J_-}e^{\ln(\frac{1}{1+|\gamma|^2})J_z}e^{-\gamma^* J_+}|j,j\rangle \\
&= e^{\gamma J_-}e^{\ln(\frac{1}{1+|\gamma|^2})J_z}|j,j\rangle \\
&= \left(\frac{1}{1+|\gamma|^2}\right)^j e^{\gamma J_-}|j,j\rangle \\
&= \left(\frac{1}{1+|\gamma|^2}\right)^j \sum_{m=-j}^{j}\binom{2j}{j-m}^{\frac{1}{2}}\gamma^{j-m}|j,m\rangle \\
&= \sum_{m=-j}^{j}\binom{2j}{j-m}^{\frac{1}{2}}\sin^{j-m}\frac{\theta}{2}\cos^{j+m}\frac{\theta}{2}e^{i(j-m)\phi}|j,m\rangle.
\end{aligned} \tag{2.20}$$

The same result could have been obtained using the Wigner D-matrices (2.6) but this "disentangling" approach was used because it better reflects the mathematical ties between the various perspectives on quantum spin. In particular, the complex number $\gamma = e^{i\phi}\tan\frac{\theta}{2}$ from (2.19) is in fact geometrically interpreted as the image of the point (θ,ϕ) in the complex plane under the stereographic map, which is central to the stellar perspective[3].

[3]Note the conventional difference in both spherical coordinates *and* fiducial state as used in [87].

The rotation operator (2.17) of course acts on all of Hilbert space, including in particular the Dicke basis. This may be thought of as rotating the entire quantization axis (i.e. the Stern-Gerlach axis) as it sits within the spherical phase space. The resulting basis is here denoted by any of the following:

$$R(\Omega)|j,m\rangle \equiv R(\theta,\phi)|j,m\rangle \equiv |j,m;\boldsymbol{n}\rangle \equiv |j,m_{\boldsymbol{n}}\rangle. \tag{2.21}$$

where $\boldsymbol{n}$ is the Euclidean vector that points to $\Omega \equiv (\theta,\phi)$. See Fig. (2.1) for a schematic in the case of the standard Dicke basis (i.e. $\boldsymbol{n} = \boldsymbol{z}$). Note the additional piece of notation $\boldsymbol{n}^{\perp} \equiv (\theta,\phi)^{\perp} = (\pi-\theta,\pi+\phi)$, which denotes the antipode of a point on the sphere.

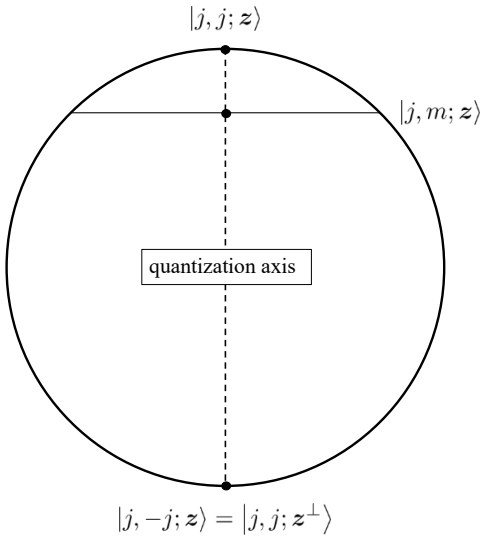

Figure 2.1: Schematic of the standard Dicke basis.

Two important and intertwined quasiprobability distributions borne from the spin coherent states are the Husimi Q function and the Glauber-Sudarshan P function [87]. The Husimi function $Q_\rho(\theta,\phi)$ may be defined as

$$Q_\rho(\theta,\phi) = \langle\theta,\phi|\rho|\theta,\phi\rangle, \tag{2.22}$$

which reduces to $Q_\phi(\theta,\phi) = |\langle\theta,\phi|\psi\rangle|^2$ for pure states. The Glauber-Sudarshan function may be implicitly defined as the expansion coefficients of a state ρ in the spin coherent state projector basis,

$$\rho = \frac{2j+1}{4\pi}\int_{S^2} P_\rho(\theta,\phi)|\theta,\phi\rangle\langle\theta,\phi|\sin\theta d\theta d\phi. \tag{2.23}$$

Given their inseparable relationship to the spin coherent states it is unsurprising that these functions are deeply connected to the structure theory of SU(2) and quantum spin. Much can be said about these functions, and various properties will be intermittently introduced as needed but for now note their faithfulness as quantum state representations essentially follows from the (over-)completeness of the spin coherent states [86, 87]:

$$\frac{2j+1}{4\pi}\int_{S^2}|\theta,\phi\rangle\langle\theta,\phi|\sin\theta d\theta d\phi = \mathbb{I}, \tag{2.24}$$

which is of course analogous to the overcompleteness of the bosonic coherent states.

As a final side remark, it is interesting to note that any set of $2j+1$ *distinct* spin coherent states form a basis for the Hilbert space $\mathbb{C}^{2j+1}$ regardless of the mutual closeness of their centroids (i.e. no matter how high their pairwise fidelities are) [128]. This may be seen as a non-trivial, finite-dimensional version of the celebrated coherent state density theorem of von Neumann, which characterizes the conditions under which a set of bosonic coherent states associated to a discrete lattice in $\mathbb{R}^2$ forms a basis for the infinite dimensional Hilbert space [129]. It essentially says (modulo minutiae) that one must have a density of one coherent state per Planck cell in order for the total set of coherent states to be complete — a higher density will yield an overcomplete basis while a lower density will yield an incomplete basis. This is mentioned because it is interesting that on the sphere there is no analogous density requirement (i.e. something like one spin coherent state per "Planck solid angle" $\sim \frac{4\pi}{2j+1}$). This is also of possible interest for generalizing the Gottesman-Kitaev-Preskill construction in quantum error-correction [130], which has a natural interpretation in terms of such von Neumann lattices [131], to spherical lattices in spin-j systems; see [132] for related work in this direction.

2.1.3 The multi-qubit and Jordan-Schwinger pictures

Two more perspectives on quantum spin are now reviewed, which may be seen as coming from different "realizations" of the $\mathfrak{su}(2)$ algebra relations (2.2) sitting within other larger quantum systems. The first one sits inside the n-qubit Hilbert space $(\mathbb{C}^2)^{\otimes n}$ via the following definitions:

$$J_i^{(\mathrm{mq})} = \sum_{l=1}^{n} \underbrace{\mathbb{I}\otimes\cdots\otimes\mathbb{I}}_{l-1}\otimes J_i\otimes\underbrace{\mathbb{I}\otimes\cdots\otimes\mathbb{I}}_{n-l} \qquad i=x,y,z \tag{2.25}$$

where the superscript denotes "multi-qubit" and J_i is from (2.1). This is just the tensor product representation of $\mathfrak{su}(2)$ over n copies. Analogous ladder operators can be defined, and it can be shown that this indeed forms an irreducible representation of SU(2) with spin $j = \frac{n}{2}$ [115]. In this *multi-qubit picture* the eigenstates of $J_z^{(\mathrm{mq})}$, often denoted as $|D_n^{(k)}\rangle$, take the form

$$|D_n^{(k)}\rangle = \binom{n}{k}^{-\frac{1}{2}} \sum_{\tau \in S_n} |\tau(\underbrace{1\cdots 1}_{k}\,\underbrace{0\cdots 0}_{n-k})\rangle, \tag{2.26}$$

where S_n is the symmetric group of order n. That is, they are the uniform superposition of all $\binom{n}{k}$ distinct computational basis states with Hamming weight k. These states are easily seen to be permutationally invariant; that is, they are states of *indistinguishable qubits*. More precisely, one can define the *symmetrizer* $\pi_n : (\mathbb{C}^2)^{\otimes n} \to (\mathbb{C}^2)^{\otimes n}$,

$$\pi_n = \frac{1}{n!} \sum_{\tau \in S_n} R_\tau, \tag{2.27}$$

where R_τ is the irreducible unitary representation of S_n. The symmetrizer is the orthogonal projection operator onto the *symmetric subspace* of n qubits, and multi-qubit Dicke basis can be understood as the (renormalized) image of the computational basis under π_n [115][4]. Thus any spin system may equivalently be thought of as the $(n+1)$-dimensional symmetric subspace of n qubits (for some n) via the identification

$$\begin{aligned} |D_n^{(k)}\rangle \quad &\longleftrightarrow \quad |\frac{n}{2}, \frac{n}{2} - k\rangle \\ |j, m\rangle \quad &\longleftrightarrow \quad |D_{2j}^{(j-m)}\rangle. \end{aligned} \tag{2.28}$$

With this in mind the Dicke states $|j, m\rangle$ may be identified with the generalized W states, first introduced in the classification of multipartite entanglement with respect to stochastic local operations and classical communication (SLOCC) [133]. In particular, the case of $(j = 3/2, m = 1/2) \equiv (n = 3, k = 1)$ recovers the original W state:

$$|\frac{3}{2}, \frac{1}{2}\rangle \simeq \frac{1}{\sqrt{3}}(|100\rangle + |010\rangle + |001\rangle). \tag{2.29}$$

It also means that as m in $|j, m\rangle$ approaches either $\pm j$, the equivalent W state has an increasingly *asymmetric* ratio of 0s to 1s, corresponding respectively to the Northern and Southern hemispheres of phase space. The special cases of $k = \{0, n\}$ correspond to the

[4]The binomial coefficient occurring in Eq. (2.20) and later in Eq. (2.36) is now less mysterious.

computational states $|0\rangle^{\otimes n}$ and $|1\rangle^{\otimes n}$, which are further identified with the North and South pole spin coherent states $|j, \pm j\rangle$ (where again and always, $n = 2j$).

Unsurprisingly, the simultaneous local rotation of each constituent qubit by $e^{i\theta \boldsymbol{k}\cdot\frac{\boldsymbol{\sigma}}{2}}$ amounts to the global rotation $e^{i\theta \boldsymbol{k}\cdot\boldsymbol{J}^{(\mathrm{mq})}}$. Hence spin coherent states in the qubit picture are the product states

$$|\theta, \phi\rangle \quad \longleftrightarrow \quad \Big(\cos\frac{\theta}{2}|0\rangle + e^{i\phi}\sin\frac{\theta}{2}|1\rangle\Big)^{\otimes 2j}. \tag{2.30}$$

Finally, it is then clear that the Greenberger–Horne–Zeilinger (GHZ) state may be seen as the balanced superposition of the North and South pole spin coherent states:

$$\frac{1}{\sqrt{2}}(|0\rangle^{\otimes n} + |1\rangle^{\otimes n}) \quad \longleftrightarrow \quad \frac{1}{\sqrt{2}}(|j, j\rangle + |j, -j\rangle). \tag{2.31}$$

Another realization of the $\mathfrak{su}(2)$ algebra is within the tensor product of two optical modes (i.e. two copies of the Heisenberg-Weyl system) via the definitions

$$J_+^{(\mathrm{op})} = a^\dagger b \qquad J_-^{(\mathrm{op})} = b^\dagger a \qquad J_z^{(\mathrm{op})} = \frac{1}{2}\left(a^\dagger a - b^\dagger b\right), \tag{2.32}$$

where the superscript stands for "optical" and a ($a^\dagger$) and b ($b^\dagger$) are the annihilation (creation) operators of the respective a and b modes [134, 101]. Here the eigenvalues of $J_z^{(\mathrm{op})}$ are

$$|j, m\rangle \quad \longleftrightarrow \quad |j + m\rangle_a |j - m\rangle_b. \tag{2.33}$$

Note that regardless of m the total number of photons shared between the two modes is fixed at $N = 2j$. Hence the Dicke states are identified optically using a fixed number of N photons distributed over two distinct modes. These *fixed-photon sectors* correspond to different spins j, and the union of all these sectors forms a full decomposition of the two-mode Hilbert space. This idea has many names including the Jordon map, boson calculus, the occupation number basis, Fock shells/layers, the Schwinger representation, or the *Jordan-Schwinger picture* of spin. See Fig. (2.2) for a schematic of how these sectors 'fit' inside the two-mode Hilbert space.

A particularly important state is the Jordan-Schwinger version of the GHZ state:

$$\frac{1}{\sqrt{2}}(|j, j\rangle + |j, -j\rangle) \quad \longleftrightarrow \quad \frac{1}{\sqrt{2}}(|N\rangle_a|0\rangle_b + |0\rangle_a|N\rangle_b). \tag{2.34}$$

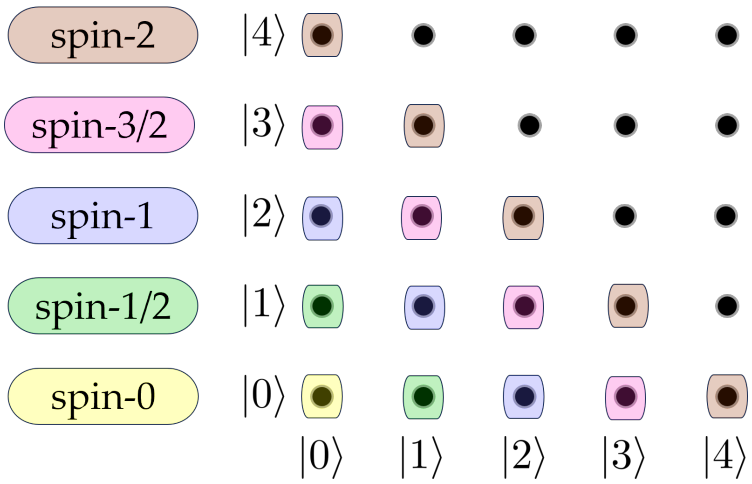

Figure 2.2: Schematic of the Jordan-Schwinger picture of spin. Diagonal dots of the same colour correspond to the Dicke states of a two-mode fixed-photon sector.

This is the famous (high-)N00N state of quantum metrology [135, 136]. While we will never work explicitly within the Jordan-Schwinger picture, its obvious physical relevance is hard to overstate. With the relationship to SU(2) in mind, it is valuable to interpret certain optical devices in the language of spin [137]. Indeed various lossless and passive (i.e. energy-conserving) components of an interferometer may be seen as a rigid rotation of the spherical phase spaces, one for each fixed-photon sector. For example, if an N-photon state (possibly highly entangled, such as the N00N state) is sent into a Mach-Zehnder interferometer with phase shifter U_ϕ characterizing the relative path-length difference, the corresponding spin-$\frac{N}{2}$ system will experience a ϕ-rotation about the y-axis [137]. Also, in quantum information the single-photon sector is exactly the *dual-rail* qubit encoding central to linear optical quantum computing [138, 139].

2.1.4 The Majorana stellar representation

The stellar representation, due to Majorana and later Schwinger, is a "baffling" [140] perspective on quantum spin that unifies all of the previous pictures. In short, it offers a description of a pure spin-j state as a unique constellation of $2j$ points on the unit sphere [113, 114]. Several applications have been established, including a generalization of the geometric phase [141, 142] and the full classification of symmetric state SLOCC

entanglement [103, 104]; see also [106] for its use in analyzing Bell nonlocality. Here the stellar representation is briefly reviewed without specific derivations. See Refs. [128, 143] for more information.

The physical state space of a two level quantum system is the projective Hilbert space under $\mathbb{C}^2$, topologically understood as the extended complex plane $\mathcal{P}\mathbb{C}^1 = \mathbb{C} \cup \{\infty\}$. This is isomorphic to the Riemann sphere S^2, with an explicit bijection given by the (inverse) stereographic projection to a sphere centred at the origin. The projection point is by convention the South pole, which is where the point at infinity is mapped. Given a qubit state in the standard polar coordinate parameterization $|\psi\rangle = \cos\frac{\theta}{2}|0\rangle + e^{i\phi}\sin\frac{\theta}{2}|1\rangle$, the ratio between the spin-down and spin-up amplitudes, $z = \tan\frac{\theta}{2}e^{i\phi}$, is the associated point in $\mathcal{P}\mathbb{C}^1$. This is the famous Bloch sphere picture of a qubit. The key insight to the stellar perspective is that a state within a higher dimensional irrep of SU(2) may be characterized by an *unordered set* of points in $\mathcal{P}\mathbb{C}^1$ rather than a single point in a larger space. Thus the correspondence between $\mathcal{P}\mathbb{C}^1$ and S^2 allows the identification of spin states with constellations on the sphere; simply perform the inverse stereographic projection on each point in $\mathcal{P}\mathbb{C}^1$ comprising the given state. Hence one of the immediate strengths of the stellar picture is that one may faithfully plot and readily imagine, for example, a 42-dimensional quantum state. The number of stars in the constellation is twice that of the spin, $n = 2j$, counting multiplicities.

On the other hand any spin-j state must of course be expandable into the Dicke basis,

$$|\Psi\rangle = \sum_{m=-j}^{j} a_m |j, m\rangle. \tag{2.35}$$

The connection between the algebraic and geometric descriptions is supplied by the zero-set of the *Majorana polynomial*,

$$P_\Psi(z) = \sum_{m=-j}^{j} (-1)^{j-m} \sqrt{\binom{2j}{j-m}}\, a_m z^{j+m}. \tag{2.36}$$

This is the polynomial over $\mathbb{C}$ with roots given by the non-infinite points in $\mathcal{P}\mathbb{C}^1$ characterizing a quantum state,

$$P_{|\Psi\rangle}(z) = a_j \prod_{i=1}^{2j} (z - z_i) \qquad z_i = \tan\frac{\theta_i}{2} e^{i\phi_i} \neq \infty \tag{2.37}$$

with $a_j = \langle j, j|\Psi\rangle$ being the leading coefficient. If the number of roots is less than $2j$ then the remaining roots are "at infinity", and are associated with the South pole (i.e. $|z_i| \to \infty \Rightarrow \theta_i \to \pi$).

The stellar representation has a natural interpretation in the symmetric qubit picture. Consider the tensor product of n qubits

$$|\Psi\rangle = \bigotimes_{i=1}^{n} |\psi_i\rangle, \qquad |\psi_i\rangle = \cos\frac{\theta_i}{2}|0\rangle + e^{i\phi_i}\sin\frac{\theta_i}{2}|1\rangle, \tag{2.38}$$

where (θ_i, ϕ_i) are the respective Bloch vectors. This state lives in the Hilbert space $(\mathbb{C}^2)^{\otimes n}$ and is in general not invariant under permutations of the individual qubits; they are distinguishable. Permutation invariance (indistinguishability) is then enforced by application of the symmetrizer π_n (2.27). *The unifying idea is that the resulting spin state* $|\Psi_S\rangle \sim \pi_n|\Psi\rangle$ *is the one associated to the constellation defined by the original Bloch vectors* $\{(\theta_i, \phi_i)\}$*, the stereographic projections of which form the zero set of the Majorana polynomial,* $P_{\Psi_S}(z)$.

This concept is furthermore related to the zeros of the spherical Husimi function (2.22). This can be seen by noting that when the Husimi function $Q_\psi(\theta, \phi)$ vanishes at a point (θ_0, ϕ_0) on the sphere, it means that the state $|\psi\rangle$ is orthogonal to the spin coherent state $|\theta_0, \phi_0\rangle$. And because the spin coherent state in the qubit picture is simply a product of qubits each with the same Bloch vector (θ_0, ϕ_0) (2.30), together with the fact that $|\psi\rangle$ is a superposed set of the same product state but permuted, it must be the case that at least one of the constituent qubits within $|\psi\rangle$ has a Bloch vector antipodal to (θ_0, ϕ_0). This intuition is made proper with the relation

$$P_\psi(z) \sim \langle(\theta, \phi)^\perp|\psi\rangle, \tag{2.39}$$

where $z = \tan\frac{\theta}{2}e^{i\phi}$ is the stereographic projection of (θ, ϕ) and $(\theta, \phi)^\perp = (\pi - \theta, \pi + \phi)$ is the point antipodal to (θ, ϕ). In short, *Majorana stars are antipodal to Husimi function zeros*. And again resorting back to the form of the pure state Husimi function as $|\langle\theta, \phi|\psi\rangle|^2$, Eq. (2.39) also allows us to view the Majorana polynomial as a sort of "square root" of the Husimi function.[5]

[5]Note the similarity to the *stellar function* (i.e. the Segal-Bargmann function) of quantum optics: $F^\star_\psi(z) \sim \langle\bar{z}|\psi\rangle$ where $|\bar{z}\rangle$ is the complex conjugate of the optical coherent state [144]. These are examples of what is more generally called a *coherent state representation*, which may be seen as having a similar logical status as, for example, the position representation $\psi(x) = \langle x|\psi\rangle$, with the importance difference however of the coherent state basis being highly overcomplete and in bijective correspondence with points in phase space. See [129] for more information.

The stellar picture also naturally accommodates the Jordan-Schwinger picture through the use of homogeneous polynomials in two variables; we will not discuss this here but see [101] for more information.

With all of these different perspectives on quantum spin (i.e. quasiprobability, symmetric subspace, constellation, Jordan-Schwinger) melded together, it is worth reflecting on Majorana's original physical intuition: he envisioned the stars in his constellations...

> "...as if each of the representative points indicated the direction of a little gyroscope with angular momentum $\frac{\hbar}{2}$." [113, 114].

As will be discussed in Chapter 4, the stellar perspective offers valuable insight to the characterization of nonclassicality that would otherwise be be quite difficult to obtain let alone interpret.

For a simple example consider the Dicke state constellations. Begin with the computational basis state of $n = 2j$ distinguishable qubits with the last k spin-down,

$$|\psi\rangle = |\underbrace{0\cdots0}_{2j-k}\,\underbrace{1\cdots1}_{k}\rangle. \tag{2.40}$$

Symmetrize and renormalize (i.e. enforce indistinguishably):

$$\begin{aligned}\pi_{2j}|\psi\rangle &= \frac{1}{(2j)!}\sum_{\tau\in S_{2j}}|\tau(\underbrace{0\cdots0}_{2j-k}\,\underbrace{1\cdots1}_{k})\rangle \\ &\mapsto \binom{2j}{k}^{-\frac{1}{2}}\frac{1}{(2j-k)!k!}\sum_{\tau\in S_{2j}}|\tau(\underbrace{0\cdots0}_{2j-k}\,\underbrace{1\cdots1}_{k})\rangle \\ &:= |j, j-k\rangle.\end{aligned} \tag{2.41}$$

The Majorana polynomial of this state is then by definition

$$P_{|j,j-k\rangle}(z) = \sum_{m=-j}^{j}(-1)^{j-m}\sqrt{\binom{2j}{j-m}}\delta_{m,j-k}z^{j+m} = (-1)^k\sqrt{\binom{2j}{k}}z^{2j-k}. \tag{2.42}$$

This is a monomial with a $(2j-k)$-degenerate zero at $z=0$. Thus there are $(2j-k)$ stars on the North pole via the stereographic map. The remaining k stars must then be on the South pole, matching the original Bloch vectors in Eq. (2.40).

For a final side remark, the stellar representation of spin was generalized to mixed states in 1986 [145] but was largely overlooked until 2020 [110]. Given its centrality in the pure state setting we are likely to see some big results and applications for it in the coming years. The basic idea is to assign a different Majorana polynomial to each multipole sector then plot their roots on nested concentric spheres, one for each multipole. The radii of these spheres correspond to the population of the state in that multipole. This generalization naturally meshes with the multi-qubit picture where tracing out qubits removes higher-degree multipole constellations while keeping the lower-degree ones fixed [110, 112]. See also [146, 147] for recent work on generalizing the stellar picture to other domains of finite dimensional quantum theory and quantum information. The stellar picture is also well-defined in single-mode optical systems[6]; see for example [144, 148, 149] for recent works on *stellar rank* as an information-theoretic measure of continuous-variable non-Gaussianity.

2.2 The Stratonovich axioms

For a brief history of the phase space picture and its generalizations refer to the introduction together with Refs. [90, 91, 92, 93, 94, 96, 97, 98, 99] and especially [89, 84] for more information on the spherical Wigner function. In short the Stratonovich axioms, also known as the Stratonovich-Weyl axioms, represent the necessary rules that any generalized Wigner function ought to satisfy when defined in the presence of a dynamical symmetry. Here we present some results for the case of SU(2) dynamical symmetry then briefly summarize the case of the original Wigner function. Also note that in this thesis we are concerned entirely with kinematics and not dynamics, at least not explicitly. A full treatment of the Moyal theory on the sphere as an autonomous construction of quantum theory yet fully equivalent to the other formulations must include the twisted product, also known as the Moyal bracket.

As discussed above the phase space associated to SU(2) is the sphere. Let $A \in L(\mathbb{C}^{2j+1})$ be an operator over the spin-j Hilbert space and let $\pi : SU(2) \to L(\mathbb{C}^{2j+1})$ be an irreducible representation of SU(2). Let $W_A(\Omega)$ denote a hypothetical Wigner function of the operator A. Then the official Stratonovich axioms for a linear injective map $A \mapsto W_A(\Omega)$ are

$$W_{A^\dagger}(\Omega) = [W_A(\Omega)]^* \qquad \text{realness} \tag{2.43a}$$

[6] And also conceivably in any phase space picture based on a Perelomov system [81] simply by changing the definition of the constellation to be zero set of the associated Husimi function or, equivalently, the zero-set of the associated coherent state representation.

$$\mathrm{tr}[A] = \int d\Omega\, W_A(\Omega) \qquad \text{standardization} \tag{2.43b}$$

$$\mathrm{tr}[AB] = \int d\Omega\, W_A(\Omega)\, W_B(\Omega) \qquad \text{traciality} \tag{2.43c}$$

$$W_{\pi(g)\rho\pi^\dagger(g)}(\Omega) = W_\rho(g^{-1}\,\Omega) \qquad \text{covariance} \tag{2.43d}$$

where $g^{-1}\Omega$ denotes a rotation of the sphere and $d\Omega = \alpha \sin\theta d\theta d\phi$ is the invariant measure on the sphere up to an *a priori* unknown scaling factor α. That being said, as linearity demands the identity operator be mapped to the unit function, it immediately follows from standardization (2.43b) that this factor[7] is $\alpha = \frac{2j+1}{4\pi}$. Standardization then also implies that $W_A(\Omega)$ be normalized. Furthermore, by re-interpreting this factor in terms of spherical coordinates, we may also conclude the geometric property that the *radius* of the spherical phase space is

$$R = \sqrt{\frac{2j+1}{4\pi}}. \tag{2.44}$$

Vastly more important however is covariance (2.43d), which demands compatibility between a rotation of phase space and the rotation operator acting on Hilbert space. As shown in Appendix A this property alone determines the majority of the structure of the spherical Wigner function. Traciality (2.43c) is the second most important, which, together with realness (2.43a), ensures that the Born rule is mapped to the L^2-inner product between Wigner functions:

$$\mathrm{tr}[\rho A] = \int W_\rho(\Omega) W_A(\Omega) d\Omega \tag{2.45}$$

for an observable A. This is what allows the theory to make predictions in a manner similar to classical statistical physics (which of course is the primary motivation for studying the phase space picture). These simple and reasonable axioms completely determine the spherical Wigner function up to a finite set of real numbers taking values in $\{1, -1\}$, and even this degree of freedom is removed by slightly modifying the traciality axiom as to incorporate the Husimi and Glauber-Sudarshan functions.

To explicitly find such a Wigner function, if it exists, the linearity of any such map $A \mapsto W_A(\Omega)$ may be realized by introducing an operator-valued function over phase space, $\Delta : S^2 \to L(\mathbb{C}^{2j+1})$, called the *kernel*, then defining the Wigner function as

$$W_A(\Omega) := \mathrm{tr}[A\, \Delta(\Omega)]. \tag{2.46}$$

[7] This factor comes up often and sometimes goes by the name *Racah's normalization*.

This is sometimes called the generalized *Weyl rule*, and virtually all quasiprobability distributions used in physics can be thought of in this way, with the individual values $\Delta(\Omega)$ often being called *phase-point operators*. The Stratonovich axioms may then be equivalently expressed as conditions on the kernel. They are

$$\Delta(\Omega)^\dagger = \Delta(\Omega) \qquad \text{realness} \tag{2.47a}$$

$$\mathbb{I} = \int d\Omega\, \Delta(\Omega) \qquad \text{standardization} \tag{2.47b}$$

$$\Delta(\Omega) = \int d\Omega'\, \Delta(\Omega')\, \mathrm{tr}[\Delta(\Omega')\Delta(\Omega)] \qquad \text{traciality} \tag{2.47c}$$

$$\Delta(g\,\Omega) = \pi(g)\Delta(\Omega)\pi^\dagger(g) \qquad \text{covariance} \tag{2.47d}$$

Note that realness (2.47a), standardization (2.47b), and covariance (2.47d) together quickly imply that the kernel is a Hermitian operator with $\mathrm{tr}[\Delta(\Omega)] = 1$ at every point Ω. Traciality may be seen as demanding that $\frac{2j+1}{4\pi}\,\mathrm{tr}[\Delta(\Omega)\Delta(\Omega')]$ behave like a delta function $\delta(\Omega - \Omega')$ in the space of functions over phase space. Traciality (2.47c) also implies an *inverse Weyl rule*

$$A = \int d\Omega\, W_A(\Omega)\Delta(\Omega), \tag{2.48}$$

which allows us to also see the Wigner function as a set of expansion coefficients over a very particular set of operators in Hilbert space. It is worth stressing that the same kernel is used in the Weyl rule (2.46) and the inverse Weyl rule (2.48). This turns out to be unique to Wigner functions within the landscape of quasiprobability theory and may quite generally be seen as a defining characteristic. Indeed all of the ideas mentioned here are applicable for many other dynamical symmetry groups, in particular the original Heisenberg-Weyl case.

2.2.1 Example: the Heisenberg-Weyl group

The (continuous) Heisenberg-Weyl group in one spatial dimension, denoted H_1, is the group generated by the canonical commutation relations $[x, p] = i\mathbb{I}$. The phase space is of course $\mathbb{R}^2$, which as mentioned earlier is obtained by a natural quotient of H_1 [84][8]. This non-compact phase space describes many physical scenarios, including a bosonic field mode and a one-dimensional non-relativistic spinless particle. The analog of the spherical

[8]More precisely the phase space is the Perelomov system of H_1 generated by $|0\rangle$, the optical vacuum.

rotation (2.17) is the displacement operator $D(x,p) = e^{i(p\hat{x}-x\hat{p})}$, which enacts in Hilbert space the translation of phase space from the origin to the point (x,p).

Major insight was brought by Grossman [19] and Royer [20] who in the 1970s showed that the Heisenberg-Weyl kernel is in fact a set of *displaced parity operators*. In particular, consider the operator Π defined as

$$\Pi\hat{x}\Pi = -\hat{x} \qquad\qquad \Pi\hat{p}\Pi = -\hat{p} \tag{2.49}$$

This enacts in Hilbert space the reflection in phase space that sends $(x,p) \mapsto (-x,-p)$[9]. The displaced parity operator

$$\Pi(x,p) = D(x,p)\Pi D^{\dagger}(x,p) \tag{2.50}$$

is then the reflection about the point (x,p) instead of the origin. With these in mind, Ref. [20] showed that the common and original definition of the Wigner function,

$$W_{\psi}(x,p) = 2\int_{-\infty}^{\infty} ds\, e^{-2ips}\psi(x-s)\psi^{*}(x+s), \tag{2.51}$$

is equivalent to the Weyl rule

$$W_{\rho}(x,p) = 2\,\mathrm{tr}[\rho\,\Pi(x,p)]. \tag{2.52}$$

See also the quote

> The Wigner function...[is thus]...the expectation value of the parity operator about (x,p). Alternatively, $W_{\psi}(x,p)$ is proportional to the overlap of ψ with its mirror image about (x,p), which is clearly a measure of how much ψ is "centered" about (x,p). [20]

This showed the deep relationship between the Wigner function and phase space symmetry and now these *Grossman-Royer operators* play a critical role in modern developments [150], which is also sometimes referred to as the *parity operator framework*. This idea applies more broadly to other dynamical symmetry groups but now the notion of reflection is more subtle and of course depends on the phase space manifold; see [92, 97] for discussions on the sphere.

[9] This is perhaps more appropriately called an *inversion* rather than a reflection as there is no axis of symmetry to reflect upon (at least not within the plane).

2.3 The spherical Wigner function

Given the importance of this topic here, a full understanding of how to obtain the SU(2)-covariant Wigner functions is required. The derivation presented in Appendix A is an expounded combination of Várilly & Gracia-Bondía in [89] and Heiss & Weigert in [93], together with some original supplements and minor omissions. While longer than necessary to obtain the final result, it is has been catered to best illustrate the relative power of each Stratonovich axiom, as well as their collective interaction with the structure theory of quantum spin. The general idea is to expand the kernel in various operator bases and use clever application of the axioms to constrain the expansion coefficients. See also [95] for a broader and more rigorous treatment. One key result is that the set of all spherical kernels satisfying the Stratonovich axioms may be expressed as

$$\Delta(\Omega) = \sqrt{\frac{4\pi}{2j+1}} \sum_{\ell=0}^{2j} \epsilon_\ell \sum_{m=-\ell}^{\ell} T^{(j)\dagger}_{\ell m} Y_{\ell m}(\Omega). \tag{2.53}$$

where $\epsilon_\ell = \pm 1$ for all non-trivial multipoles (i.e. for $\ell \in \{1, ..., 2j\}$). Hence there are 2^{2j} different cases.

From Eq. (2.53) we see that the kernel (and therefore also the Wigner function) is naturally constructed in terms of multipole sectors $\ell \in \{0, ..., 2j\}$, each of which show a nice pairing between the spherical harmonics and the spherical tensor operators – which are just the operator versions of the spherical harmonics (2.11). We can also say that any Wigner function of a spin-j state lives in the Hilbert subspace of $L^2(S^2)$ generated by spherical harmonics of degree no larger than $\ell = 2j$. And as spherical harmonics are eigenfunctions of the spherical Laplace operator this therefore places an upper bound on the scale of angular resolution of the Wigner function[10]. Finally we can say that the orthogonality of the spherical tensor operators implies through the Weyl rule (2.46) that the Wigner function of the spherical tensor operator is proportional to the spherical harmonic of the same parameters[11]:

$$W_{T^{(j)}_{\ell,m}}(\theta, \phi) \sim Y_{\ell,m}(\theta, \phi). \tag{2.54}$$

Another property derived in Appendix A is that the phase-point operators share the same rotationally-invariant spectrum but the kernel at the point Ω is diagonal in the basis

[10] From the perspective of Fourier theory this means that the spherical Wigner function is *band-limited* [151]. Intuitively, the maximum "wiggliness" of the Wigner function depends on j.

[11] The Q and P functions of the multipole operators are also proportional to spherical harmonics but with an ℓ-dependent pre-factor [152]; see also Eq. (2.56) below.

associated (2.21) to the quantization axis $\boldsymbol{n}$ pointing to Ω. These eigenvalues for the canonical Wigner function are given in (2.58).

2.3.1 Uniqueness

As just discussed there are 2^{2j} distinct Wigner functions. And while this appears to be a problem, the Wigner function associated to the choice $\epsilon_\ell = +1$ for all $\ell \in \{0, ..., 2j\}$ may be singled out using two independent and natural arguments.

The first is to incorporate the spherical s-ordered class of functions $f^{(s)}(\Omega)$ into the picture. This is done by modifying the traciality axiom (2.43c) to

$$\mathrm{tr}[AB] = \int d\Omega \, f_A^{(s)}(\Omega) \, f_B^{(-s)}(\Omega). \tag{2.55}$$

Analogous to the Glauber-Cahill operator orderings, the Husimi function corresponds to $Q_\rho = f_\rho^{(-1)}$ while the Glauber-Sudarshan function corresponds to $P_\rho = f^{(1)}$. This modified traciality axiom may be thought to be a spherical version of the optical equivalence theorem [99]. As shown in [89] the only Wigner function to sit within this s-parameterized set of quasiprobability distributions is the one where $\epsilon_\ell = +1 \; \forall \, \ell$. Indeed the s-parameterized kernel $\Delta^{(s)}$ is [99, 84, 97]

$$\Delta^{(s)}(\Omega) = \sqrt{\frac{4\pi}{2j+1}} \sum_{\ell=0}^{2j} \sum_{m=-\ell}^{\ell} \left\langle \begin{matrix} j & \ell \\ j & 0 \end{matrix} \middle| \begin{matrix} j \\ j \end{matrix} \right\rangle^{-s} T^{(j)\dagger}_{\ell,m} Y_{\ell,m}(\Omega), \tag{2.56}$$

which by comparison to (2.53) clearly shows that it is associated to $(s = 0)$ just like the optical case.

In my view this is more than enough to grant the title of "canonical" to the kernel $\Delta^{(0)}(\Omega)$, but there is another excellent reason to choose it. An interesting property of the entire SU(2) apparatus described in this chapter is that it is subject to a Lie algebra contraction to the Heisenberg-Weyl algebra [87, 126]. There is much to be said about this contraction but the takeaway is that under a particular limit of $j \to \infty$ the J_z operator becomes the number operator N, the ladder operators become the creation and annihilation operators, and the Dicke state becomes the Fock state:

$$\lim_{j\to\infty} |j, j-n\rangle = |n\rangle. \tag{2.57}$$

In terms of phase space manifolds, the idea is to "zoom in" to the North pole of the sphere at a fixed rate relative to the increasing spin j. The result is an increasingly flatter phase space until finally in the limit the Heisenberg-weyl plane of $\mathbb{R}^2$ is all that remains [97]. More will be said about this in Chapter 3. In terms of uniqueness, Ref. [92] showed that the only Wigner function compatible with this contraction is again the one with $\epsilon_\ell = +1$ $\forall\, \ell$.

2.3.2 Summary

The following is the canonical spherical Wigner function for states and operators in $L(\mathbb{C}^{2j+1})$:

$$W_\rho(\theta,\phi) := \mathrm{tr}[\rho\,\Delta(\theta,\phi)] \qquad \text{where} \qquad \begin{aligned} \Delta_j(\theta,\phi) &= \sum_{m=-j}^{j} \Delta_{j,m} |j,m_{\boldsymbol{n}}\rangle\langle j,m_{\boldsymbol{n}}| \\ \Delta_{j,m} &= \sum_{\ell=0}^{2j} \frac{2l+1}{2j+1} \left\langle \begin{matrix} j & \ell \\ m & 0 \end{matrix} \middle| \begin{matrix} j \\ m \end{matrix} \right\rangle . \end{aligned} \tag{2.58}$$

Equivalent expressions are

$$W_\rho(\theta,\phi) = \sqrt{\frac{4\pi}{2j+1}} \sum_{\ell=0}^{2j} \sum_{m=-\ell}^{\ell} \rho_{\ell,m} Y_{\ell,m}(\theta,\phi) \qquad \Delta(\Omega) = \sqrt{\frac{4\pi}{2j+1}} \sum_{\ell=0}^{2j} \sum_{m-=-\ell}^{\ell} T^{(j)\dagger}_{\ell,m} Y_{\ell,m}(\Omega), \tag{2.59}$$

where $\rho_{\ell,m} = \mathrm{tr}[\rho T^{(j)}_{\ell,m}]$ are state multipoles. The definition of Wigner negativity is

$$\delta(\rho) := \frac{1}{2}\left(\frac{2j+1}{4\pi} \int_{S^2} |W_\rho(\theta,\phi)| \sin\theta d\theta d\phi - 1 \right). \tag{2.60}$$

The Dicke state Wigner function is

$$\begin{aligned} W_{|j,m\rangle}(\theta,\phi) &= \langle j,m|\Delta(\theta,\phi)|j,m\rangle \\ &= \sum_{l=0}^{2j} \frac{2l+1}{2j+1} \left\langle \begin{matrix} j & l \\ m & 0 \end{matrix} \middle| \begin{matrix} j \\ m \end{matrix} \right\rangle P_l(\cos\theta) . \end{aligned} \tag{2.61}$$

Chapter 3

Common pure states

Chapters 3 and 4 are approximately based (respectively) on the works

> Davis, J., Kumari, M., Mann, R. B., & Ghose, S. (2021). Wigner negativity in spin-j systems. *Physical Review Research*, 3(3), 033134. [1]
>
> Davis, J., Hennigar, R. A., Mann, R. B., & Ghose, S. (2023). Stellar representation of extremal Wigner-negative spin states. *Journal of Physics A: Mathematical and Theoretical*, 56(26), 265302. [2]

Here we begin to study the spherical Wigner function, (5.7), of various symmetric multi-qubit states often seen in the quantum information and quantum communication literature. These include spin coherent, spin cat (i.e. GHZ/N00N), and Dicke (i.e. W). Several surprising results will be reported. The first is that spin coherent states must have a non-zero amount of Wigner negativity regardless of their dimension. The second is that the most Wigner-negative Dicke basis element is spin-dependent. This is in contrast to several entanglement measures, where the most entangled Dicke state is always the balanced/equatorial state: $|j, 0\rangle$ for integer spin or $|j, \pm 1/2\rangle$ for half-integer spin. Third, GHZ states are found to score relatively low, and are not significantly Wigner-negative relative to their Dicke state counterparts of equal dimension.

But before doing so we briefly give an immediate and interesting example of how the planar and spherical Wigner functions have different global properties. In particular, their pointwise upper and lower bounds are distinct. This can be seen by comparing the two

kernel spectra and by noting from the generalized Weyl rule, (5.7), that the maximum eigenvalue gives the pointwise upper bound while the minimum eigenvalue gives the pointwise lower bound. Also recall that all phase-point operators have the same spectrum due to the covariance property. See Fig. 3.1 for some examples of typical SU(2) kernel spectra. We see that the pointwise upper bound at a point (θ, ϕ) is attained by the Dicke state eigenvector $m = j$ quantized along the axis $\boldsymbol{n}$ pointing to (θ, ϕ), which is exactly the spin coherent state with centroid (θ, ϕ). The pointwise lower bound is associated to the eigenstate $|j, j-1; \boldsymbol{n}\rangle\langle j, j-1; \boldsymbol{n}|$, which is incidentally the W state centred at (θ, ϕ). Hence spin coherent states and W states are a sort of opposite to each other, at least in a pointwise sense. This will come up again in Chapter 5 where we discuss mixed states in more detail. Note that the bounds approach ± 2 as spin increases; this is guaranteed because in the optical scenario the infinite-dimensional kernel operators, (2.52), are highly degenerate with only two eigenvalues, ± 2. This behaviour is one manifestation of the spin-to-optical contraction [92]. See also [97] for similar eigenvalue distributions associated to other spherical quasiprobability functions and their infinite-spin limits. It also should

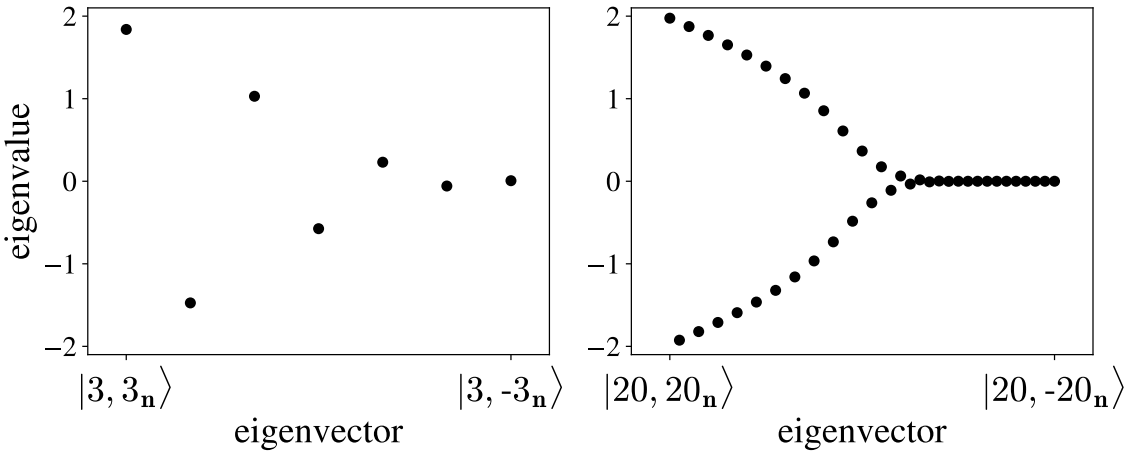

Figure 3.1: Typical phase-point operator spectra. Left is $j = 3$ and right is $j = 20$.

be noted that in every case checked it was numerically found that the kernel eigenvalues oscillate in sign and strictly decrease in absolute value; see Fig. 3.1. It is reasonable to conjecture that this remains true for all finite spin, though a formal proof has not been made. Assuming this is indeed true, the pointwise upper bound of the spherical Wigner function is always larger in absolute value than its pointwise lower bound. This remains true when considering mixed states due to the pointwise-convexity of the Wigner function

with respect to density matrix decompositions.

In the case of a single qubit (i.e. $j = 1/2$) the pointwise bounds are

$$\begin{aligned} \max_{(\theta,\phi)} [W_{\text{qubit}}(\theta,\phi)] &= \frac{1}{2}\left(1+\sqrt{3}\right) \approx 1.37 \\ \min_{(\theta,\phi)} [W_{\text{qubit}}(\theta,\phi)] &= \frac{1}{2}\left(1-\sqrt{3}\right) \approx -0.37. \end{aligned} \tag{3.1}$$

3.1 Spin coherent

As discussed in Sec. 2.1.2, spin coherent states are the spin analogs of the optical coherent states. They are realized in the qubit picture as the product state of qubits with all Bloch vectors pointing in the same direction.

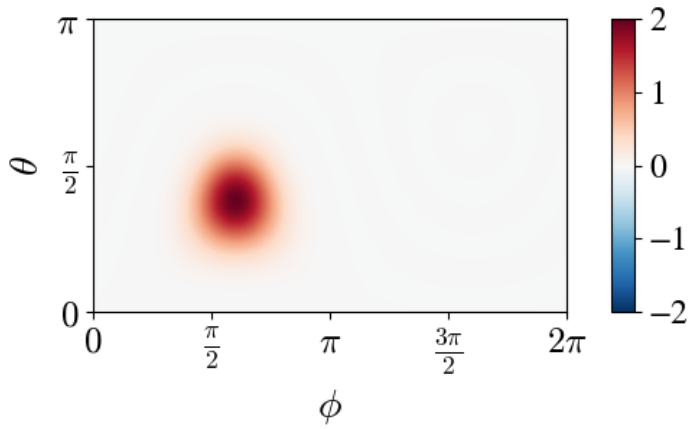

Figure 3.2: Typical spin coherent state Wigner function. Here the centroid is $(\theta, \phi) = (1.2, 1.9)$ and $j = \frac{9}{2}$.

3.1.1 Non-vanishing negativity

A natural question to ask is whether the spin coherent state attains negative values in its Wigner function somewhere on the spherical phase space. This would be interesting to know because in optical systems, Hudson's theorem, also known as the Hudson-Soto-Claverie theorem in a multi-mode setting, establishes the equivalence between Wigner

function Gaussianity and non-negativity in pure states [40, 41]. And so because coherent states are Gaussian they are therefore Wigner-positive. See [153, 154, 155] for further studies on planar positivity, [156] for rotor/cylindrical positivity, and [51] for an extension and rephrasing of the Gottesman-Knill theorem as toroidal positivity[1]. A natural question is then: is there an analogous statement that characterizes positivity on the sphere? Using a short and simple argument, we give a partial answer to this question and show that spin coherent states are never Wigner-positive.

Begin by noting that a consequence of Hudson's theorem is that any two Gaussian states $|\psi_1\rangle$ and $|\psi_2\rangle$ have non-vanishing overlap, $\langle\psi_1|\psi_2\rangle \neq 0$. This can be seen in the phase space picture via the traciality axiom, Eq. (2.43c), where the associated Wigner functions have non-vanishing Gaussian tails that will always overlap each other by a non-zero amount regardless of the location of the centroids. The coherent state basis $\{|\alpha\rangle\}$ is a special case with $\langle\alpha|\beta\rangle \neq 0$ for any $\alpha, \beta \in \mathbb{C}$. This property is not true in the case of spin: any two spin coherent states with antipodal centroids are orthogonal. This follows from the orthogonality of the Dicke basis along any quantization axis $\boldsymbol{n}$, specialized to the highest and lowest weight states: $\langle j, j_{\boldsymbol{n}}|j, -j_{\boldsymbol{n}}\rangle = 0$. These two states are related by a π-rotation about any equatorial axis, which preserves negativity because such a rotation is an SU(2) displacement. So with the fully spin-up Dicke state identified with the spin-j coherent state $|\Omega\rangle$ and the fully spin-down with $|\Omega^\perp\rangle$, where $\Omega^\perp = (\pi - \theta, \pi + \phi)$ is the coordinate antipodal to Ω, traciality becomes

$$|\langle j, j_{\boldsymbol{n}}|j, -j_{\boldsymbol{n}}\rangle|^2 = \frac{2j+1}{4\pi}\int_{S^2} W_{|\Omega\rangle}(\theta,\phi)W_{|\Omega^\perp\rangle}(\theta,\phi)\sin\theta d\theta d\phi = 0. \tag{3.2}$$

Eq. (3.2) cannot be satisfied by two strictly positive functions. So they either have disjoint support or at least one of them — and therefore both via the π-rotation — goes negative somewhere. The former can be ruled out by appealing to the general form of the Dicke state Wigner function, Eq. (2.61). By restricting to an arc of constant longitude between the two poles, their azimuthal symmetry allows them to be effectively viewed as real-valued functions over the interval $[0, \pi]$. And as they are each a linear combination of Legendre polynomials, which in turn are combinations of powers of their arguments, the Dicke state Wigner function can be seen as a finite-degree polynomial in $\cos\theta$. Being such a polynomial with real coefficients, their real zero sets will be finite, ranging in principle

[1] This final example, using toroidal positivity, also characterized the interesting *bound magic states*, which represent a slight mismatch between non-stabilizer-ness and magic distillability.

from no roots to $2j$ roots. So any two such polynomials have mutual support on $[0, \pi]$ up to some finite set of points (i.e. measure zero).

We conjecture that spin coherent states furthermore minimize Wigner negativity over all pure states. The above result, together with this conjecture, would imply that no pure spin states is Wigner-positive and therefore is non-classical in some sense. This likely non-existence of a Gaussian/stabilizer analog may then reflect the non-classicality of spin symmetry itself, and so offer some intuition for why quantum mechanical spin has no perfect classical analogue.

3.1.2 Location of the negativity

Because the negativity of a spin coherent state is unaffected by rotations we restrict attention to the North pole Dicke state:

$$\begin{aligned} W_{|j,j\rangle}(\theta,\phi) &= \sum_{l=0}^{2j} \frac{2l+1}{2j+1} \left\langle \begin{matrix} j & l \\ j & 0 \end{matrix} \middle| \begin{matrix} j \\ j \end{matrix} \right\rangle P_l(\cos\theta) \\ &= \frac{(2j)!}{\sqrt{2j+1}} \sum_{l=0}^{2j} \frac{(2l+1)}{\sqrt{(2j-l)!(2j+1+l)!}} P_l(\cos\theta). \end{aligned} \tag{3.3}$$

As spin increases, we have numerically confirmed that the Wigner negativity of a spin coherent state rapidly approaches zero, although it does not vanish for the finite j considered ($j < 30$). In each case the negativity contributions come from tiny oscillations in the Wigner function, generally present in the Southern hemisphere; see Fig. (3.3). In planar phase space, such oscillations are usually associated with a superposition of distinct macroscopic states (e.g. a planar cat state), which are commonly seen as highly non-classical. However, the spin coherent state is typically considered the most classical-like spin state because of its analogy to Gaussian coherent states on the plane. Thus Wigner negativity helps identify the important differences between planar and spin coherent states that exist despite their similarities. The non-vanishing negativity for finite spin seems to result from the compact spherical phase space compared to the non-compact planar phase space of Gaussian coherent states. Intuitively, the spin coherent state appears to be as close as possible to a Gaussian function on the sphere. The compactness of the phase space however stops this from truly happening and these tiny ripples are the consequence. In the spin contraction limit, Eq. (2.57) for $n = 0$, these ripples are "pushed to infinity" and no longer contribute towards the optical Wigner function.

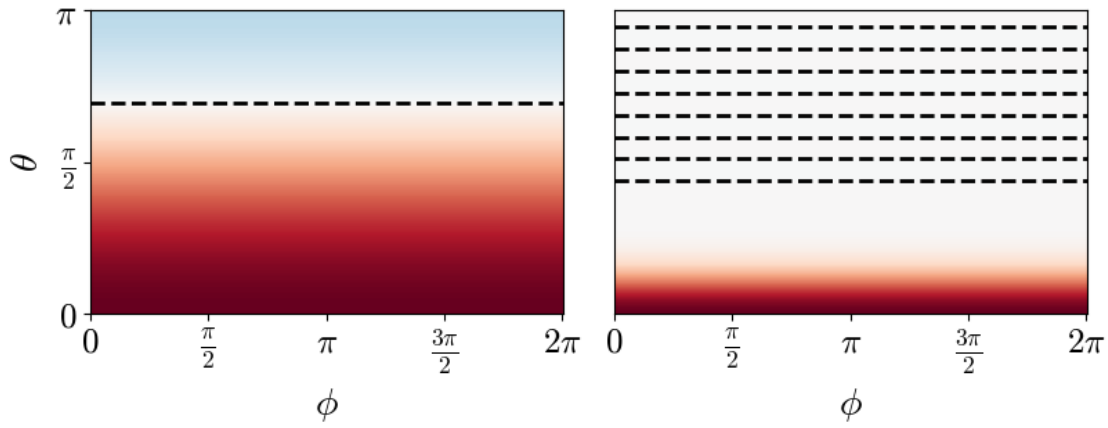

Figure 3.3: Spin coherent states on the North pole ($\theta = 0$). Left is a single spin-up qubit, i.e. the computational basis state $|0\rangle$. Right is spin-6. Dashed lines are nodal lines where the Wigner function vanishes.

We also find a surprising result that refutes a conjecture in [89] proposing that all Dicke state Wigner functions with spin j have $2j$ distinct nodal lines of constant latitude. We numerically give a counterexample: the spin coherent state of 12 qubits has only 8 distinct roots as illustrated in Fig. 3.4.

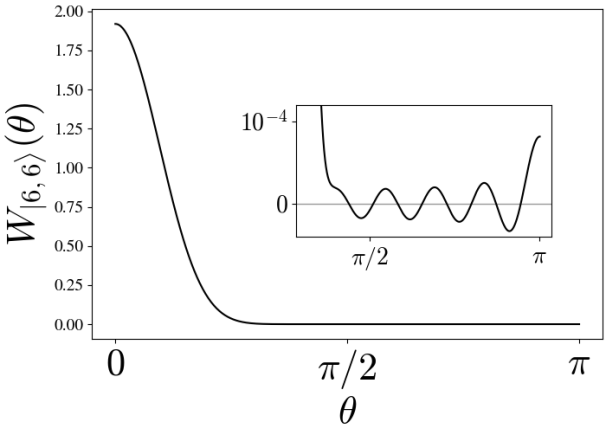

Figure 3.4: Cross section of the spin-6 North pole spin coherent state Wigner function.

3.2 Greenberger–Horne–Zeilinger

The Greenberger-Horne-Zeilinger (GHZ) state was first introduced to generalize Bell's theorem on quantum nonlocality to a multipartite setting [157, 158, 159]. Incidentally, a closely related set of states now called N00N states, Eq. (2.34), were introduced in the same year for their use in understanding decoherence of fragile cat-like states [160]. Both of these have since been intensively studied within quantum information, quantum optics, and quantum metrology [161, 162, 136, 163, 164]. These states, together with their higher multipartite generalizations, are also known as spin cat states in reference to their inherent superposition of two macroscopically distinct states. They are nicely viewed as elements of a spin system where they take the general form $\alpha|j, j_{\boldsymbol{n}}\rangle + \beta|j, -j_{\boldsymbol{n}}\rangle$. The multi-qubit and Jordan-Schwinger realizations, Eqs. (2.26) and (2.33), readily show their mutual equivalence as abstract spin states; see also [135]:

$$\underbrace{\frac{1}{\sqrt{2}}(|0\rangle^{\otimes 2j} + |1\rangle^{\otimes 2j})}_{\text{GHZ}} \longleftrightarrow \underbrace{\frac{1}{\sqrt{2}}(|2j\rangle|0\rangle + |0\rangle|2j\rangle)}_{N00N} \longleftrightarrow \underbrace{\frac{1}{\sqrt{2}}(|j, j\rangle + |j, -j\rangle)}_{\text{spin cat}} \tag{3.4}$$

See Fig. 3.5 for numerical plots of typical GHZ Wigner functions.

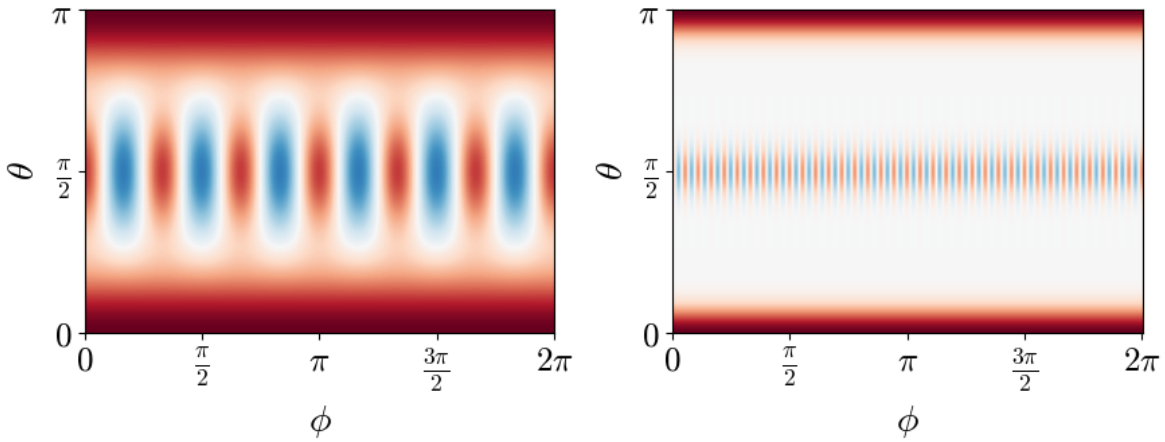

Figure 3.5: Typical GHZ Wigner functions without a relative phase. Left is for $j = 3$ and right is for $j = 18$. Note that the colour scales are different and have been saturated on the max/min values of the Wigner function to help bring out the interference patterns.

Here we consider the following family of cat states, including those with an asymmetric

balancing:

$$|j;\vartheta,\varphi\rangle = \cos\left(\frac{\vartheta}{2}\right)|j,j\rangle + e^{i\varphi}\sin\left(\frac{\vartheta}{2}\right)|j,-j\rangle, \tag{3.5}$$

where $0 \leq \vartheta \leq \pi$ and $0 \leq \varphi \leq 2\pi$[2]. Using the Weyl rule and the kernel, (5.7), the Wigner function of Eq. (3.5) splits into two antipodal spin coherent contributions and two cross-term contributions, $\langle j,\pm j|\Delta(\Omega)|j,\mp j\rangle$, which contain the characteristic interference pattern:

$$\begin{aligned} W_{|j;\vartheta,\varphi\rangle}(\theta,\phi) &= \langle j;\vartheta,\varphi|\Delta(\theta,\phi)|j;\vartheta,\varphi\rangle && (3.6)\\ &= \cos^2\frac{\vartheta}{2}\langle j,j|\Delta(\theta,\phi)|j,j\rangle + \sin^2\frac{\vartheta}{2}\langle j,-j|\Delta(\theta,\phi)|j,-j\rangle && (3.7)\\ &\quad + \sin\frac{\vartheta}{2}\cos\frac{\vartheta}{2}(e^{i\varphi}\langle j,j|\Delta(\theta,\phi)|j,-j\rangle + e^{-i\varphi}\langle j,-j|\Delta(\theta,\phi)|j,j\rangle) && (3.8)\\ &= \cos^2\frac{\vartheta}{2}W_{|j,j\rangle}(\theta,\phi) + \sin^2\frac{\vartheta}{2}W_{|j,-j\rangle}(\theta,\phi) + \sin\varphi\,\underbrace{\Re[e^{i\varphi}\langle j,j|\Delta(\theta,\phi)|j,-j\rangle]}_{\text{interference}}. && (3.9) \end{aligned}$$

The cross-term matrix element in the interference term evaluates to

$$\langle j,j|\Delta(\Omega)|j,-j\rangle = \sqrt{\frac{4\pi}{2j+1}}\sum_{l=0}^{2j}\sum_{k=-l}^{l}Y_{lk}^*(\Omega)\left[\sqrt{\frac{2l+1}{2j+1}}\left\langle\begin{matrix} j & l \\ -j & k\end{matrix}\middle|\begin{matrix} j \\ j\end{matrix}\right\rangle\delta_{k,2j}\right] \tag{3.10}$$

which is non-zero only for simultaneous $l = 2j$ and $k = 2j$, giving

$$\langle j,j|\Delta(\Omega)|j,-j\rangle = \sqrt{\frac{4\pi}{2j+1}}(-1)^{2j}Y_{2j,2j}^* \tag{3.11}$$

where we have used

$$\left\langle\begin{matrix} j & 2j \\ -j & 2j\end{matrix}\middle|\begin{matrix} j \\ j\end{matrix}\right\rangle = (-1)^{2j}\sqrt{\frac{2j+1}{4j+1}}. \tag{3.12}$$

The interference term becomes

$$\sin\vartheta\sqrt{\frac{2j+1}{4j+1}}\Re\left[e^{i\varphi}(-1)^{2j}Y_{2j,2j}^*(\Omega)\right] = \sin\vartheta N_j\sin^{2j}(\theta)\cos(2j\phi-\varphi) \tag{3.13}$$

[2]Bacry introduced and called members of this family "crown states" in 1978 [120], just over a decade before the GHZ and N00N papers.

where

$$N_j = \frac{1}{2^{2j}(2j)!}\sqrt{(4j+1)!/(2j+1)} \tag{3.14}$$

and the following relation has been used:

$$Y_{l,l}(\theta,\phi) = \frac{(-1)^l}{2^l l!}\sqrt{\frac{(2l+1)!}{4\pi}}\sin^l(\theta)e^{il\phi}. \tag{3.15}$$

The general GHZ Wigner function is then

$$W_{|j;\vartheta,\varphi\rangle}(\theta,\phi) = \cos^2\left(\frac{\vartheta}{2}\right)W_{|j,j\rangle}(\theta,\phi)+\sin^2\left(\frac{\vartheta}{2}\right)W_{|j,-j\rangle}(\theta,\phi)+\sin\vartheta\ N_j\sin^{2j}(\theta)\cos(2j\phi-\varphi) \tag{3.16}$$

where

$$N_j = \frac{1}{2^{2j}(2j)!}\sqrt{\frac{(4j+1)!}{2j+1}}. \tag{3.17}$$

While Eq. (3.16) appears new, at least in the quantum information community, an asymptotic form of the GHZ Wigner function, valid only for integer spin, has been given in [165]. The first two terms correspond to the Wigner functions of the spin coherent states, and the interference term is expressed throughout phase space as a band of fringes along the equator, with the number of distinct negative regions equal to $2j = N$, the number of qubits. As spin increases the interference pattern becomes more concentrated along the equator and the spatial extent of the positive polar regions shrinks. This is a consequence of the polar regions locally approaching that of a planar coherent state. This, in addition to the $\sin^{2j}(\theta)$ factor for asymmetric cats, highly suppresses the Wigner function in the regions between the equator and the two poles; see Fig. (3.5) for $j = 3$ and $j = 18$ in the GHZ case of $(\vartheta,\varphi) = (\pi/2, 0)$. The constellations of these states are characterized by $2j$ stars at colatitude ϑ with an equiangular distribution along the azimuth and phase-shifted by φ [120]. It is perhaps interesting that the polar positioning of the constellation is dependent on ϑ while the interference pattern is not.

In the context of optical cats via Jordan-Schwinger, the $(N\phi)$ oscillation frequency in the interference pattern is exactly the metrological power behind the $N00N$ state in precision measurements. Such a path-entangled state of light passing through a Mach-Zehnder interferometer with a phase-shifter U_ϕ will pick up a relative phase of $N\phi$, which may be exploited to achieve the Heisenberg bound in sensitivity measurements [136]. And so the super-resolution property of such states is nicely visualized as highly oscillatory

bands on the spherical Wigner function [164], which furthermore contain the vast majority of the Wigner negativity of the state[3]. See also [166] for recent and related work on "sub-Planckian" structures on phase space using this Wigner function.

It is clear that the interference pattern is the primary contribution to the Wigner negativity of the state and that any contributions from the spin coherent components are either cancelled out or rapidly become negligible as spin increases. An approximation for the negativity can thus be achieved by focusing on the fringes and ignoring the pointwise-convex interaction between the fringes and the antipodal spin coherent contributions. To that end, Eq. (3.13) has polar symmetry about $\theta = \pi/2$ as well as an azimuthal splitting into $2j$ identical regions. We have set $\varphi = 0$ without loss of generality due to the periodic boundary conditions of the fringes. Focusing on where the cosine becomes negative, integrate (3.13) over the region $[0, \frac{\pi}{2}] \cup \frac{1}{2j}\left[\frac{\pi}{2}, \frac{3\pi}{2}\right]$ then multiply the result by $2 \cdot 2j = 4j$:

$$4j \sin\vartheta N_j \frac{2j+1}{4\pi} \int_0^{\pi/2} \sin^{2j}(\theta) \sin\theta d\theta \int_{\pi/4j}^{3\pi/4j} \cos(2j\phi) d\phi. \tag{3.18}$$

The azimuthal integral yields $-1/j$, the negative sign of which is removed to ensure that the negativity is a positive number. The polar component must employ the recursive relation

$$\int_0^{\pi/2} \sin^n(\theta) d\theta = \frac{n-1}{n} \int_0^{\pi/2} \sin^{n-2}(\theta) d\theta \tag{3.19}$$

for integer n, which leads to the known identity

$$\int_0^{\pi/2} \sin^n(\theta) d\theta = \tilde{\sigma}(n) \frac{(n-1)!!}{n!!} \tag{3.20}$$

where $\tilde{\sigma}(n) = \pi/2$ for even n and $\tilde{\sigma}(n) = 1$ for odd n. The approximation then becomes

$$\delta(|j;\vartheta,\varphi\rangle) \lesssim \sin\vartheta N_j \frac{\sigma(j)}{\pi} \frac{(2j)!!}{(2j-1)!!} \tag{3.21}$$

where $\sigma(j) = 1$ for integer spin, $\sigma(j) = \pi/2$ for half-integer spin. The explicit special cases are obtained from the identities $n!! = 2^k k!$ for even integer $n = 2k$ and $n!! = (2k)!/(2^k k!)$

[3]Not to claim that the negativity is necessarily causing the metrological advantage, just that it is interesting to see the correlation between the two.

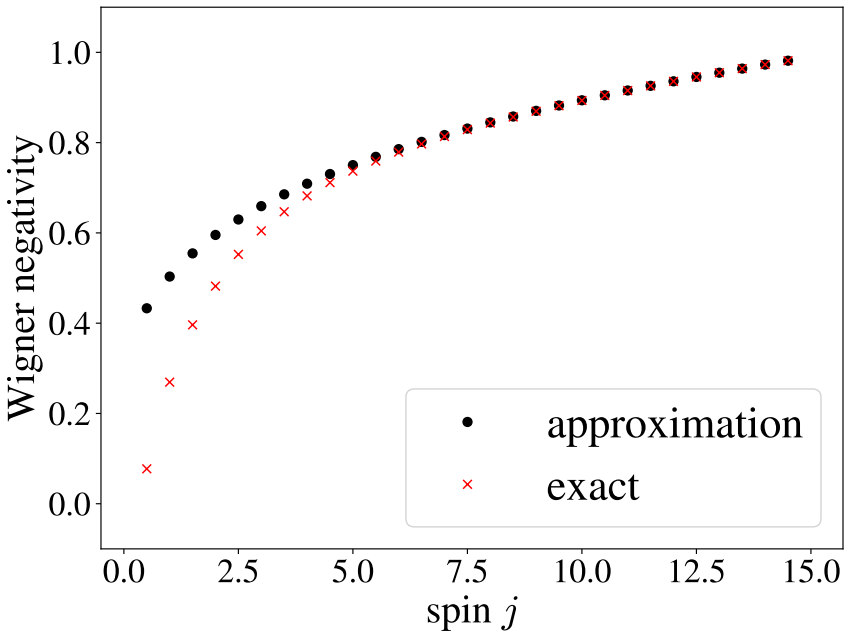

Figure 3.6: Comparison between the approximate and exact negativity for GHZ states as a function of spin.

for odd integer $n = 2k - 1$. The two cases explicitly are:

$$\begin{aligned} \delta^{(\text{int})} &\lesssim \frac{1}{\pi} \sin\vartheta \sqrt{\frac{(4j+1)!}{2j+1}} \left(\frac{j!}{(2j)!}\right)^2 \\ \delta^{(\text{half-int})} &\lesssim \sin\vartheta \sqrt{\frac{(4j+1)!}{2j+1}} \frac{1}{2^{4j}} \frac{1}{(j-\frac{1}{2})!^2}. \end{aligned} \tag{3.22}$$

See Fig. 3.6 for a comparison between the numerically obtained exact negativity and Eq. (3.21) as a function of j. This approximation provides a reasonable estimate of the Wigner negativity for $j \gtrsim 5$.

3.3 Dicke

Having analyzed spin coherent states and a class of superpositions thereof, we now turn our attention to the individual Dicke states, $|j, m\rangle$. Such states are equivalent to the gener-

alized W states of quantum information, first introduced in the classification of multipartite entanglement with respect to stochastic local operations and classical communication (SLOCC) [133]. As mentioned in Sec. 2.1.3, these states have a multi-qubit representation: The W state of weight $k \in \{0, ..., N\}$ is the symmetrized superposition of $N = 2j$ qubits where $k = j - m$ out of N of them are in the computational state $|1\rangle$:

$$|D_N^{(k)}\rangle = \binom{N}{k}^{-\frac{1}{2}} \sum_{\tau_i \in S_n} |\tau_i(\underbrace{1 \cdots 1}_{k} \underbrace{0 \cdots 0}_{N-k})\rangle \leftrightarrow |j, j-k\rangle. \tag{3.23}$$

where S_n is the symmetric group of order n. The case $k = 1$ is the standard W state, while the two extremal cases $|j, \pm j\rangle$ correspond to antipodal spin coherent states. A collective spin-flip of a Dicke state, $\sigma_x^{\otimes N}|D_N^{(k)}\rangle$, is its conjugate state

$$\overline{|D_N^{(k)}\rangle} := |D_N^{(2j-k)}\rangle \leftrightarrow |j, -j+k\rangle. \tag{3.24}$$

As m approaches either $\pm j$, the equivalent W state has an increasingly asymmetric ratio of ground to excited qubits – i.e. mostly 0s or mostly 1s, which here corresponds to the northern and southern hemispheres respectively.

The Dicke state Wigner function, Eq. (2.61), is

$$W_{|j,m\rangle}(\theta, \phi) = \sum_{l=0}^{2j} \frac{2l+1}{2j+1} \left\langle \begin{matrix} j & l \\ m & 0 \end{matrix} \middle| \begin{matrix} j \\ m \end{matrix} \right\rangle P_l(\cos\theta). \tag{3.25}$$

Typical plots of these azimuthally-invariant functions are in Fig. 3.7. They are characterized by a principal band of positive density localized along a circle of constant latitude associated to m, with additional alternating bands along the sphere. If the principal band is distinctly in one hemisphere, the fringes in the opposing hemisphere are reduced in amplitude; see Figs. 3.4 and 3.7. As mentioned earlier, the number of roots for all m values is in general not equal to $2j$.

The Wigner negativity of Dicke states reveals a surprisingly rich structure. This is best seen by focusing on the entire Dicke basis and how its negativities change with increasing j. See Fig. 3.8 for a few numerical examples of such sets of negativities. Note that conjugate Dicke states within the same basis must have equal negativity; this is because they are related by a global π rotation about any axis in the equatorial plane. The least negative states of a Dicke basis are always found to be the two spin coherent states as conjectured. For fixed spin the negativity generally tends to increase as m moves away from the poles

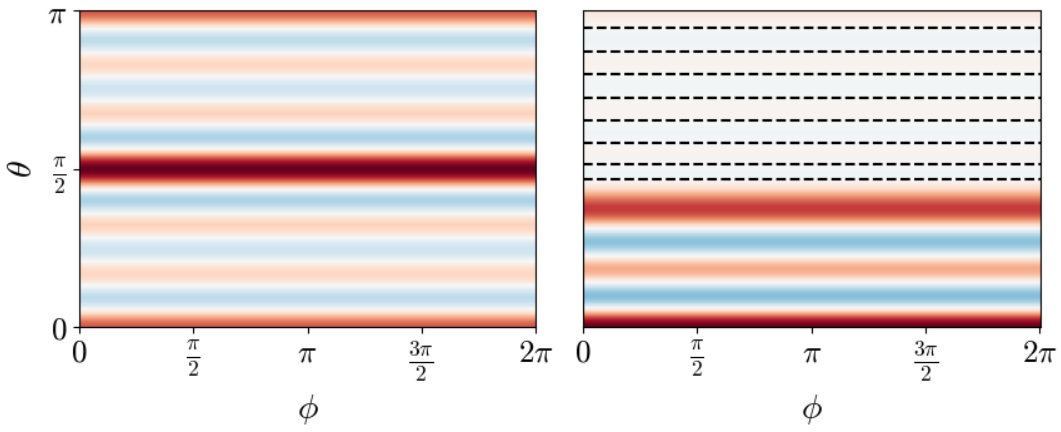

Figure 3.7: Typical Dicke state Wigner functions. Left is the balanced state $|6,0\rangle$, Right is the slightly unbalanced state $|6,2\rangle$. Dashed lines mark roots that are difficult to see. The unbalanced state displays reduced amplitude in the southern hemisphere region, typical of all such Dicke states. The colour scales are different and have been saturated on the max/min values of each the Wigner function to help bring out their features.

and towards the equator, i.e. as $m \to 0$. For low spins, $j \lesssim 30$, this pattern of increasing Wigner negativity with decreasing $|m|$ culminates with the most negative Dicke state being the balanced/equatorial one: $|j,0\rangle$ for integer spin and $|j,\pm 1/2\rangle$ for half-integer spin. In the qubit picture this corresponds to a pattern of increasing non-classicality as the ratio between 0s and 1s approaches one. Surprisingly, this pattern changes when $j \gtrsim 30$, where now the maximally Wigner-negative Dicke state bifurcates away from the equator into a spin-dependent conjugate pair: $|j,\pm m'_j\rangle$ with $m'_j \notin \{0, \frac{1}{2}, -\frac{1}{2}\}$. See Fig. 3.8. For example, the maximally Wigner-negative Dicke state for $j = 80$ happens to be $|80,\pm 16\rangle$ rather than $|80,0\rangle$. The projection eigenvalue m'_j corresponding to the maximally negative state does not settle to a fixed value for the spins considered (up to $j = 80$, or 160 qubits).

Another way to explore this result is to track their behaviour throughout the spin-to-optical contraction, where they limit to the oscillator number states [87, 92, 97]. To that end we numerically investigated Eq. (2.57),

$$\lim_{j\to\infty} |j, j-n\rangle = |n\rangle, \tag{3.26}$$

by computing the Wigner negativity of state sequences $\{|j, j-n\rangle\}_j$ for a handful of fixed n. The basic idea is to fix a number n, then begin with the totally excited multi-qubit

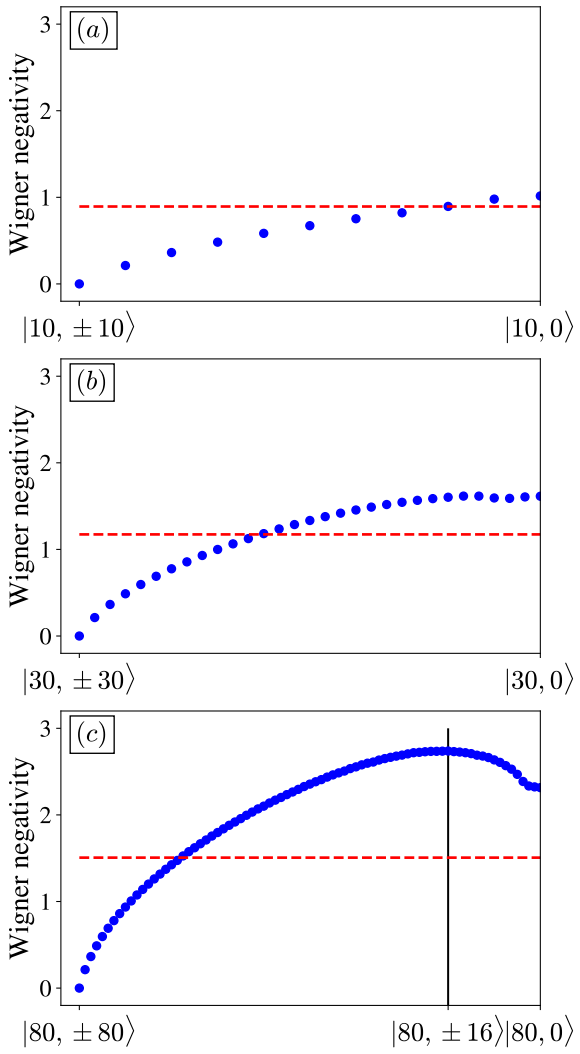

Figure 3.8: The blue dots are Wigner negativities of the Dicke basis $\{|j, \pm m\rangle\}$ corresponding to (a) $j = 10$, (b) $j = 30$, and (c) $j = 80$. The solid vertical line in (c) denotes the maximally Wigner-negative Dicke state. The red dashed line corresponds to the GHZ states of equal dimension.

state $|1\rangle^{\otimes n}$, which corresponds to the South pole spin coherent state in the $\mathbb{C}^{n+1}$ Hilbert space. The sequence $\{|j, j-n\rangle\}_j$ amounts to adding more and more ground qubits $|0\rangle$ while keeping the number of 1s fixed, with each such addition raising the Hilbert space dimension by 1. This effectively sources more Dicke states from the South pole and so

"pushes" our tracked state upwards and into the Northern hemisphere. From a column-vector/coordinate perspective, this amounts to simply padding the bottom of a state array with an ever-increasing amount of zeroes. For example, the following is the beginning of the $n = 2$ sequence:

$$|1,-1\rangle = \begin{bmatrix}0\\0\\1\end{bmatrix} \quad \mapsto \quad |\frac{3}{2},-\frac{1}{2}\rangle = \begin{bmatrix}0\\0\\1\\0\end{bmatrix} \quad \mapsto \quad |2,0\rangle = \begin{bmatrix}0\\0\\1\\0\\0\end{bmatrix} \quad \mapsto \quad |\frac{5}{2},\frac{1}{2}\rangle = \begin{bmatrix}0\\0\\1\\0\\0\\0\end{bmatrix}.$$

The Wigner negativities are plotted in Fig. 3.9. To help read this figure, here are three features common to each sequence. The first is that they all begin at some point along the bottom $\{|j,j\rangle\}_j$ curve (i.e. the $n = 0$ curve). As just mentioned, this is because the starting state for any sequence is always the South pole spin coherent state $|j,-j\rangle$, which has the same negativity as $|j,j\rangle$. The second is that when $j = n + \frac{1}{2}, n$, or $n - \frac{1}{2}$, each sequence is respectively at $|j,-\frac{1}{2}\rangle, |j,0\rangle$ or $|j,+\frac{1}{2}\rangle$. This means that each curve will meet the black equatorial curve $\{|j,m=0,\pm\frac{1}{2}\rangle\}_j$ three times in a row (see the above example). The third is that each sequence must eventually approach the negativity of its limiting number state $|n\rangle$ (see the visible flatline values).

Despite these common properties, there is clearly nontrivial behaviour happening as n changes. Low n sequences ($n \lesssim 8$) contain states that are more Wigner-negative than their number state limit, while for $n \gtrsim 8$ this is no longer true, with some sequences strictly increasing. There is also a different behaviour for $n \gtrsim 30$, where such large-n sequences cross over the equatorial curve before they flatline to their appropriate Fock state. This matches with the aforementioned bifurcation of the most Wigner-negative Dicke state around $j \approx 30$. Consider a vertical cross-section in Fig. 3.9; this corresponds to Dicke basis of fixed j. For vertical cross-sections corresponding to $j \lesssim 30$, all spin-j Dicke states lie below the spin-j equatorial state. On the other hand, for vertical cross-sections corresponding to $j \gtrsim 30$, there are states above the equatorial state, with this effect increasingly exaggerated as j increases.

Overall, these results on the spin-dependent properties of maximally Wigner-negative Dicke states reflect an intriguing and unexpected structure to the non-classicality of Dicke states and spin systems in general. The geometric significance suggests a non-trivial effect

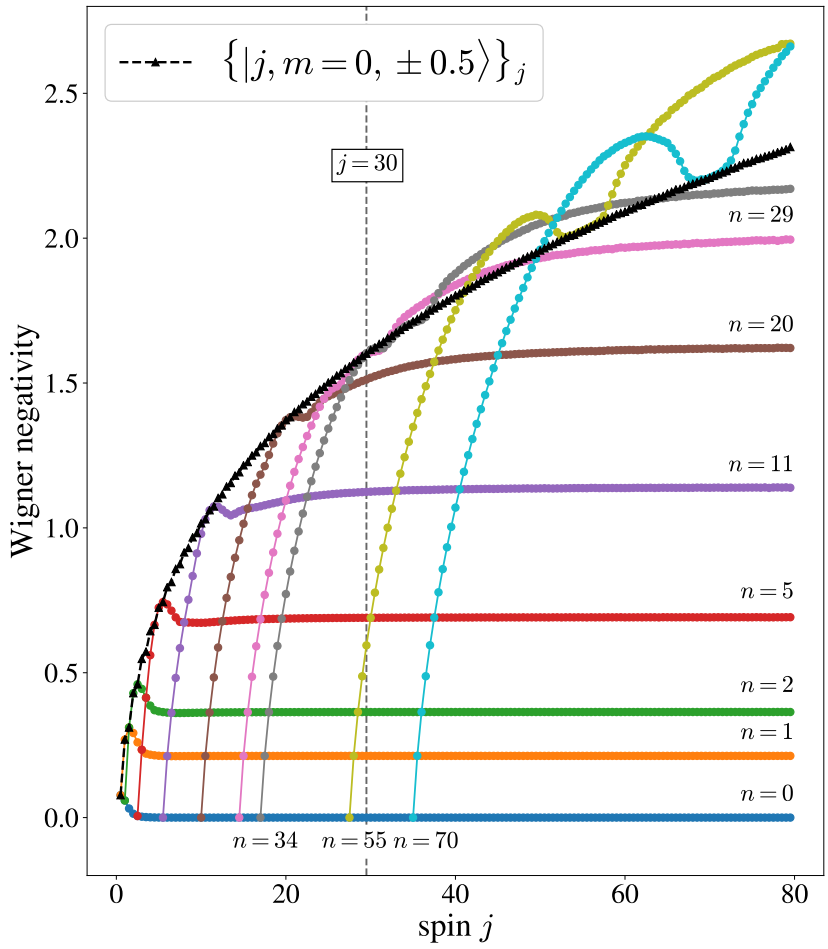

Figure 3.9: Wigner negativity of sequences of states $|j, j-n\rangle$ as j increases for various fixed values of n. The asymptotic flatlines of a given sequence match the number state negativity $|n\rangle$ as expected. The dashed curve with triangular markers corresponds to the equatorial states $|j, 0\rangle$ and $|j, \pm 0.5\rangle$. Around $j \gtrsim 30$ (vertical dashed line) there is emergent behaviour, in which sequences cross over the black equatorial curve.

that the size of phase space (or perhaps other properties, such as curvature) has on state non-classicality. Indeed, the negativity behavior investigated here is a result of the interplay between the geometry of the phase space and the structure of the spherical Wigner function, which both change with spin. This is different from the planar case except in the large spin limit which approaches the planar geometry as shown above.

3.4 Relationship to entanglement

It is interesting to compare the Wigner negativity of a spin state with the state's entanglement in the multi-qubit picture. Here we briefly touch on this topic, and dig deeper in Chapters 4 and 5. It can be shown that within a Dicke basis of arbitrary spin j, the balanced/equatorial state is always the most entangled as measured by the entropy across *arbitrary* bi-partitioning in the multi-qubit picture [167]. The geometric measure of entanglement similarly witnesses the balanced/equatorial Dicke state as having the most entanglement within the Dicke basis in all finite dimensions [105]. These are of course in contrast to Wigner negativity, where the most Wigner-negative Dicke state bifurcates from $|j, 0\rangle$ to $|j, \pm m_j'\rangle$ around $j \gtrsim 30$. On the other hand, the entanglement entropy of sequences $\{|j, j-n\rangle\}_j$ across specifically half-bipartitions (i.e. an even splitting of the $2j$ qubits for integer spin) seem to approach a constant value for any fixed n [168][4]. See Fig. 2a in [168] for a nice comparison to our Fig. 3.9. In a similar fashion as established here, the Wigner negativity of $\{|j, j-n\rangle\}_j$ also approaches a constant value; i.e. that of the number state $|n\rangle$ for any fixed n[5].

Thus the behavior of spherical Wigner negativity somewhat qualitatively agrees with entanglement entropy when considering half-bipartitions of sequences $\{|j, j-n\rangle\}_j$, but disagrees on which Dicke basis element is the most nonclassical. Furthermore, the GHZ state is relatively less Wigner negative than most Dicke states with the same spin value as seen in Fig. 3.8. This suggests that Wigner negativity and entanglement capture different aspects of the non-classicality of states.

[4]It should be mentioned however that the entanglement entropy of the sequence $\{|j, j-n\rangle\}_j$ across a $1 : (2j-1)$ qubit bipartition vanishes in the limit of infinite j for any fixed n [167], and thus does not approach a finite constant nonzero value like the half-bipartition entropy.

[5]It is interesting to observe that, in light of the spin-to-optical contraction, the work of [168] can in some sense be understood as assigning a non-zero entanglement value to certain single-mode pure states.

Chapter 4

Maximally Wigner-negative pure states

Chapters 3 and 4 are approximately based (respectively) on the works

Davis, J., Kumari, M., Mann, R. B., & Ghose, S. (2021). Wigner negativity in spin-j systems. *Physical Review Research*, 3(3), 033134. [1]

Davis, J., Hennigar, R. A., Mann, R. B., & Ghose, S. (2023). Stellar representation of extremal Wigner-negative spin states. *Journal of Physics A: Mathematical and Theoretical*, 56(26), 265302. [2]

In this chapter we extend the previous results in two ways. The first is to go beyond the states commonly used in information processing and focus on pure spin states that maximize Wigner negativity. As mentioned in the introduction, this is motivated by the behaviour of Wigner negativity in a quantum computational setting, where it acts as a magic monotone. The second is to dig deeper into the relationship between Wigner negativity and entanglement. In particular, we use the stellar picture to compare states that maximize Wigner negativity with those that maximize various measures of entanglement in the multi-qubit picture of spin (see Sec. 2.1.3). These three entanglement-based notions are anticoherence, geometric entanglement, and Glauber-Sudarshan negativity, which we briefly review. This comparison lends insight to the general structure of spin non-classicality and, in line with the results from the previous chapter, reveals a surprisingly non-trivial

structure to maximally Wigner-negative spin states.

4.1 Alternative notions of nonclassicality in phase space

4.1.1 Anticoherence

Perhaps the first and most natural approach one may take to quantify the entanglement within a composite state is to compute the entanglement entropy (i.e. the von Neumann entropy, a.k.a. the quantum Shannon entropy) of a state relative to a bi-partition somewhere across the tensor product structure of the underlying Hilbert space. For bipartite systems this perspective is relatively straightforward as there is only one way to chop up the Hilbert space, but for a many-body system it becomes unclear how to use this notion of entropy to build an unambiguous hierarchy of entanglement.

While the general problem of entanglement classification remains open, much progress has been made in the past two decades[1]. A natural idea that emerged during this effort was to consider states that have maximally mixed reductions (i.e. maximally mixed reduced states with respect to the partial trace) [170, 171]. This idea now goes under many names and variants, including m-uniformity [172], Verstraete normal forms [173], and Absolutely Maximally Entangled (AME) states [174].

Anticoherence, from an entropic perspective, is essentially this idea but restricted to the symmetric subspace of a collection of n qubits. This entropic perspective however came later: the phrase anticoherence, which will be explained shortly, comes from the spin-$\frac{n}{2}$ structure that the symmetric subspace affords. In particular, an *anticoherent spin state of order* m was originally defined in 2006 [175] as a spin state having zero average spin together with isotropic moments:

$$|\psi\rangle \ m\text{-anticoherent} \quad \Longleftrightarrow \quad \langle \boldsymbol{J} \rangle = 0 \quad \& \quad \langle (\boldsymbol{n} \cdot \boldsymbol{J})^k \rangle \neq f(\boldsymbol{n}) \quad \forall\, k = 1, ..., m. \tag{4.1}$$

As spin coherent states have the strongest spin expectation allowable (i.e. $|\langle \boldsymbol{J} \rangle| = j$), the above definition was designed to capture those states that were the exact opposite, hence

[1] One modern perspective on the task of entanglement classification is to induce a partial order on the set of quantum states via the specification of a resource theory (i.e. an operational task that requires the consumption of a particular resource). For example, an EPR state is consumed to perform quantum teleportation. See [169] and references therein for the general theory.

*anti*coherent state. The relatively recent works of [107, 108] (circa 2015) established the deep connection between moment isotropy and the aforementioned entanglement entropy:

$$\langle \boldsymbol{J} \rangle = 0 \quad \& \quad \langle (\boldsymbol{n} \cdot \boldsymbol{J})^k \rangle \neq f(\boldsymbol{n}) \quad \Longleftrightarrow \quad \mathrm{tr}_{\neg k}(|\Psi\rangle\langle\Psi|) = \frac{I}{k+1} \tag{4.2}$$

where k runs from 1 to m on both sides and $\mathrm{tr}_{\neg k}$ denotes tracing out all but k qubits. Note that due to permutation invariance all reductions of the same size are equivalent, hence one can refer to the *the* k-qubit reduction. As moments are directly related to the spherical harmonic expansion of a quasiprobability representation (see below), Eq. (4.2) thus establishes the *equivalence between the "wiggliness" of the spherical Wigner function and the entanglement within the underlying many-body state.* In particular, all anticoherent states of any degree have a Wigner function with vanishing "centre of mass".

One may define quantitative measures of anticoherence, applicable to any pure spin state [176]. For example, consider the multipole expansion of a density matrix ρ with fixed spin j,

$$\rho = \sum_{K=0}^{2j} \sum_{q=-K}^{K} \rho_{Kq} T^{(j)}_{Kq}, \qquad \rho_{Kq} = \mathrm{tr}[\rho T^{(j)\dagger}_{Kq}], \tag{4.3}$$

where $T^{(j)}_{Kq}$ are the spherical tensor operators (2.12). The state multipoles ρ_{Kq} contain information on the amplitude of a density matrix to have a specific multipole pattern, and the quantity $\sum_q |\rho_{Kq}|^2$ is the overlap with the entire K multipole. Higher K reflects finer angular structure in the Wigner function (recall Eq. (2.59)), so it is natural to analyze the cumulative overlap

$$\mathcal{A}^{(j)}_m = \sum_{K=1}^{m} \sum_{q=-K}^{k} |\rho_{Kq}|^2. \tag{4.4}$$

Spin-j coherent states by design maximize the above quantity for all orders m, and so states that minimize Eq. (4.4) are interpreted as spin coherent "opposites". States for which $\mathcal{A}^{(j)}_m$ vanish are m-anticoherent, or in the parlance of quantum optics, *mth-order unpolarized* due to their polarization information having been pushed to higher multipoles. States with the highest degree of anticoherence allowed (given a fixed spin/dimension) are also sometimes referred to as the Kings of Quantum. Various King states of spin j and order m have been calculated [177, 178], experimentally realized [179], and are of critical metrological use in, for example, reference frame alignment [180] and quantum rotosensing [181, 182, 183].

In an optical setting (specifically polarimetry), anticoherence is about quantifying the quantum mechanical departure from the classical fact that fully polarized monochromatic light always has a Stokes vector (S_x, S_y, S_z) on the Poincaré sphere. Increasing the intensity of the beam continuously enlarges the Poincare radius but not the angular information of the Stokes vector. In the quantized picture the Poincaré radii become discrete due to the indivisibility of the photon, and higher layers permit the vanishing of polarization expectation $\langle \boldsymbol{J} \rangle$, even for pure states [184]. A semiclassical intuition for this is that each photon in a pure Fock state of monochromatic light may have its own polarization (represented by a Majorana star), allowing for the possibility of collective cancellation.

As the above intuition suggests, anticoherence is naturally compatible with the stellar picture. For example, anticoherence puts strong restrictions on the point-group symmetry of a state's constellation [185, 181]; see also [110] for analogous results in the mixed Majorana setting. All together, it is clear that anticoherence is an extremely rich notion of non-classicality with several fruitful interpretations[2].

As a loosely related but interesting final remark, the notion of anticoherence may make one wonder if there is any connection to the so-called barycentric measure of entanglement, introduced by Ganczarek, Kuś, and Życzkowski [186][3]. This measure of entanglement is constructed via the following: interpret the stars as unit point masses then compute their centre of mass (i.e. their barycentre). The measure is then defined as $(1 - d_B^2(\psi))$ where $d_B(\psi)$ is the Euclidean distance between the barycentre and the centre of the sphere. This measure vanishes on product states and is preserved under symmetric local operations (i.e. rotations). Interestingly and perhaps unexpectedly, there exist anticoherent states that have non-vanishing barycentre [107, 185]. As anticoherence is related to spin expectation, which amounts to weighted integrals over the Wigner function via traciality, the lesson here is that one must not confuse the centre of mass of a Wigner function with the centre of mass of a constellation.

4.1.2 Geometric entanglement

Broadly speaking, an alternative way of quantifying entanglement is via the distance to the set of product states (with respect to some appropriate Hilbert space metric). A concrete

[2] Anticoherence is in my view the (second) best notion of non-classicality on the sphere.

[3] This concept however may be almost entirely traced back to Bacry's *degree of coherence* from 1978 [120].

realization of this idea is the *geometric degree of entanglement*, E_G, which is commonly attributed to Shimony from 1995 [187]. Here we express the definition in the context of SU(2) symmetry where the set of product states are symmetric [188]:

$$E_G(|\psi\rangle) = \frac{1}{2} \min_{|\phi\rangle \in \mathcal{C}_{\text{scs}}} |||\psi\rangle - |\phi\rangle||^2_{\text{HS}}, \tag{4.5}$$

where $||A||_{\text{HS}} = \sqrt{\text{tr}[A^\dagger A]}$ is the Hilbert-Schmidt norm and

$$\begin{aligned} \mathcal{C}_{\text{scs}} &= \{|\chi\rangle^{\otimes 2j},\ |\chi\rangle = \cos\frac{\theta_\chi}{2}|0\rangle + e^{i\phi_\chi}\sin\frac{\theta_\chi}{2}|1\rangle\} \\ &= \{|\theta,\phi\rangle,\ (\theta,\phi) \in S^2\} \end{aligned} \tag{4.6}$$

is the set of spin product states, which is equivalent to the set of spin coherent states. Combining Eq. (4.5) with the fact that the ($s = -1$) Husimi kernel may also be expressed as is the spin coherent POVM over the sphere (2.22),

$$Q_\rho(\theta,\phi) := f_\rho^{(-1)}(\theta,\phi) = \text{tr}[\,\rho\,|\theta,\phi\rangle\langle\theta,\phi|\,] = \langle\theta,\phi|\rho|\theta,\phi\rangle, \tag{4.7}$$

together shows that

$$E_G(|\psi\rangle) = \min_{(\theta,\phi)\in S^2}(1 - |\langle\psi|\theta,\phi\rangle|^2) = 1 - \max_{(\theta,\phi)\in S^2} Q_\psi(\theta,\phi). \tag{4.8}$$

Hence the geometric measure of a state may be thought of as the relative difference between the maximal pointwise height of the state's Husimi function and its theoretical upper bound of unity. Consequently, maximally geometric-entangled states may be thought of as those with the "flattest" possible Husimi function despite being pure. The requirement of purity forces the function to fluctuate in some manner as the truly flat Husimi function must be the maximally mixed state. This latter point is a consequence of the standardization axiom, Eq. (2.43b), which ensures that the identity operator on Hilbert space is mapped to the unit function on phase space. A somewhat analogous notion exists on the bosonic phase space, where the set of classical pure states are the coherent states [189][4]. An interesting distinction here is that the intuition behind the classicality of the single-mode bosonic coherent states does not come from entanglement theory as there is only one quantum

[4]One can furthermore imagine a similar definition for any phase space picture based on a Perelmov construction (i.e. using G-coherent states). When $G = \text{SU}(d)$ the flatness of the Husimi function may furthermore be interpreted as quantifying the entanglement of a pure state in the symmetric subspace of n qudits, $\text{Sym}[(\mathbb{C}^d)^{\otimes n}]$, though the phase space manifold will likely be too complicated to visualize.

object under consideration. While this is perfectly fine, it may also be worth saying that in light of the SU(2)-optical contraction, (2.57), one can still in some sense actually think of coherent states as pure product states, but of an infinite number of qubits.

We end by noting that while the notion of geometric entanglement has become a mainstay in the quantum information era, a strong conceptual ancestor may be found at least 20 years prior in the classic reference of Arecchi *et al.* [87]. In it they define pure product states of N 2-level atoms as $|a_1, b_1, ..., a_N, b_N\rangle = \bigotimes_{n=1}^{N}(a_n|e_1\rangle + b_n|e_2\rangle)$ where $\{e_1, e_2\}$ is a basis, then remark:

> "For any normalized state $|\psi\rangle$ of the N-atom assembly, a degree of correlation can be defined in the following manner: One forms the overlap integral $|\langle\psi|a_1, b_1, ..., a_N, b_N\rangle|^2$ and maximizes the result with respect to the set (a_i, b_i), $i = 1$ to N. The complement to one of this maximized overlap integral is defined as the degree of atomic correlation of the state $|\psi\rangle$." [87].

While not in the language of information theory nor explicitly discussing entanglement, the underlying idea of a correlation measure is obviously present and their definition is precisely the same as Eq. (4.8) but expressed in the more general case of distinguishable qubits. This situation is quite similar to the above footnote on barycentric entanglement.

4.1.3 Glauber-Sudarshan negativity

P-representability is quite similar to the geometric measure of entanglement, but now the set of states deemed classical is enlarged to the convex hull of spin coherent states [102, 190]. With the Glauber-Sudarshan P function seen as the collection of expansion coefficients over the spin coherent projector basis, the classical set is comprised of those states that admit a positive P-function:

$$\mathcal{P}(\rho) = \min_{\rho_c \in \mathcal{C}} ||\rho - \rho_c||_{\text{HS}} \tag{4.9}$$

where, using the appropriate Stratonovich kernel, Eq. (5.7),

$$\mathcal{C} = \{\rho \,|\, P_\rho(\theta, \phi) = \text{tr}[\rho \Delta_j^{(1)}(\theta, \phi)] \geq 0 \quad \forall\, (\theta, \phi) \in S^2\} \tag{4.10}$$

for a given spin j. An alternative way to compare the geometric measure and P-representability is to keep the convex hull fixed for both; the geometric measure is then effectively seen as

minimizing the Bures distance rather than the Hilbert-Schmidt distance [191]. In any case, the motivation behind this notion of nonclassicality comes from interpreting the values of a positive P-function as a collection of epistemic/statistical weights in an incoherent mixture of spin coherent states. Thus *a symmetric multi-qubit state is separable if and only if it's Glauber-Sudarshan P function is positive.* States that are maximally far away from the set of those with a positive P function are known as the Queens of Quantum [102, 190]. This entanglement-based notion of non-classicality is well-suited for mixed states and will be discussed further in Chapter 5.

To summarize, we have recalled three alternative and insightful notions of non-classicality that each have a natural interpretation as some geometric or functional property of some quasiprobability distribution on phase space. By comparing states that maximize Wigner negativity to states that maximize these other notions, we will learn about the structure of Wigner negativity on the sphere.

4.2 Maximal states

4.2.1 Spin 1/2

For the single qubit system ($j = 1/2$) the stellar representation reduces to the Bloch sphere picture. The Wigner functions of the spin-up and spin-down states along the z-axis (i.e. the standard computational basis states $|0\rangle$ and $|1\rangle$) are given by

$$W_{\uparrow}(\theta,\phi) = \frac{1}{2} + \frac{\sqrt{3}}{2}\cos\theta \qquad W_{\downarrow}(\theta,\phi) = \frac{1}{2} - \frac{\sqrt{3}}{2}\cos\theta \tag{4.11}$$

Since all pure qubit states are trivially spin coherent states connected through rigid rotation, they all have the same non-zero amount of Wigner negativity. This can be quickly calculated by hand to be $\frac{1}{2} - \frac{1}{\sqrt{3}} \approx 0.077$ [1, 192].

Thoughts on the single qubit

Here I briefly indulge in some short, semi-formal comments on interpreting the other notions of non-classicality discussed here in the special case of spin-1/2: anticoherence, geometric entanglement, and Glauber-Sudarshan positivity. Is the single pure qubit a *bona*

fide quantum object? The intuitive answer is a simple "yes" yet many well-motivated definitions of non-classicality offer a surprisingly diverse array of different answers (including a quick and easy "no"). This discussion of course all boils down to exactly what is meant by "qubit" and "quantum". For sake of consistency let us say that the qubit is the self-representation of SU(2). More explicitly, it is the Hilbert space $\mathbb{C}^2$ of pure states together with the three Pauli matrices (2.2) viewed as observables.

The simplest and bluntest analysis out of the three considered here is Glauber-Sudarshan positivity. By construction the P function is positive for every qubit state. Hence from this perspective the qubit is explicitly not quantum. The next simplest is anticoherence, and the reasoning is related. While (much) more sophisticated in higher dimensions, the case of $j = 1/2$ is special because all pure qubit states are spin-coherent; i.e. the Hilbert space is too small to contain anything "anti" coherent. As a result, no pure state in $\mathbb{C}^2$ is anticoherent and so it is not unreasonable to conclude that the qubit is also non-quantum from this perspective. The geometric measure is a bit more of a stretch as its original meaning was only intended for multi-partite systems. That being said one can argue that the alternative definition via Husimi-function-height (4.8) is a natural extension to the single qubit. If this is accepted then again the qubit is classical because all pure states have unit height. If not accepted, one could alternatively argue more generally that if such entanglement-based non-classicality is fundamentally concerned with how two objects are connected, then a single indivisible object in isolation is not necessarily inherently "quantum".

So in one way or another all three of the other notions of non-classicality view the qubit as a non-quantum object[5]. While this by no means whatsoever constitutes a reason to discontinue their use — in particular due to their proven track record of success, both in theory and experiment — I believe that the spherical Wigner function displaying an unambiguous "quantumness" of the single pure qubit should be seen as meaningful, and not dismissed as a quirk or fault in the generalized Moyal-Stratonovich research programme as it applies to quantum spin. See Chapter 6 (conclusions) for a broader outlook.

4.2.2 Spin 1

Spin systems with $j = 1$, equivalent to the symmetric subspace of two qubits, are characterized by two-point constellations. Here we go into detail on how to characterize all

[5]Even with a more skeptical stance on the above arguments, surely at the very least they are all neutral, with none giving a resounding "yes".

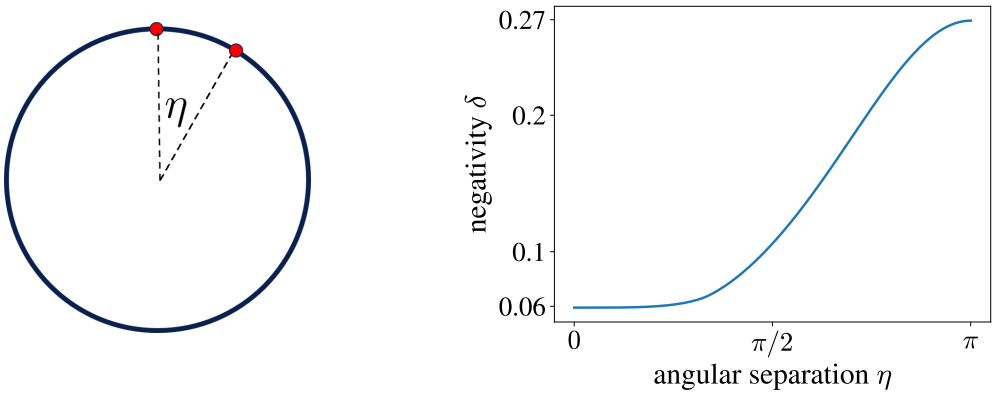

Figure 4.1: Left: parameterization of all spin-1 states up to rotational equivalence. Right: Wigner negativity as a function of polar separation. The minimum is attained by the degenerate constellations (spin coherent states) while the maximum is obtained by the antipodal constellations (symmetric Bell states).

such pure states; higher dimensions follow similarly. Negativity is invariant under global rotation and so without loss of generality we fix one of the stars on the North pole. The second is placed on the ZX plane with a polar separation η relative to the former – see Fig. 4.1[6]. Using the symmetrizer (2.27), this amounts to projecting the state $|0\rangle R_y(\eta)|0\rangle$ to the symmetric subspace followed by renormalization. The family of η-parameterized states in the Dicke basis is calculated to be

$$|\psi_\eta\rangle = \frac{1}{\sqrt{1+\cos^2\eta/2}}\left(\sqrt{2}\cos\frac{\eta}{2}|1,1\rangle + \sin\frac{\eta}{2}|1,0\rangle\right). \tag{4.12}$$

The corresponding family of Wigner functions is

$$W_{|\psi_\eta\rangle}(\theta,\phi) = \frac{1}{1+\cos^2\eta/2}\left[2\cos^2\frac{\eta}{2}\,W_{|1,1\rangle}(\theta,\phi) + \sin^2\frac{\eta}{2}\,W_{|1,0\rangle}(\theta,\phi) + \frac{1}{\sqrt{2}}\sin\eta\,W_{\text{int}}(\theta,\phi)\right] \tag{4.13}$$

[6]In line with sometimes-used parlance in quantum information, one could perhaps call this object a *spin redit*. (a "ree-dit", short for "real qudit", is a qudit with only real coefficients in some privileged basis).

where the two Dicke state terms, Eq. (2.61), reduce to

$$\begin{aligned} W_{|1,1\rangle}(\theta,\phi) &= \frac{1}{3}(1-\sqrt{\frac{5}{8}}) + \sqrt{\frac{1}{2}}\cos\theta + \frac{1}{2}\sqrt{\frac{5}{2}}\cos^2\theta, \\ W_{|1,0\rangle}(\theta,\phi) &= \frac{1}{3}(1+\sqrt{\frac{5}{2}}) - \sqrt{\frac{5}{2}}\cos^2\theta \end{aligned} \tag{4.14}$$

and the interference term is

$$W_{\text{int}}(\theta,\phi) = \sin\theta(1+\sqrt{5}\cos\theta)\cos\phi. \tag{4.15}$$

The Wigner negativity is then numerically computed for each polar separation η. Every spin-1 pure state has a negativity value along the curve in Fig. 4.1. This curve does not touch the horizontal axis and so, similar to the single qubit case, there is no pure state with vanishing negativity. The states with minimal negativity are those with degenerate stars and correspond to the two-qubit spin coherent states. We find, perhaps unsurprisingly, that the antipodal constellations maximize Wigner negativity. This class of states is generated by one of the symmetric Bell states: $\frac{1}{\sqrt{2}}(|01\rangle+|10\rangle) = |1,0\rangle$ or $\frac{1}{\sqrt{2}}(|00\rangle+|11\rangle) = \frac{1}{\sqrt{2}}(|1,1\rangle+|1,-1\rangle)$, together with their global rotations $\frac{1}{\sqrt{2}}(|+-\rangle+|-+\rangle)$ or $\frac{1}{\sqrt{2}}(|++\rangle+|--\rangle)$, etc. The exact upper and lower bounds of the negativity are computed to be

$$\begin{aligned} \max_{\eta}\delta(W_\eta) &= \frac{1}{3}\sqrt{\frac{2}{15}(55+17\sqrt{10})} - 1 \approx 0.2693 \\ \min_{\eta}\delta(W_\eta) &= \frac{4}{5\sqrt{92+29\sqrt{10}}} \approx 0.0590 \end{aligned} \tag{4.16}$$

The alternative measures of nonclassicality are also minimized by degenerate configurations and maximized by antipodal configurations.

4.2.3 Spin 3/2

The number of free parameters needed to describe a pure $j = \frac{3}{2}$ state up to global rotations is three: two polar angles and one relative azimuthal angle. Without loss of generality we again place one star on the North pole and another on the ZX plane with polar angle $0 \leq \vartheta_1 \leq \pi$. The final star has no constraints, having polar angle $0 \leq \vartheta_2 \leq \pi$ and azimuthal angle $0 \leq \varphi \leq \pi$ relative to the second star. To avoid double counting the

equivalent constellations $(\vartheta_1, \vartheta_2, \varphi)$ and $(\vartheta_2, \vartheta_1, \varphi)$ we also impose $\vartheta_2 \geq \vartheta_1$. See Fig. 4.2. The family of states associated with these constellations is the projection of

$$|0\rangle \otimes R_y(\vartheta_1)|0\rangle \otimes R_z(\varphi)R_y(\vartheta_2)|0\rangle \tag{4.17}$$

to the symmetric subspace, given by

$$\begin{aligned} |\psi_{\vartheta_1,\vartheta_2,\varphi}\rangle = N\Big[3\cos\frac{\vartheta_1}{2}\cos\frac{\vartheta_2}{2}|\frac{3}{2},\frac{3}{2}\rangle + \sqrt{3}\left(\sin\frac{\vartheta_1}{2}\cos\frac{\vartheta_2}{2} + \cos\frac{\vartheta_1}{2}\sin\frac{\vartheta_2}{2}e^{i\varphi}\right)|\frac{3}{2},\frac{1}{2}\rangle \\ + \sqrt{3}\sin\frac{\vartheta_1}{2}\sin\frac{\vartheta_2}{2}e^{i\varphi}|\frac{3}{2},-\frac{1}{2}\rangle\Big] \end{aligned} \tag{4.18}$$

up to normalization N. The corresponding family of Wigner functions is similarly found via the generalized Weyl rule with respect to the $j = 3/2$ SU(2) kernel. Fig. 4.2 shows a selection of Wigner negativities.

Similar to the spin-1 system, the degenerate constellations have minimum but not vanishing negativity. A representative constellation that maximizes negativity has $\vartheta_1 = \vartheta_2 = \frac{2\pi}{3}$ and $\varphi = \pi$, corresponding to the roots of unity along a great circle in the ZX plane. This is rotationally equivalent to the GHZ/$N00N$ state quantized along the z-axis,

$$\frac{1}{\sqrt{2}}(|000\rangle + |111\rangle) \simeq \frac{1}{\sqrt{2}}(|3\rangle|0\rangle + |0\rangle|3\rangle) \simeq \frac{1}{\sqrt{2}}(|\frac{3}{2},\frac{3}{2}\rangle + |\frac{3}{2},-\frac{3}{2}\rangle) \tag{4.19}$$

respectively expressed in the computational basis, the two-mode occupation (Schwinger) representation, and the Dicke basis (see Chapter 2). This state has the same constellation but along the equator, and has widespread application in quantum information science and quantum metrology [136, 193]. Note that the GHZ state maximizing negativity in this low-dimensional setting must be an exceptional case because our previous results in Chapter 3 (see Fig. 3.8) clearly show that the generalized GHZ state generically contains rather low amounts of negativity relative to the Dicke basis, let alone all of Hilbert space.

By comparison, both anticoherence and P-representability similarly observe such states (also sometimes called 3-cats in quantum information) as maximally nonclassical. The geometric measure however is saturated by the antipodal constellation but with the North pole being two-star degenerate [105]. This corresponds to the W state $\frac{1}{\sqrt{3}}(|001\rangle + |010\rangle + |100\rangle)$, which is incomparable to the spin cat state when restricted to LOCC operations in the qubit picture [133]. Nonetheless, it is worth explicitly saying that the W state has less Wigner negativity than the GHZ state in four dimensions.

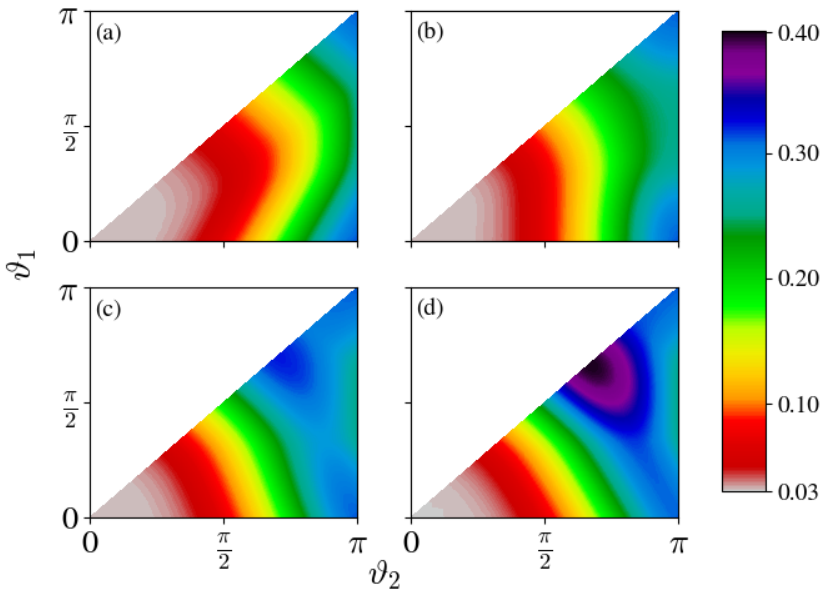

Figure 4.2: Cross-sections of the parameter space of three star constellations. The value of each point represents the Wigner negativity of the spin-1 state associated with that constellation. The axes represent the two polar angles ϑ_1 and ϑ_2, and each panel represents a different azimuthal separation φ: (a) $\varphi = 0$, (b) $\varphi = \frac{\pi}{2}$, (c) $\varphi = \frac{3\pi}{4}$, (d) $\varphi = \pi$. The most nonclassical constellation, $\vartheta_1 = \vartheta_2 = \frac{2}{3}\pi$ and $\varphi = \pi$, is rotationally equivalent to the GHZ/$N00N$ state.

Note on higher spins

Moving forward to higher spins, the problem of determining the extremal quantum states is technically more difficult, and we proceed primarily through numerical methods. We brute-force evaluate the integral (2.60) using Mathematica's built-in numerical optimization techniques, seeking a precision of 5 digits in the final result. To increase the likelihood that the constellation output is the true maximum of the Wigner negativity we perform many iterations of the procedure, seeding the numerical optimization with different initial constellations selected randomly and uniformly across the sphere.

In general the output will consist of several constellations that appear distinct. However, many of the constellations reached by the numerical solver will be related to one

another by a rotation. A simple technique to determine whether two constellations are definitively distinct is as follows. We first take the constellation and write the Cartesian vectors for each star in a matrix:

$$A = [\vec{v}_1, \vec{v}_2, \ldots, \vec{v}_n] \ . \tag{4.20}$$

We then take the matrix AA^T and compute its spectrum. If any two constellations have distinct spectra, then we can be certain the two constellations are also distinct. Because AA^T is invariant if the individual vectors are acted upon by a rotation, if the spectra for two constellations are the same, then those constellations may be related by a rotation.

Using these optimization and classification techniques a careful search is done to determine the constellation of maximum Wigner negativity. After a candidate has been determined, we run a secondary numerical optimization, this time constraining the search region to within $\pm 5\%$ of the previously determined values for the stars and working at machine precision. The actual value for the negativity (up the precision we seek) of the final candidate constellation is then independently cross-checked using the methods described in Refs. [97, 194]. Using many thousands of samplings of initial points, we check to ensure we find a global maximum rather than a local one.

4.2.4 Spin 2

Spin systems with $j = 2$ are characterized by four-star constellations. As usual, we fix the symmetries of the system by placing one star at the North pole, another along the ZX plane characterized just by its polar angle, and the remaining two are specified by both polar and azimuthal angles. The remaining sections continue this pattern. We find that the minimally Wigner-negative state corresponds to the constellation with all stars coincident at the North pole. That is, up to rigid rotations the spin-2 coherent state is of minimal but not vanishing nonclassicality.

The state of maximal negativity is determined to be the following *tetrahedron state*

$$|\psi_{\text{tetra}}\rangle = \frac{1}{\sqrt{3}}|2,2\rangle + \sqrt{\frac{2}{3}}|2,-1\rangle \tag{4.21}$$

The constellation consists of one point at the North pole and three points distributed with equiangular spacing along the azimuthal direction at a fixed polar angle of $\theta = 2\arccos(\frac{1}{\sqrt{3}})$ (Fig. 4.3). It is interesting to note that all three comparative measures – anticoherence,

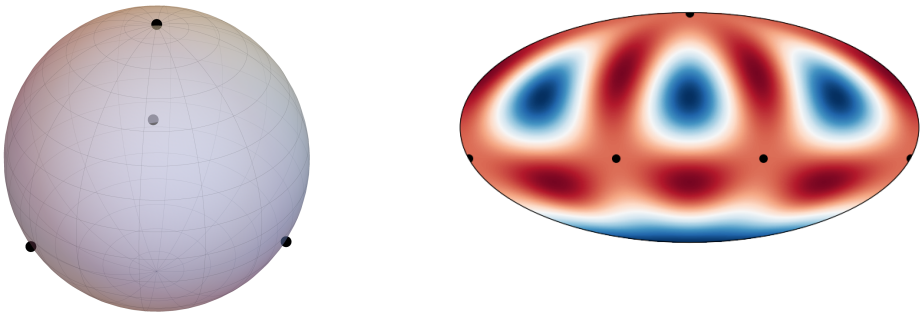

Figure 4.3: Extremal state for spin 2. Left is the associated constellation and right is the associated Wigner function in the Mollweide projection with the constellation superimposed.

P-representability, and geometric entanglement – also agree that the tetrahedron state is maximally nonclassical for four qubit. This arrangement also solves several common spherical optimization problems such as the Thompson problem and the Tóth problem [105]. In addition to the perhaps expected cases of antipodal 2-qubit constellations and 3-qubit GHZ states, we will see this is the last instance where Wigner negativity agrees with any of the other nonclassicality measures.

4.2.5 Spin 5/2

Again, we have confirmed numerically that the spin coherent state is indeed the state of minimal Wigner negativity. For the maximal constellation we obtain the configuration shown in Fig. 4.4. This differs from those found using other state nonclassicality measures. Compared to those alternative extremal states, it is not a particularly symmetric arrangement, and forms the beginning of a pattern of partially symmetric configurations as spin increases.

We can make a further observation for $j = 5/2$: There is a second state with a local negativity maximum notably close in value to the global maximum but with an appreciably different constellation structure. The constellation for this second state is shown in Fig. 4.5. It is an embedded right square pyramid characterized by the base having polar angle $\theta \approx 1.841$ radians. The Wigner negativity of this state is $\delta = 0.57015604$, which differs from maximum only at $\mathcal{O}(10^{-5})$. To ensure this is robust we ran our numerical

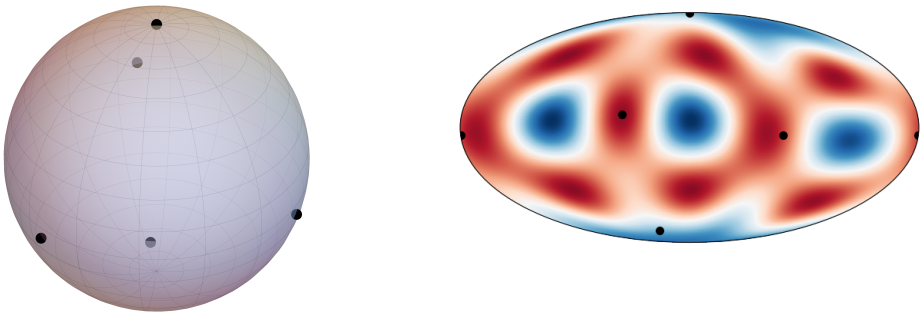

Figure 4.4: Extremal state for spin 5/2. Left is its constellation and right is its Wigner function.

optimization scheme in a small neighbourhood of each constellation to higher precision – again with independent verification from the methods described in Refs. [97, 194] – and found increasing numerical stability. This pyramidal state is therefore an especially Wigner-negative spin-5/2 state, though not maximally negative. Interestingly, a regular square pyramid is also identified as the extremal constellation with respect to geometric entanglement [105]. However, the two states are different as shown in Fig. 4.5. The maximally entangled pyramid has a base slightly further from the apex, with a larger polar angle of $\theta \approx 1.874$. As an aside for reference, note that a pyramid state with base polar angle $\theta = \pi$ is equivalent to the 5-qubit W state, which has a negativity ≈ 0.26 as seen in Fig. 4.5.

4.2.6 Spin 3

Spin systems with $j = 3$ are characterized by six-star constellations. The minimal constellation is again found to be the spin coherent state, and the maximal constellation is shown in Fig. 4.6. It is characterized by four co-planar points that together form a rectangle, along with the star at the North pole and another displaced along the arc $\varphi = 0$ (i.e. the ZX plane). The case of spin 3 is notable because a different state, $\frac{1}{\sqrt{2}}(|3,2\rangle + |3,-2\rangle)$, simultaneously maximizes all of the alternative measures. This is the so-called *octahedron state*, and is characterized by a constellation with stars along the vertices of an embedded octahedron. With an *a priori* presumption that nonclassicality correlates with constellation symmetry, one would perhaps expect the Wigner case to follow suit because the

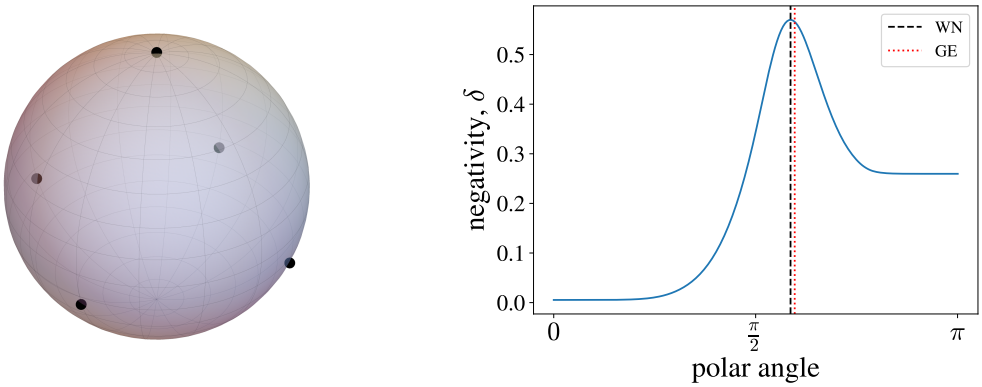

Figure 4.5: Left: Constellation of a state that locally maximizes Wigner negativity in Hilbert space. Right: Wigner negativities of the family of "square pyramid" states parameterized by the polar angle of the pyramid base. The stars in the base have azimuthal angles $\{0, \pi/2, \pi, 3\pi/2\}$. The state that maximizes geometric entanglement (red dotted line) has a slightly larger pyramid height than the Wigner-maximal pyramid state (black dashed line).

octahedron is the next available Platonic solid as the number of stars increase. Yet the most Wigner-negative state identified here is approximately 5% more negative than the octahedron state, a significantly higher gap than the pyramidal runner-up in the five qubit system.

Nonetheless, the $j = 3$ constellation is not without symmetry. As shown in Fig. 4.7, the configuration respects C_{2v} point-group symmetry. The stars can also be bi-partitioned into two identical triangles in six different ways; see Fig. 4.8. The first two partitions, shown in the upper-left and upper-middle plots of Fig. 4.8, yield a pair of isosceles triangles. The remaining partitions are made of pairs of identical scalene triangles. The octahedron constellation by comparison can be partitioned into two identical triangles in ten different ways, which is the maximal number of such partitions. For reference, in the upper-left partition the triangles have angles 53.9°, 53.9°, and 72.2° with edge lengths 1.51, 1.51, and 1.78. The upper-middle triangles have angles 58.3°, 58.3°, and 63.4° with edge lengths 1.69, 1.69, and 1.77.

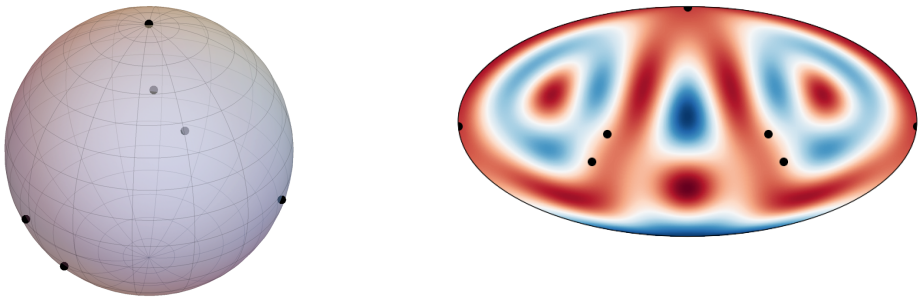

Figure 4.6: Extremal state for spin 3. Left is the constellation and Right is the Wigner function. This state is approximately 5% more Wigner-negative than the octahedron state, which maximizes all the alternative notions of nonclassicality.

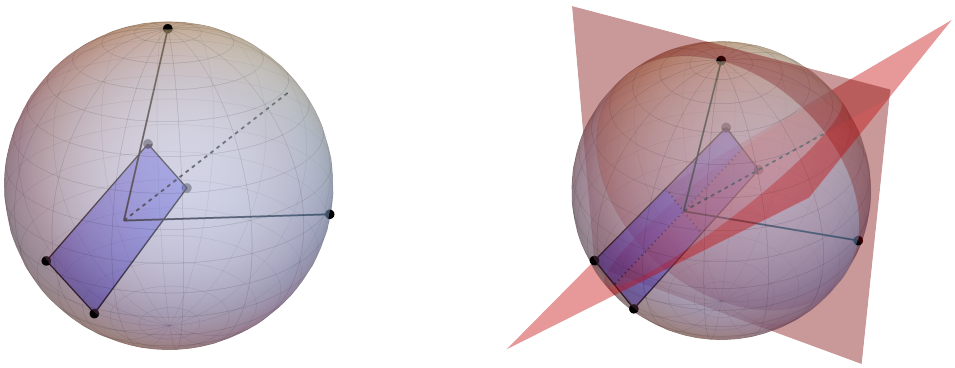

Figure 4.7: Demonstrating C_{2v} point symmetry of the maximal spin 3 constellation. Left: π-rotation about dotted line. Right: Two mirror planes parallel to the axis of rotation.

4.2.7 Spin 7/2

Spin systems with $j = 7/2$ correspond to seven stars. The maximal constellation is characterized by two parallel equilateral triangles with matching orientation, together with a star along the diameter going through the centroids of the triangles; see Figs. 4.9 and 4.10.

Using a similar argument as the six star system, such constellations can be seen to have C_{3v} point-group symmetry. The maximally anticoherent state is also of this "two

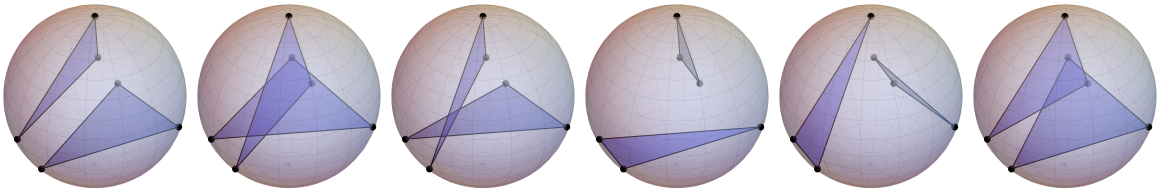

Figure 4.8: Bi-partitions of the spin-3 maximal state into identical triangles. In the top-left and top-middle plots the pair of triangles are isosceles; the others are scalene. In every case the triangles are identical — their angles and edge lengths are equal within working precision. In maintaining a common perspective this may be less apparent in some cases.

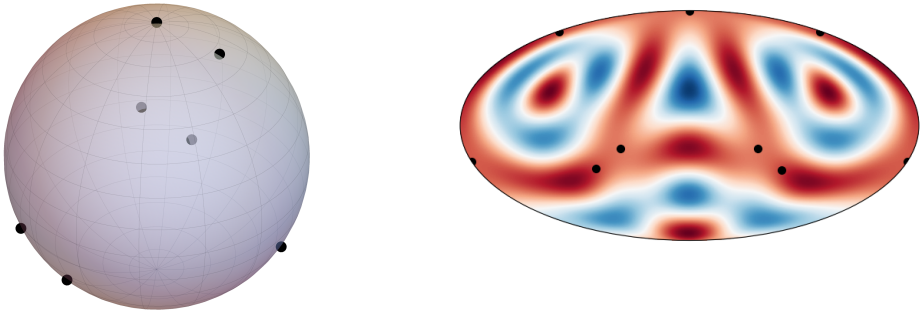

Figure 4.9: Maximal spin-$\frac{7}{2}$. Left is the constellation and right is the Wigner function.

triangles + pole" form but with different heights of the triangles along the rotational axis [177]. In particular, the two triangles in the Wigner case are significantly closer to each other: $\Delta d_{\text{Wigner}} \approx 0.43$ and $\Delta d_{\text{ac}} \approx 0.82$ as measured by their axial distance along the diameter. See Fig. 4.11 for a comparison between all such constellations as parameterized by the polar angles of the two triangles (polar with respect to the axis pointing towards the 7th star). By comparison, the maximal constellations of both geometric entanglement and P-representability are described by a pentagon along the equator together with a star on each pole [105, 190].

Using a method similar to the previous section, we have found another highly negative spin-7/2 state by modifying the maximal state. Note that combining the isolated point with either of the triangles results in a triangular pyramid as shown in the middle and right plots of Fig. 4.10. These pyramids are in general irregular in the sense that they are built from one equilateral face and three identical isosceles faces. In our particular instance

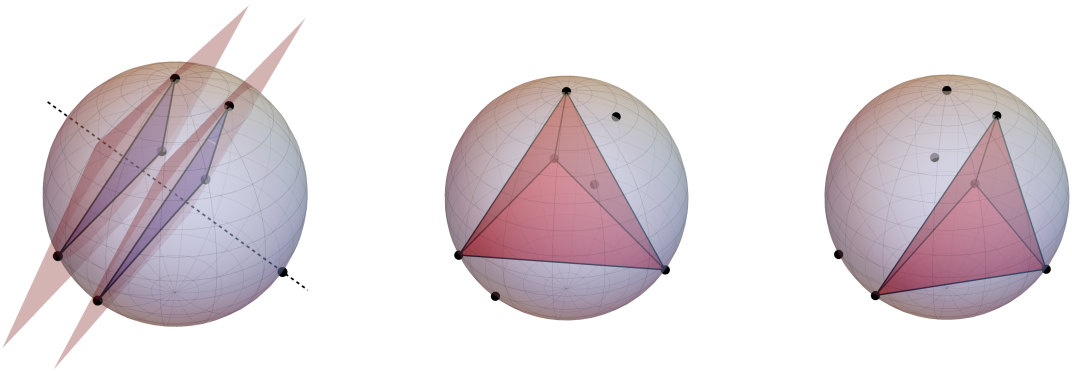

Figure 4.10: Left: parallel planes extended by two equilateral triangles within the maximal spin-$\frac{7}{2}$ constellation. The dotted line is a diameter passing through the centroid of the triangles and the remaining point. Middle and Right: irregular tetrahedra within the constellation, with the right closely approximating a regular tetrahedron.

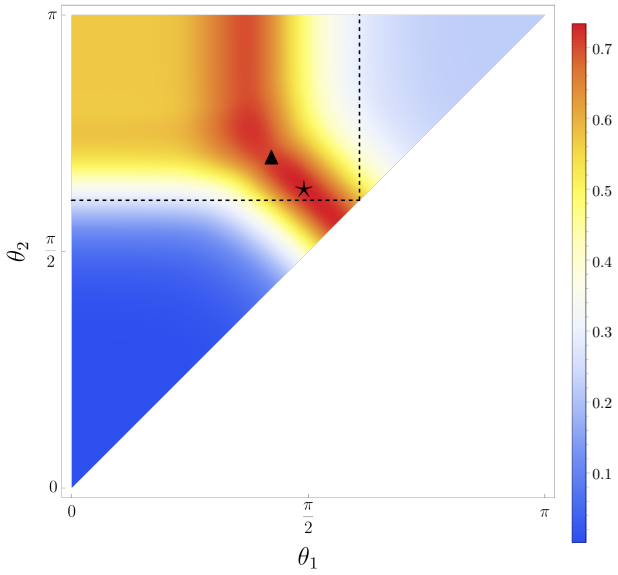

Figure 4.11: Wigner negativity landscape of "two triangles + pole" constellations. Parameters are the polar angles of each triangle with respect to the axis of rotational symmetry. The dashed lines indicate when one of the triangles forms a tetrahedron with the pole. The star indicates the Wigner extremal state, while the triangle indicates the anticoherence extremal state.

of this general pattern, the smaller pyramid has a characteristic isosceles face with angles $\{52°, 52°, 77°\}$ and the larger has $\{62°, 62°, 56°\}$. The latter configuration is somewhat close to an equilateral triangle, which if true would turn the pyramid into a tetrahedron.

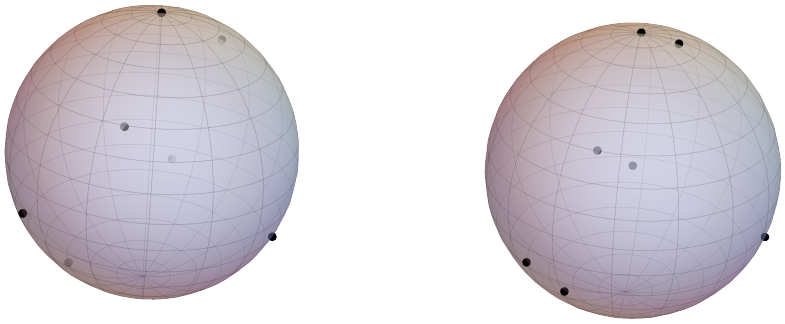

Figure 4.12: Left: maximal spin-$\frac{7}{2}$ state with four highlighted stars that approximate a regular tetrahedron. Right: constrained optimization after snapping the four points to a regular tetrahedron. The right has a Wigner negativity of 0.73243.

Pursuing this, we can consider the constrained problem where four of the seven stars are snapped to a tetrahedron while the remaining three are varied through the numerical optimization. The result of this is shown on the right of Fig. 4.12. The constellation is similar to the maximal one, though different enough to be visually distinguished. This state also has a high Wigner negativity of 0.73243. This differs from the true maximum slightly, within one part in a thousand. We mention this because although this state is not maximal, it is nonetheless interesting to see a Platonic solid as a sub-constellation to an extremely negative state with spin 7/2 despite the six-qubit extremal state not being the octahedron.

4.2.8 Summary of maximal states

Here are some data tables summarizing the maximally Wigner-negative spin states:

Spin	Wigner negativity	Maximal constellation (θ, ϕ)
1	0.26935	$(0,0),(\pi,0)$
3/2	0.39634	$(0,0),(2\pi/3,0),(2\pi/3,\pi)$
2	0.50078	$(0,0),(\theta_T,0),(\theta_T,2\pi/3),(\theta_T,4\pi/3)$ $\theta_T = 2\cos^{-1}(1/\sqrt{3})$
5/2	0.57016	$(0,0),(1.66,0),(1.43,2.21),$ $(2.86,2.23),(1.65,4.43)$
3	0.65354	$(0,0),(1.62,0),(1.71,2.03),$ $(1.71,4.25),(2.02,4.54),(2.02,1.75)$
7/2	0.73395	$(0,0),(1.97,0),(1.83,2.18),(2.07,4.51),$ $(1.83,4.09),(2.06,1.76),(0.43,6.25)$

Table 4.1: Table of maximal Wigner negative values and the associated constellations.

Spin	Dicke coefficients $(m = -j, \cdots, j)$
1	$(0,1,0)$
3/2	$(0,-\sqrt{3/2},0,1/2)$
2	$(0,\sqrt{2/3},0,0,1/\sqrt{3})$
5/2	$(0,-0.594+0.373i,0.090+0.034i,0.053+0.200i,$ $-0.391+0.507i,0.216)$
3	$(0,0.743-0.001i,-0.02,0.156,0.37,-0.111,0.523)$
7/2	$(0,0.299-0.008i,0.687-0.006i,-0.227-0.005i,$ $0.299-0.001i,0.215-0.003i,-0.074-0.005i,0.496)$

Table 4.2: Table of Dicke coefficients for Wigner extremal states. Exact numbers are used when available.

4.3 Random state analysis

This section summarizes a brief analysis of the statistical properties of spherical Wigner negativity over Hilbert space.

Given a fixed spin j, random unitaries are sampled with respect to the Haar measure on $\mathrm{U}(2j+1)$ – i.e. the circular unitary ensemble (CUE)[7]. These unitaries are applied to an irrelevant fiducial state to produce a uniform sample of random states in the Hilbert space

[7]See [195] for alternative ways of obtaining random constellations.

$\mathbb{C}^{2j+1}$. Fig. 4.13 shows the distribution of Wigner negativity over $N = 200{,}000$ random states for $1 \leq j \leq \frac{7}{2}$. The results indicate that random states on average are highly Wigner negative relative to the allowed range, though the exact distribution depends on the particular spin. Apart from the two and three qubit systems, each distribution has a similar form with a high peak relatively close to the upper bound. As spin increases the peak narrows, creating a more rapid decay towards maximal negativity.

Additional distributions were computed for higher spins up to and including $j = 6$, and they continue to have the same general form as the $j \geq 2$ set in Fig. 4.13. The increasingly sharper decays from each peak indicate that the maximal state(s) and those with a similar degree of negativity become increasingly rare as spin increases. Fig. 4.14 plots the percentage of random states from the CUE sample that have a negativity within two percent of their theoretical maximum; see section 4.2.8 for the list of maxima. On average, across all spins $j \geq 2$, only $\approx 0.2\%$ of states are within 2% of their respective maximum negativity value, indicating the rarity of the highly Wigner-negative states in Hilbert space. For spins $j \geq 4$ the maximum is taken to be the highest negativity sampled; the true maximal value can only be higher, making the average (dashed red line) almost certainly an upper bound. By comparison, we computed the linear entropy of the $(1 : n-1)$ bipartition in the qubit representation of the same CUE sample and find that, on average across all spins $j \geq 2$, approximately 7.3% of them are within 2% of the maximum value 1/2. This number increases with spin, with the case of $j = 6$ having around 12.6% of random states within 2% of the linear entropy maximum. In the specific case of an 11-qubit system for example, one is approximately 70 times more likely to randomly sample a state with an almost maximally mixed one-qubit reduction than a state with an almost maximal Wigner negativity.

We also note that, as expected, all random states sampled were found to have strictly less negativity than the determined maximal state of the same dimension.

4.4 Discussion

Determining the exact Wigner negativity of a state in general requires the identification of the zero set of its associated Wigner function, followed by an integration over that set. This rapidly becomes analytically intractable as spin increases. Even in the azimuthally symmetric case of Dicke states for example, the form of the Wigner function (2.61) requires exact knowledge of the zeroes of the Legendre polynomials. Hence we are left with

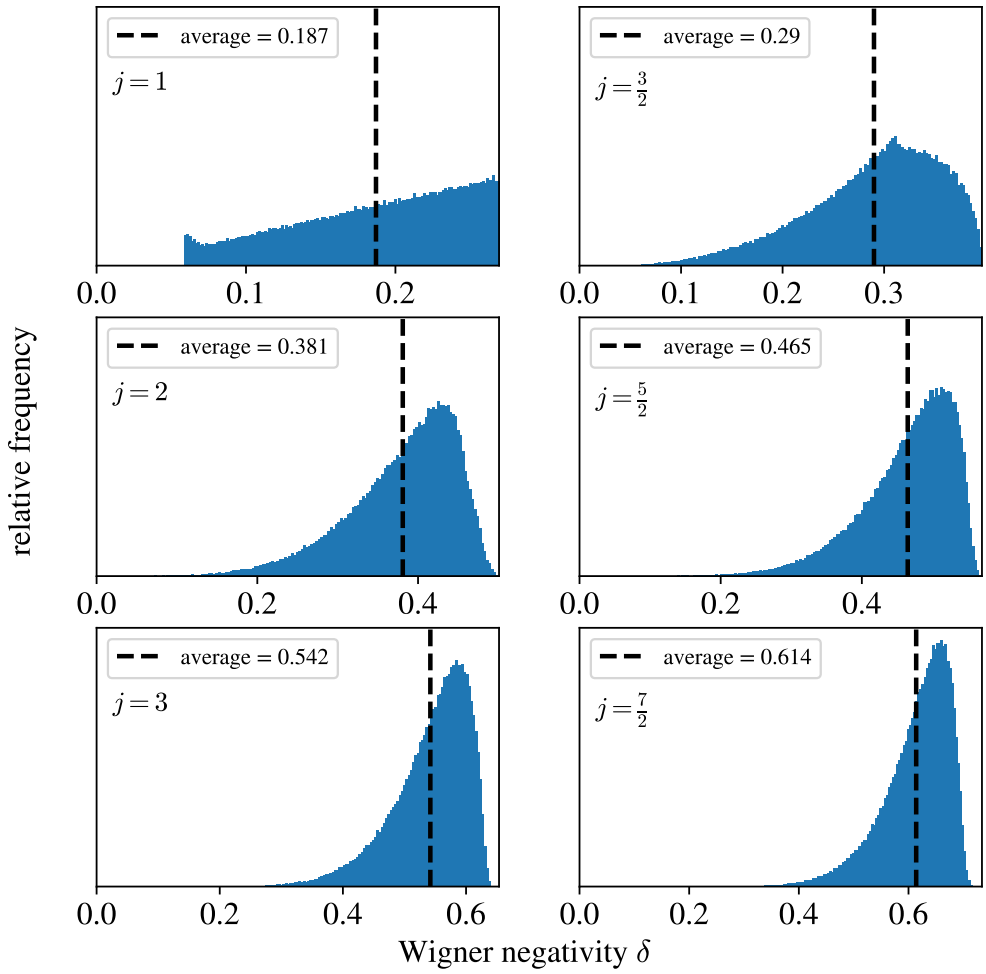

Figure 4.13: Distribution of Wigner negativity over $N = 200{,}000$ randomly sampled states for spins $1 \leq j \leq 7/2$. The horizontal axis gives the absolute Wigner negativity, and cuts off on the right at the maximal value. In each case the vertical dashed line indicates the CUE average.

computational techniques and general heuristics. Here we discuss some observations in

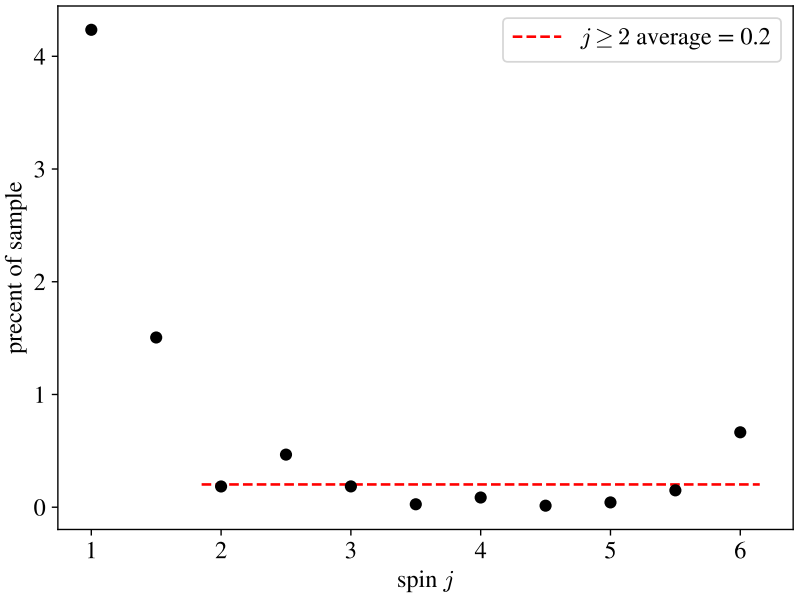

Figure 4.14: For each spin j on the horizontal axis, the vertical axis is the percentage of the N =200,000 random states that have a negativity within 2% of their respective maximum. The dashed red line is the average for $j \geq 2$. For spins $j \geq 4$ the maximum is the highest negativity sampled.

the context of states that maximize other measures of nonclassicality. In particular, the constellations of such alternative maximal states are in general highly symmetric, highly delocalized, or both [185, 109]. And while the Wigner-maximal constellations partially display these qualities in the spins considered, they do not follow an obvious geometric guiding principle.

First consider constellation symmetry. The relatively weak correlation between configuration symmetry and Wigner negativity begins with the spin 3 system where, despite the Wigner-maximal state having partial symmetry (i.e. a C_{2v} point-group), it is definitively not the highly symmetric octahedron state. This continues to higher spin despite the global maximum being unknown. See Fig. 4.15 for a comparison between all extremal states up to spin 6. For $j \geq 4$ the most negative random state drawn from the CUE sample is used in place of the unknown global maximum(s). Only for $j \leq 2$ does the highest Wigner-negative state coincide with one of the alternative maxima. Each larger dimensional system with $j > 2$ contains at least one state in Hilbert space with a Wigner

negativity larger than the negativity of the alternative extremal states. This difference in negativity furthermore appears to grow with spin. The last case of spin 6, corresponding to 12 indistinguishable qubits, is particularly interesting because that is the number of vertices of the icosahedron, another Platonic solid with high constellation symmetry. Indeed the *icosahedron state* simultaneously maximizes the other measures of nonclassicality yet is approximately $\approx 13\%$ less negative than the statistical maximum, and actually scores below average across Hilbert space, $\mathbb{C}^{13}$. Fig. 4.16 compares the icosahedron state and the most negative random state sampled. There is a passing similarity between the Wigner functions of the 12 qubit statistical maximum and both the 6 and 7 qubit global maxima, with two roughly dual "lobes" in the upper hemisphere together with somewhat concentric regions in the opposing hemisphere. It is plausible that the 12-qubit global maximum may sharpen this similarity and demonstrate a more concrete pattern in Wigner-maximal spin states.

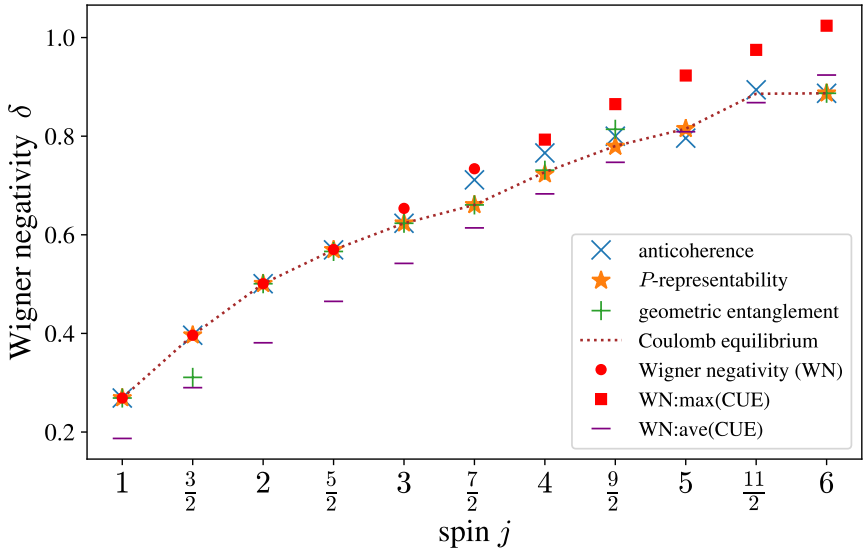

Figure 4.15: Wigner negativity of alternative maximal states and Thomson/Coulomb global equilibria. For $j \geq 2.5$ (five qubits and larger), there exists a state with higher negativity than the other maxima considered. For $j \geq 4$ this state is taken to be the most negative of the CUE random sample. The lack of a marker indicates no available data.

We also briefly mention the two other Platonic states within $1/2 \leq j \leq 6$: the cube and

the tetrahedron. The cube state is interesting because anticoherence is the only measure that witnesses it as maximal. It is additionally the first time all four measures have different maximal states. By contrast, the tetrahedron state is the only non-trivial case where all four measures agree. This consensus offers evidence that the tetrahedron state may be of practical use in various quantum-enhanced applications. This is also in part what motivated us to pursue modifications of the maximal states revolving around fixed tetrahedra within a given constellation.

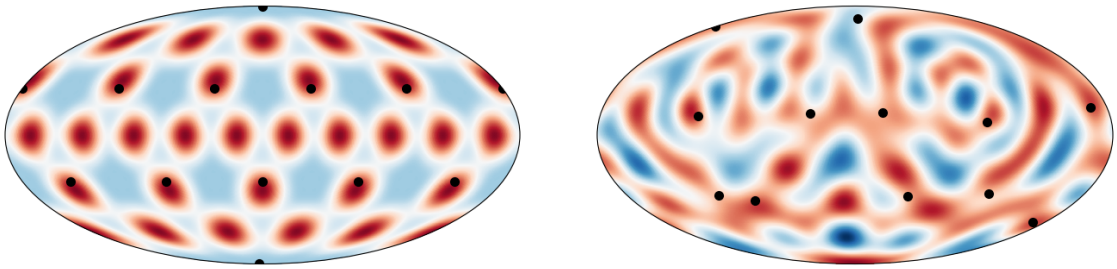

Figure 4.16: Left: Wigner function of the icosahedron state. Right: Wigner function of the most negative state found in the spin 6 CUE sample.

Now consider constellation delocalization. To compare the Wigner-maximal states against those with a uniform distribution of Majorana stars we consider the Thompson problem, defined as the electrostatic configuration of n point charges confined to the sphere that minimizes the Coulomb potential energy [196]. The solutions to the Thompson problem are one of many inequivalent benchmarks for distributional uniformity over the sphere [197], however the intuitive description of the problem makes it a reliable reference point. The exact configurations to this problem are not generally known for an arbitrary number of points, though numerically optimized solutions exist in many cases [198, 199]. The dotted line in Fig. 4.16 denotes the Wigner negativity of such Thomson solutions. Similar to the case of constellation symmetry, the Coulomb equilibria have sub-maximal negativity for $j > 2$. The difference between the equilibria and the highest known negativity also grows with system dimension, culminating again in the below-average negativity from the spin 6 icosahedron state.

We note a related observation that Wigner-maximal constellations sometimes contain groups of stars confined to a relatively small region of phase space. This is seen in the

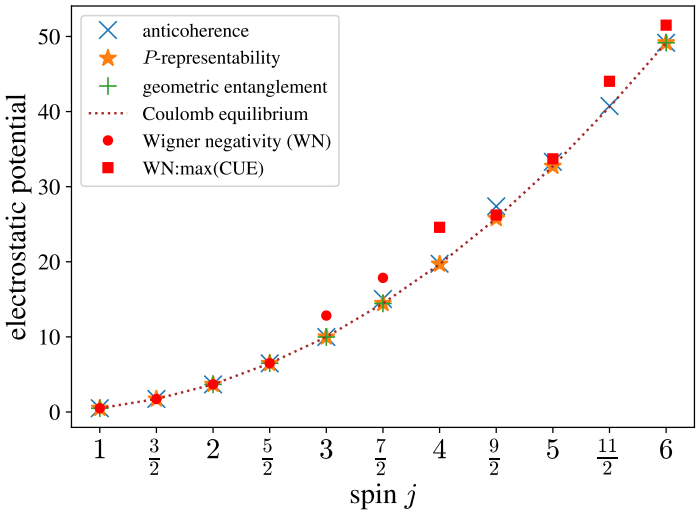

Figure 4.17: Coulomb electrostatic potential energy of alternative extremal constellations. Highly Wigner-negative states tend to have a higher potential energy, indicating the presence of clustering of stars within their constellations. The lack of a marker indicates no available data or, as in some cases of geometric entanglement, when two stars are degenerate.

small edges of the rectangle structure within spin 3 (Fig. 4.6), and the two triangles within spin 7/2 (Fig. 4.9). Qualitatively, such grouping is not generally seen in the non-Wigner maximal states, with the exception of geometric entanglement in the spin-3/2 case having two stars degenerate on the same point. The geometric measure configurations for spins greater than 7/2 continue to occasionally have degenerate stars [105], however they are still relatively uniform over the sphere if such degenerate points are seen as singular. This "clustering" of stars, i.e. being close but not degenerate, appears to be specific to Wigner negativity. See Fig. 4.17 for a comparison of all the maximal states as measured by the electrostatic potential energy of their constellations. States with high negativity tend to have higher potential energy, indicating the presence of relatively closer stars.

In summary, given the data from the spins considered, it appears that while Wigner negativity is sensitive to both constellation symmetry and delocalization, they are not guiding principles to be individually optimized over.

Chapter 5

Wigner negativity and state purity

This chapter is based on the following work:

> Denis, J., Davis, J., Mann, R. B., & Martin, J. (2023). Polytopes of absolutely Wigner bounded spin states. *arXiv:2304.09006*, [3].

and is largely a lift from [3] with various modifications and additions.

5.1 Introduction

Negative quasiprobability in the phase space representation has long been an indicator of non-classicality in quantum systems. The three most studied types of quasiprobability are those associated with the Wigner function, the Glauber-Sudarshan function, and the Kirkwood-Dirac function, particularly so in recent years due to the rise of quantum information theory. Wigner negativity in particular has received special attention because of its relationship to quantum advantage in the magic state injection model of universal fault-tolerant quantum computation [51, 45, 58, 61, 62]. In this setting Wigner negativity acts as a magic monotone with respect to Gaussian/Clifford group operations, and so offers some credence to the idea that more negativity implies more non-classicality [65, 67, 68].

For pure states in bosonic systems the set of Wigner-positive states is fully characterized by Hudson's theorem, be it Gaussian states in the continuous variable regime or stabilizer

states in the discrete variable regime [40, 32]. However the relationship between negative quasiprobability and state mixedness is not well understood. For both practical and theoretical reasons this relationship is important. In the mixed bosonic setting, Gaussianity is no longer necessary to infer Wigner function positivity and the situation becomes more complicated [200, 201, 202]. A general observation is that negativity tends to decrease as purity decreases. This may be attributed to the point-wise convexity of Wigner functions over state decompositions, together with the maximally mixed state guaranteed to be Wigner-positive (at least in a limiting sense of increasingly flatter Gaussians), although the precise relationship is not fully understood. Even less understood is how Wigner negativity manifests in spin-j systems, equivalent to the symmetric subspace of $2j$ qubits, which have a Moyal representation on a spherical phase space [88, 89, 91, 98, 97, 115]. Evidence suggests that no pure spin state is completely Wigner-positive [2], and the question of mixed spin states remains largely unexplored.

Inspired by work on characterizing mixed spin state entanglement in the symmetrized multi-qubit picture, in particular that of absolute separability [203, 204], here we address the question of Wigner positivity by investigating unitary orbits of spin states. The unitary orbit of a spin-j state ρ is defined as the set of states $\{U\rho U^\dagger : U \in \mathrm{SU}(2j+1)\}$. In particular, we call a general spin state *absolutely Wigner-positive* (AWP) if its spherical Wigner function remains positive under the action of all global unitaries $U \in \mathrm{SU}(2j+1)$.

In order to position our work in a wider context, we begin with a brief note on related research. Recent works have studied the sets of AWP states [205, 206, 207, 208] taking a broad perspective on the Moyal picture in finite dimensions by simultaneously considering the set of all candidate SU(N)-covariant Wigner functions for each dimension N. It is in this general setting where the relationship between generalized Moyal theory, the existence of Wigner-positive polytopes, and the Birkoff-von Neumann theorem was first established. It was furthermore abstractly demonstrated that there always exists a compatible reduction to an appropriate N-dimensional SU(2) symbol correspondence on the sphere.

By contrast, here we work exclusively with the symmetry group SU(2) in each dimension, as well as a single concrete Wigner function, Eq. (5.2), which we consider to be the canonical Wigner function for spin systems because it is the only SU(2)-covariant Wigner function to satisfy, in addition to the usual Stratonovich-Weyl axioms, either of the following two properties:

- Compatibility with the spherical s-ordered class of functions: it is exactly "in between" the Husimi Q function and the Glauber-Sudarshan P function (as generated

by the standard spin-coherent state $|j, j\rangle$) [89].

- Compatibility with Heisenberg-Weyl symmetry: its infinite-spin limit is the original Wigner function on $\mathbb{R}^2$ [92].

In addition to offering a related but alternative argument showing the existence of such polytopes, here we go beyond previous investigations in three ways. The first is that we extend the argument to include orbits of Wigner functions lower-bounded by numbers not necessarily zero. These one-parameter families of polytopes, which we refer to as *absolutely Wigner bounded* (AWB) polytopes, are of interest not only for Wigner functions but also for other quasiprobability distributions. The second is that we go into explicit detail on the geometric properties of these polytopes and explore their relevance in the context of spin systems and quantum information. The third is that we contrast the Wigner negativity structure to the Glauber-Sudarshan negativity structure, which amounts to an accessible comparison between Wigner negativity and entanglement in the mixed state setting.

Having established the context for this work with the above description, our first result is the complete characterization of the set of AWB spin states in all finite dimensions, with AWP states appearing as a special case. As similarly discussed in [207], this may be phrased as a natural application of the Birkhoff-von Neumann theorem on doubly stochastic matrices, though here we extend and specialize to the SU(2)-covariant Wigner kernel associated with the canonical Wigner function on the sphere. In particular, the set of AWB states forms a polytope in the simplex of density matrix spectra, the $(2j + 1)!$ hyperplane boundaries of which are defined by permutations of the eigenvalues of the phase-point operators. Centred on the maximally mixed state for each dimension, we also exactly find the largest possible Hilbert-Schmidt ball containing nothing but AWB states, which amounts to the strictest AWB sufficiency criterion based solely on the purity of mixed states. We also obtain an expression that we conjecture describes the smallest Hilbert-Schmidt ball containing all AWB states, which amounts to a tight necessity criterion. Numerical evidence supports this conjecture. For both criteria, we discuss their geometric interpretation in relation to the full AWB polytope. We then specialize to absolute Wigner positivity and compare it with symmetric absolute separability (SAS), which in the case of a single spin-j system is equivalent to absolute Glauber-Sudarshan positivity [102, 209, 210].

Our paper is organized as follows. Section 5.2 briefly outlines the generalized phase space picture using the parity-operator/Stratonovich framework for the group SU(2). Section 5.3 proves our first result on AWB polytopes, while Sec. 5.4 determines and conjectures, respectively, the largest and smallest Hilbert-Schmidt ball sitting inside and outside

the AWB polytopes. Section 5.5 explores low-dimensional cases in more detail and draws comparisons to entanglement. Finally, conclusions are drawn and perspectives are outlined in Sec. 5.6.

5.2 Background

The parity-operator framework is the generalization of Moyal quantum mechanics to physical systems other than a collection of non-relativistic spinless particles. Each type of system has a different phase space, and the various types are classified by the system's dynamical symmetry group [84]. In each case the central object is a map, Δ, called the *kernel*, which takes points in phase space to operators on Hilbert space. A quasi-probability representation of a quantum state, evaluated at a point in phase space, is the expectation value of the phase-point operator assigned to that point. Different kernels yield different distributions but all must obey the Stratonovich-Weyl axioms, which ensure, among other properties, the existence of an inverse map and that the Moyal picture is as close as possible to classical statistical physics over the same phase space (i.e. the Born rule as an L^2 inner product).

When applied to the Heisenberg-Weyl group (i.e. the group of displacement operators generated by the canonical commutation relations, $[x, p] = i\mathbb{I}$) this framework reduces to the common phase space associated with n canonical degrees of freedom, $\mathbb{R}^{2n}$, and the phase-point operators corresponding to the Wigner function appear as a set of displaced parity operators [84, 19, 20]. A spin-j system on the other hand corresponds to the group SU(2), which yields a spherical phase space, S^2. Here we list some necessary results from this case; see Refs. [88, 89, 91, 98, 97] for more information.

5.2.1 Wigner function of a spin state

Consider a single spin system with spin quantum number j. Pure states live in the Hilbert space $\mathcal{H} \simeq \mathbb{C}^{2j+1}$, which carries an irreducible SU(2) representation that acts as rotations up to global phase: $U_g|\psi\rangle \simeq R(\theta, \phi)|\psi\rangle$ where $g \in \mathrm{SU}(2)$. Mixed states live in the space of operators, $\mathcal{L}(\mathcal{H})$, where SU(2) acts via conjugation: $U_g \rho U_g^\dagger$. This action on operator space is not irreducible and may be conveniently decomposed into irreducible multipoles.

The SU(2) Wigner kernel of a spin-j system is

$$\begin{aligned}\Delta &: S^2 \to \mathcal{L}(\mathcal{H}) \\ \Delta(\Omega) &= \sqrt{\frac{4\pi}{2j+1}} \sum_{L=0}^{2j} \sum_{M=-L}^{L} Y^*_{LM}(\Omega) T_{LM},\end{aligned} \tag{5.1}$$

where $\Omega = (\theta, \phi) \in S^2$, $Y_{LM}(\Omega)$ are the spherical harmonics, and $T_{LM} \equiv T^{(j)}_{LM}$ are the spherical tensor operators associated with spin j [116]. To avoid cluttered notation we do not label the operator Δ with a j; the surrounding context should be clear on which dimension/spin is being discussed. The Wigner function of a spin state ρ is defined as

$$\begin{aligned}W_\rho(\Omega) &= \mathrm{Tr}\left[\rho \Delta(\Omega)\right] \\ &= \frac{1}{2j+1} + \sqrt{\frac{4\pi}{2j+1}} \sum_{L=1}^{2j} \sum_{M=-L}^{L} \rho_{LM} Y_{LM}(\Omega),\end{aligned} \tag{5.2}$$

where $\rho_{LM} = \mathrm{tr}[\rho\, T^\dagger_{LM}]$ are state multipoles [99]. This function is normalized according to

$$\frac{2j+1}{4\pi} \int_{S^2} W_\rho(\Omega)\, d\Omega = 1, \tag{5.3}$$

and, as Eq. (5.2) suggests, the maximally mixed state (MMS) $\rho_0 = \mathbb{I}/(2j+1)$ is mapped to the constant function

$$W_{\rho_0}(\Omega) = \frac{1}{2j+1}. \tag{5.4}$$

An important property is SU(2) covariance:

$$W_{U_g \rho U_g^\dagger}(\Omega) = W_\rho(g^{-1}\,\Omega), \tag{5.5}$$

where the right hand side denotes the spatial action of SU(2) on the sphere. As this is simply a rigid rotation, analogous to an optical displacement operator rigidly translating $\mathbb{R}^{2n}$, the overall functional form of any Wigner function is unaffected. Hence the Wigner negativity defined as [9, 1]

$$\delta(\rho) = \frac{1}{2}\left(\int_\Gamma |W_\rho(\Omega)|\, d\mu(\Omega) - 1\right), \tag{5.6}$$

often used as a measure of non-classicality, is invariant under SU(2) transformations. Note that the action of a general unitary $U \in \mathrm{SU}(2j+1)$ on a state ρ can of course radically

change its Wigner function and thus also its negativity. The quantity $d\mu(\Omega) = (2j + 1)/(4\pi)\sin\theta d\theta d\phi$ is the invariant measure on the phase space.

A related consequence of SU(2) covariance is that all phase-point operators have the same spectrum [93]. The set of kernel eigenvectors at the point Ω is the Dicke basis quantized along the axis $\mathbf{n}$ pointing to Ω, such that we have

$$\Delta(\Omega) = \sum_{m=-j}^{j} \Delta_{j,m} |j, m; \mathbf{n}\rangle\langle j, m; \mathbf{n}|, \tag{5.7}$$

with rotationally-invariant eigenvalues

$$\Delta_{j,m} = \sum_{L=0}^{2j} \frac{2L+1}{2j+1} C^{j,m}_{j,m;L,0} \tag{5.8}$$

where $C^{J,M}_{j_1,m_1;j_2,m_2}$ are Clebsch-Gordan coefficients. In particular, at the North pole ($\Omega = 0$) the kernel is diagonal in the standard Dicke basis and its matrix elements are

$$[\Delta(0)]_{mn} = \langle j, m|\Delta(0)|j, n\rangle = \Delta_{j,m}\delta_{mn}. \tag{5.9}$$

The kernel is guaranteed to have unit trace at all points and in all dimensions:

$$\sum_{m=-j}^{j} \Delta_{j,m} = 1 \quad \forall\, j, \tag{5.10}$$

and satisfies the relationship [206]

$$\sum_{m=-j}^{j} \Delta^2_{j,m} = 2j + 1 \quad \forall\, j, \tag{5.11}$$

for which we give a proof of in Appendix 5.7.1 for the sake of consistency.

Finally, we note the following observations on the set of kernel eigenvalues (5.8):

$$\begin{aligned} &|\Delta_{j,m}| > |\Delta_{j,m-1}| \neq 0, \\ &\mathrm{sgn}(\Delta_{j,k}) = (-1)^{j-k} \end{aligned} \tag{5.12}$$

for all $m \in \{-j + 1, ..., j\}$. That is, as m ranges from j to $-j$ the eigenvalues alternate in sign (starting from a positive value at $m = j$) and strictly decrease in absolute value

without vanishing. Numerics support this assumption though we are not aware of any proof; see also [1, 97] for discussions on this point. Note this implies that the kernel has multiplicity-free eigenvalues for all finite spin. This is in contrast to the Wigner function on $\mathbb{R}^2$, which has a highly degenerate kernel (i.e. it acts on an infinite-dimensional Hilbert space but only has two eigenvalues) [20]. Only some of our results depend on (5.12), and we will highlight when this is the case.

In what follows we use the vector notation $\boldsymbol{\lambda}$ for the spectrum $(\lambda_0, \lambda_1, \ldots, \lambda_{2j})$ of a density operator ρ, and likewise $\boldsymbol{\Delta}$ for the spectrum $(\Delta_{j,-j}, \Delta_{j,-j+1}, ..., \Delta_{j,j})$ of the kernel Δ. We also alternate between the double-subscript notation $\Delta_{j,m}$, which refers directly to Eq. (5.8), and the single-subscript notation Δ_i where $i \in \{0, ..., 2j\}$, which denotes a vector component, similar to λ_i.

5.3 Polytopes of absolutely Wigner bounded states

We present in this section our first result. We prove there exists a polytope containing all absolutely Wigner bounded (AWB) states with respect to a given lower bound, and fully characterize it. When this bound is zero we refer to such states as absolutely Wigner positive (AWP). We also determine a necessary and sufficient condition for a state to be inside the AWB polytope based on a majorization criterion. These results offer a strong characterization of the classicality of mixed spin states.

We start with the following definition of AWB states:

Definition 1. *A spin-j state ρ is absolutely Wigner bounded (AWB) with respect to $W_{\min}$ if the Wigner function of each state unitarily connected to ρ is lower bounded by $W_{\min}$. That is, if*

$$W_{U\rho U^\dagger}(\Omega) \geq W_{\min} \qquad \begin{array}{l} \forall\ \Omega \in S^2 \\ \forall\ U \in \mathrm{SU}(2j+1). \end{array} \tag{5.13}$$

When $W_{\min} = 0$ we refer to such states as absolutely Wigner positive (AWP). Hence, an AWP state has only non-negative Wigner function states in its unitary orbit.

5.3.1 Full set of AWB states

The following proposition is an extension and alternative derivation of a result on absolute positivity obtained in [207, 206]. It gives a complete characterization of the set of states

whose unitary orbit contains only states whose Wigner function is larger than a specified constant value, and is valid for any spin quantum number j.

Proposition 1. *Let $\boldsymbol{\Delta}^{\uparrow}$ denote the vector of kernel eigenvalues sorted into increasing order, and let*

$$W_{\min} \in [\Delta_0^{\uparrow}, \tfrac{1}{2j+1}]. \tag{5.14}$$

Then a spin state ρ has in its unitary orbit only states whose Wigner function satisfies $W(\Omega) \geq W_{\min}\, \forall\, \Omega$ iff its decreasingly ordered eigenvalues $\boldsymbol{\lambda}^{\downarrow}$ satisfy the following inequality

$$\sum_{i=0}^{2j} \lambda_i^{\downarrow} \Delta_i^{\uparrow} \geq W_{\min}. \tag{5.15}$$

Remark. While not necessary for the proof to hold, note that according to Eq. (5.12) the sorted kernel eigenspectrum becomes $\boldsymbol{\Delta}^{\uparrow} = (\Delta_{j,j-1}, \Delta_{j,j-3}, ..., \Delta_{j,-j}, ..., \Delta_{j,j-2}, \Delta_{j,j})$ and so $W_{\min} \in [\Delta_{j,j-1}, \frac{1}{2j+1}]$. The upper bound comes from Eq. (5.3), which implies that any Wigner function with $W_{\min} > 1/(2j+1)$ would not be normalized. Furthermore, for $W_{\min} = 0$, this proposition provides a characterisation of the set of AWP states, as previously found in a more abstract and general setting in [207, 206].

Proof. Consider a general spin state ρ. We are first looking for a necessary condition for any element $U\rho U^{\dagger}$ of the unitary orbit of ρ to have a Wigner function $W(\Omega) \geq W_{\min}$ at any point $\Omega \in S^2$. Since the unitary transformation applied to ρ may correspond, in a particular case, to an SU(2) rotation, the value of the Wigner function of ρ at any point Ω corresponds to the value of the Wigner function at $\Omega = 0$ of an element in its unitary orbit (the rotated version of ρ). But since we are considering the full unitary orbit, i.e. all possible U's, we can set the Wigner function argument to $\Omega = 0$ via the following reasoning. The state ρ can always be diagonalized by a unitary matrix M, i.e. $M\rho M^{\dagger} = \Lambda$ with $\Lambda = \mathrm{diag}(\lambda_0, ..., \lambda_{2j})$ a diagonal positive semi-definite matrix. The Wigner function at $\Omega = 0$ of $U\rho U^{\dagger}$ is then given by

$$\begin{aligned} W_{U\rho U^{\dagger}}(0) &= \mathrm{Tr}\left[U\rho U^{\dagger}\Delta(0)\right] \\ &= \mathrm{Tr}\left[UM^{\dagger}\Lambda M U^{\dagger}\Delta(0)\right]. \end{aligned}$$

By defining the unitary matrix $V = UM^{\dagger}$ and calculating the trace in the Dicke basis, we obtain (where we drop the Wigner function argument in the following)

$$W_{U\rho U^{\dagger}} = \mathrm{Tr}\left[V\Lambda V^{\dagger}\Delta(0)\right]$$

$$
\begin{aligned}
&= \sum_{p,q,k,l=0}^{2j} V_{pq}\lambda_q\delta_{qk}V_{lk}^*\Delta_l\delta_{lp} \\
&= \sum_{q,p=0}^{2j} \lambda_q \left|V_{qp}\right|^2 \Delta_p.
\end{aligned}
$$

The positive numbers $|V_{qp}|^2$ in the previous equation define the entries of a unistochastic (hence also doubly stochastic) matrix of dimension $(2j+1)\times(2j+1)$ which we denote by X,

$$
X_{qp} = \left|V_{qp}\right|^2. \tag{5.16}
$$

By the Birkhoff-von Neumann theorem, we know that X can be expressed as a convex combination of permutation matrices P_k,

$$
X = \sum_{k=1}^{N_p} c_k P_k, \tag{5.17}
$$

where $N_p = (2j+1)!$ is the total number of permutations $\pi_k \in S_{2j+1}$ with S_{2j+1} the symmetric group over $2j+1$ symbols,

$$
c_k \geq 0 \quad \forall\, k \quad \text{and} \quad \sum_{k=1}^{N_p} c_k = 1. \tag{5.18}
$$

Consequently, we have

$$
\begin{aligned}
W_{U\rho U^\dagger} &= \sum_{p,q=0}^{2j} \lambda_p X_{pq} \Delta_q \\
&= \sum_{k=1}^{N_p} c_k \sum_{p,q=0}^{2j} \lambda_p \left[P_k\right]_{pq} \Delta_q \\
&= \sum_{k=1}^{N_p} c_k \sum_{p=0}^{2j} \lambda_p \Delta_{\pi_k(p)}
\end{aligned}
$$

For a state ρ whose eigenspectrum $\boldsymbol{\lambda}$ satisfies the N_p inequalities

$$
\sum_{p=0}^{2j} \lambda_p \Delta_{\pi(p)} \geq W_{\min} \qquad \forall\, \pi \in S_{2j+1} \tag{5.19}
$$

we then have

$$W_{U\rho U^\dagger} = \sum_{k=1}^{N_p} c_k \sum_{p=0}^{2j} \lambda_p \Delta_{\pi_k(p)} \geq W_{\min}$$

for any unitary U and we conclude.

Conversely, a state has in its unitary orbits only states whose Wigner function satisfies $W(\Omega) \geq W_{\min}\ \forall\, \Omega$ if

$$W_{U\rho U^\dagger} = \sum_{k=1}^{N_p} c_k \sum_{p=0}^{2j} \lambda_p \Delta_{\pi_k(p)} \geq W_{\min} \qquad \forall\, U. \tag{5.20}$$

In particular, the unitary matrix U can correspond to any permutation matrix P, so that we have

$$W_{P\rho P^\dagger} = \sum_{p=0}^{2j} \lambda_p \Delta_{\pi(p)} \geq W_{\min} \qquad \forall\, \pi \tag{5.21}$$

and we conclude that the state satisfies (5.19).

In fact, it is enough to consider the ordered eigenvalues $\boldsymbol{\lambda}^\downarrow$ so that a state is AWB iff it verifies the most stringent inequality

$$\boldsymbol{\lambda}^\downarrow \cdot \boldsymbol{\Delta}^\uparrow = \sum_{p=0}^{2j} \lambda_p^\downarrow \Delta_p^\uparrow \geq W_{\min} \tag{5.22}$$

with the ordered eigenvalues of the kernel $\boldsymbol{\Delta}^\uparrow$. □

The proof provided for Proposition 1 can in fact be reproduced for any quasiprobability distribution $\mathcal{W}$ defined on the spherical phase space S^2 as the expectation value of a specific kernel operator $\tilde{\Delta}(\Omega)$ in a quantum state ρ; that is, via $\mathcal{W}_\rho(\Omega) = \mathrm{Tr}[\rho\tilde{\Delta}(\Omega)]$, see also Refs. [207, 206] for other generalizations. A polytope in the simplex of states will describe the absolute positivity of each quasiprobability distribution and its vertices will be determined by the eigenvalues of the defining kernel. A family of such (normalized) distributions is obtained from the s-parameterized Stratonovich-Weyl kernel (see e.g. Refs. [99, 89, 83])

$$\Delta^{(s)}(\Omega) = \sqrt{\frac{4\pi}{2j+1}} \sum_{L,M} \left(C^{jj}_{jj,L0}\right)^{-s} Y^*_{LM}(\Omega) T_{LM} \tag{5.23}$$

with $s \in [-1, 1]$. For $s = 0$, it reduces to the Wigner kernel given in Eq. (5.1).

As negative values of the Wigner function are generally considered to indicate non-classicality, the value $W_{\min} = 0$ plays a special role. Nevertheless, since Proposition 1 holds for any $W_{\min} \in [\min\{\Delta_i\}, \frac{1}{2j+1}]$ the corresponding sets of states also form polytopes, which become larger as $W_{\min}$ becomes more negative, culminating in the entire simplex when $W_{\min}$ is the smallest kernel eigenvalue $\min\{\Delta_i\}$ (which according to Eq. (5.12) is $\Delta_{j.j-1}$). There is thus a continuous transition between the one-point polytope, which represents the maximally mixed state, and the polytope containing the whole simplex. As discussed later, Fig. 5.4 in Sec. 5.4 shows a special example of this family for spin-1.

Quasiprobability distributions other than the Wigner function, such as the Husimi Q function derived from the s-ordered SW kernel (5.23) for $s = -1$, are positive by construction, implying that the polytope for $Q_{\min} = 0$ contains the entire simplex of state spectra. In this case it becomes especially interesting to consider lower bounds $Q_{\min} > 0$ and study the properties of the associated polytopes.

5.3.2 AWP polytopes

Since the conditions for being AWP depend only on the eigenspectrum $\boldsymbol{\lambda}$ of a state, it is sufficient in the following to focus on diagonal states in the Dicke basis. The condition (5.15) for $W_{\min} = 0$ defines a polytope of AWP states in the simplex of mixed spin states. Indeed, we start by noting that the equalities

$$\sum_{i=0}^{2j} \lambda_i \Delta_{\pi(i)} = 0 \tag{5.24}$$

define, for all possible permutations π, $(2j+1)!$ hyperplanes in $\mathbb{R}^{2j}$. Together they delimit a particular polytope that contains all absolutely Wigner positive states. The AWP polytopes for $j = 1$ and $j = 3/2$ are respectively represented in Figs. 5.1 and 5.2 in a barycentric coordinate system (see Appendix 5.7.2 for a reminder).

If we now restrict our attention to ordered eigenvalues $\boldsymbol{\lambda}^{\downarrow}$, we get a minimal polytope that is represented in Fig. 5.3 for $j = 1$. The full polytope is reconstructed by taking all possible permutations of the barycentric coordinates of the vertices of the minimal polytope. These vertices can be found as follows. In general we need $2j+1$ independent conditions on the vector $(\lambda_0, \lambda_1, \ldots, \lambda_{2j})$ to uniquely define (the unitary orbit of) a state ρ. One of them is given by the normalization condition $\sum_{i=0}^{2j} \lambda_i = 1$. The others correspond

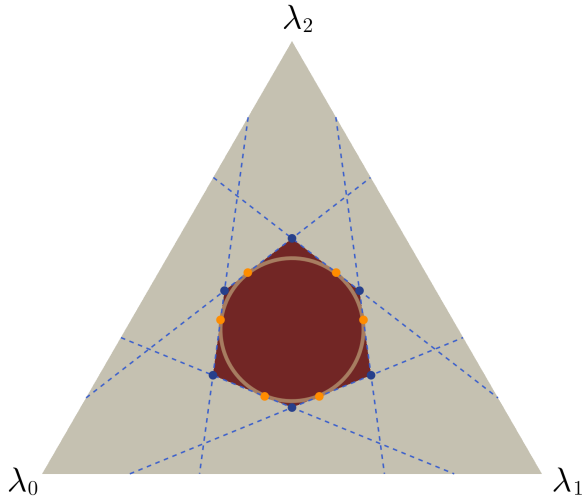

Figure 5.1: AWP polytope for $j = 1$ displayed in the barycentric coordinate system. The AWP polytope is the area shaded in dark red with the blue dashed lines marking the hyperplanes defined by Eq. (5.24). The circle is the surface of the AWP ball (see Section 5.4). The orange points represent all the permutations of the spectrum (5.37). The gray triangle corresponds to the full simplex of spin-1 states with spectrum $\boldsymbol{\lambda} = (\lambda_0, \lambda_1, \lambda_2)$.

to the fact that a vertex of the AWP polytope is the intersection of $2j$ hyperplanes each specified by an equation of the form (5.24). One of them is

$$\sum_{i=0}^{2j} \lambda_i^{\downarrow} \Delta_i^{\uparrow} = 0. \tag{5.25}$$

Let us focus on the remaining $2j - 1$. For simplicity, consider a transposition $\pi = (p, q)$ with $q > p$. The condition (5.24) becomes in this case, using (5.25),

$$\begin{aligned} & \lambda_p^{\downarrow} \Delta_q^{\uparrow} + \lambda_q^{\downarrow} \Delta_p^{\uparrow} + \sum_{\substack{i=0 \\ i \neq p,q}}^{2j} \lambda_i^{\downarrow} \Delta_i^{\uparrow} = 0 \\ \Leftrightarrow \quad & \lambda_p^{\downarrow} (\Delta_q^{\uparrow} - \Delta_p^{\uparrow}) + \lambda_q^{\downarrow} (\Delta_p^{\uparrow} - \Delta_q^{\uparrow}) = 0 \end{aligned} \tag{5.26}$$

As all the eigenvalues of the kernel are different by assumption (5.12), Eq. (5.26) is satisfied iff $\lambda_p^{\downarrow} = \lambda_q^{\downarrow}$ and, as the eigenvalues are ordered, this also means that $\lambda_k^{\downarrow} = \lambda_p^{\downarrow}$ for all k

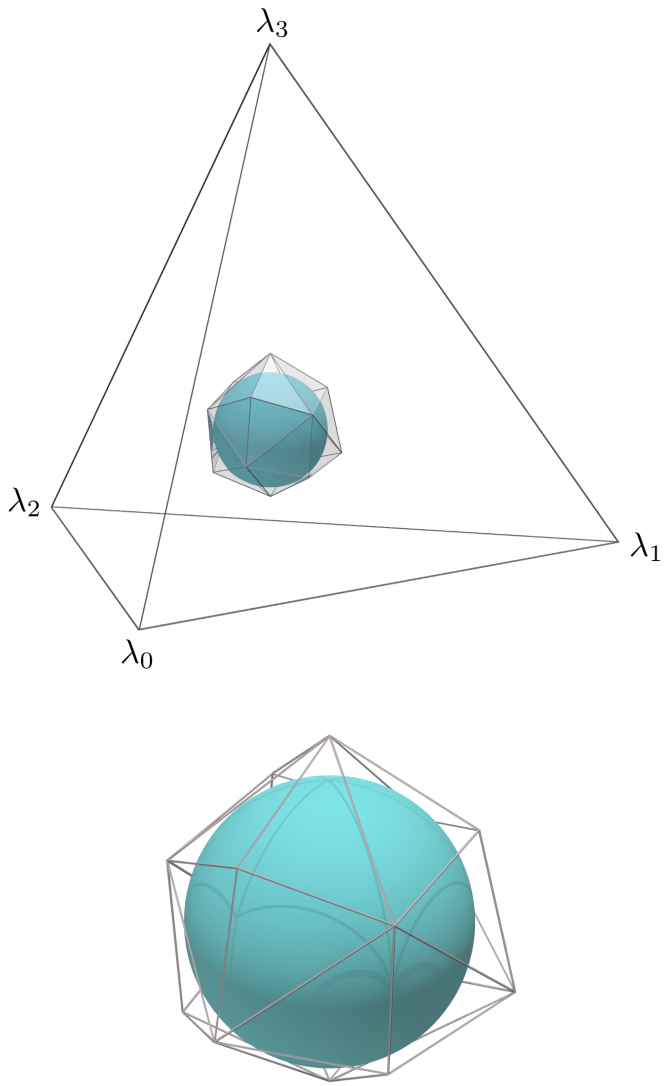

Figure 5.2: The AWP polytope for $j = 3/2$ in the barycentric coordinate system (top). The grey rods (shown in the enlarged polytope at the bottom) are the edges of the AWP polytope and the blue sphere is its largest inner ball, with radius $r_{\text{in}}^{\text{AWP}} = 1/(2\sqrt{15})$.

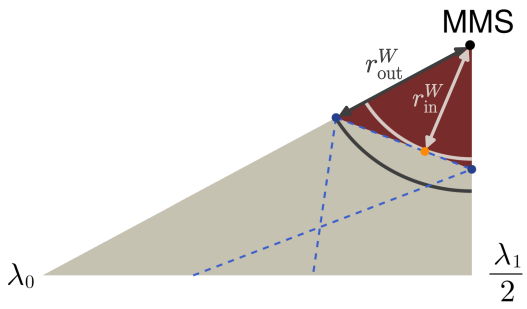

Figure 5.3: AWP minimal polytope for $j = 1$ in the barycentric coordinate system. The structure is similar to Fig. 5.1 but we only draw the part where the eigenvalues of the state are ordered in descending value. The dark point corresponds to the maximally mixed state (MMS). The inner and outer AWP balls radii, $r_{\text{in}}^{\text{AWP}}$ and $r_{\text{out}}^{\text{AWP}}$, are shown.

between p and q. Note that in this reasoning, the only forbidden transposition is $(0, 2j)$ because it would give the MMS. Hence, for a given transposition (p, q) will correspond a set of $q - p$ conditions $\lambda_l = \lambda_{l+1}$ for $l = p, \ldots, q - 1$. Therefore, as any permutation is a composition of transpositions, the $2j - 1$ conditions that follow from (5.24) eventually reduce to a set of $2j - 1$ nearest-neighbour eigenvalue equalities taken from

$$\mathcal{E} = \left(\lambda_0^{\downarrow} = \lambda_1^{\downarrow}, \lambda_1^{\downarrow} = \lambda_2^{\downarrow}, ..., \lambda_{2j-1}^{\downarrow} = \lambda_{2j}^{\downarrow}\right). \tag{5.27}$$

Since we need $2j - 1$ conditions, we can draw $2j - 1$ equalities from $\mathcal{E}$ in order to obtain a vertex. This method gives $\binom{2j}{2j-1} = 2j$ different draws and so we get $2j$ vertices for the minimal polytope. As explained previously, all other vertices of the full polytope are obtained by permuting the coordinates of the vertices of the minimal polytope. In Appendix 5.7.3, we give the barycentric coordinates of the vertices of the minimal polytope up to $j = 2$. The entirety of the preceding discussion of the AWP polytope vertices naturally extends to the AWB polytope vertices for which we must replace 0 by W_{min} in the right-hand side of the equality (5.24). However, for negative values of W_{min}, the polytope may be partially outside the simplex and some vertices will have negative-valued components, resulting in unphysical states.

A peculiar characteristic of the AWP polytope is that each point on its surface has a state in its orbit satisfying $W(0) = 0$. Indeed, for a state spectrum $\boldsymbol{\lambda}$ that satisfies (5.24)

for a given permutation π, the diagonal state ρ in the Dicke basis with $\rho_{ii} = \lambda_{\pi^{-1}(i)}$ satisfies

$$W(0) = \sum_{i=0}^{2j} \lambda_i \Delta_i = 0 \tag{5.28}$$

and is in the unitary orbit of $\boldsymbol{\lambda}$. Following the same reasoning, in the interior of the AWP polytope, there is no state with a zero-valued Wigner function.

5.3.3 Majorization condition

Here we find a condition equivalent to (5.15) for a state to be AWB based on its majorization by a mixture of the vertices of the minimal polytope.

Definition 2. *For two vectors* $\mathbf{u}$ *and* $\mathbf{v}$ *of the same length* n*, we say that* $\mathbf{u}$ *majorizes* $\mathbf{v}$*, denoted* $\mathbf{u} \succ \mathbf{v}$*, iff*

$$\sum_{k=1}^{l} u_k^{\downarrow} \geq \sum_{k=1}^{l} v_k^{\downarrow} \tag{5.29}$$

for $l < n$*, with* $\sum_{k=1}^{n} u_k = \sum_{k=1}^{n} v_k$ *and* $\mathbf{u}^{\downarrow}$ *denoting the vector* $\mathbf{u}$ *with components sorted in decreasing order.*

Proposition 2. *A state* ρ *is AWB iff its eigenvalues* $\boldsymbol{\lambda}$ *are majorized by a convex combination of the ordered vertices* $\{\boldsymbol{\lambda}_{\mathrm{v}_k}^{\downarrow}\}$ *of the corresponding AWB polytope, i.e.* $\exists\, \mathbf{c} \in \mathbb{R}_+^{2j}$ *such that*

$$\boldsymbol{\lambda} \prec \sum_{k=1}^{2j} c_k \boldsymbol{\lambda}_{\mathrm{v}_k}^{\downarrow} \tag{5.30}$$

with $\sum_{k=1}^{2j} c_k = 1$*.*

Proof. If $\boldsymbol{\lambda}$ is AWB then it can be expressed as a mixture of the vertices of the AWB polytope

$$\boldsymbol{\lambda} = \sum_{k} c_k \boldsymbol{\lambda}_{\mathrm{v}_k} \tag{5.31}$$

and the majorization (5.30) follows.

Conversely, it is known from the Schur-Horn theorem that $\mathbf{x} \succ \mathbf{y}$ iff $\mathbf{y}$ is in the convex hull of the vectors obtained by permuting the elements of $\mathbf{x}$ (i.e. the permutahedron generated by $\mathbf{x}$). Hence, if $\boldsymbol{\lambda}$ respects (5.30), it can be expressed as a convex combination of the vertices of the AWB polytope and is therefore inside it. □

5.4 Balls of absolutely Wigner bounded states

5.4.1 Largest inner ball of the AWB polytope

In this section, we calculate the radius $r_{\text{in}}^{W_{\min}}$ of the largest ball centred on the MMS contained in the polytope of AWB states and find a state ρ^* that is both on the surface of this ball and on a face of the polytope. Denoting by $r(\rho)$ the Hilbert-Schmidt distance between a state ρ and the MMS,

$$r(\rho) = \|\rho - \rho_0\|_{\text{HS}} = \sqrt{\text{Tr}\left[(\rho - \rho_0)^2\right]}, \tag{5.32}$$

we have that all valid states with $r(\rho) \leq r_{\text{in}}^{W_{\min}}$ are AWB.

Proposition 3. *The radius of the largest inner ball of the AWB polytope associated with a $W_{\min}$ value such that the ball is contained within the state simplex is*

$$r_{\text{in}}^{W_{\min}} = \frac{1 - (2j+1)W_{\min}}{2\sqrt{j(2j+1)(j+1)}}. \tag{5.33}$$

Proof. Note that the distance (5.32) is equivalent to the Euclidean distance in the simplex between the spectra $\boldsymbol{\lambda}$ and $\boldsymbol{\lambda}_0$ of ρ and the MMS respectively, i.e.

$$r(\rho) = \sqrt{\left(\sum_{i=0}^{2j} \lambda_i^2\right) - \frac{1}{2j+1}} = \|\boldsymbol{\lambda} - \boldsymbol{\lambda}_0\|.$$

In order to find the radius $r_{\text{in}}^{W_{\min}}$ (see Fig. 5.3 for $W_{\min} = 0$) of the largest inner ball of the AWB polytope, we need to find the spectra on the hyperplanes of the AWB polytope with the minimum distance to the MMS. Mathematically, this translates in the following constrained minimization problem

$$\min_{\boldsymbol{\lambda}} \|\boldsymbol{\lambda} - \boldsymbol{\lambda}_0\|^2 \quad \text{subject to} \begin{cases} \sum_{i=0}^{2j} \lambda_i = 1 \\ \boldsymbol{\lambda} \cdot \boldsymbol{\Delta} = W_{\min} \end{cases} \tag{5.34}$$

where $\boldsymbol{\Delta} = (\Delta_0, \Delta_1, ..., , \Delta_{2j})$. For this purpose, we use the method of Lagrange multipliers with the Lagrangian

$$L = \|\boldsymbol{\lambda} - \boldsymbol{\lambda}_0\|^2 + \mu_1 \left(\boldsymbol{\lambda} \cdot \boldsymbol{\Delta} - W_{\min}\right) + \mu_2 \left(1 - \sum_{i=0}^{2j} \lambda_i\right)$$

where μ_1, μ_2 are two Lagrange multipliers to be determined. The stationary points $\boldsymbol{\lambda}^*$ of the Lagrangian must satisfy the following condition

$$\frac{\partial L}{\partial \boldsymbol{\lambda}}\Big|_{\boldsymbol{\lambda}=\boldsymbol{\lambda}^*} = \mathbf{0} \quad \Leftrightarrow \quad 2\boldsymbol{\lambda}^* + \mu_1 \boldsymbol{\Delta} - \mu_2 \mathbf{1} = \mathbf{0} \tag{5.35}$$

with $\mathbf{1} = (1, 1, ..., 1)$ of length $2j+1$. By summing over the components of (5.35) and using Eq. (5.10), we readily get

$$\mu_2 = \frac{\mu_1 + 2}{2j+1}. \tag{5.36}$$

Then, by taking the scalar product of (5.35) with $\boldsymbol{\Delta}$ and using Eqs. (5.11) and (5.36), we obtain

$$\mu_1 = \frac{1 - (2j+1)W_{\min}}{2j(j+1)} \quad \text{and} \quad \mu_2 = \frac{(2j+1) - W_{\min}}{2j(j+1)}.$$

Finally, by substituting the above values for μ_1 and μ_2 in Eq. (5.35) and solving for the stationary point $\boldsymbol{\lambda}^*$, we get

$$\boldsymbol{\lambda}^* = \frac{[(2j+1) - W_{\min}]\,\mathbf{1} - [1 - (2j+1)W_{\min}]\,\boldsymbol{\Delta}}{4j(j+1)} \tag{5.37}$$

from which the inner ball radius follows as

$$r_{\text{in}}^{W_{\min}} = r(\rho^*) = \frac{1 - (2j+1)W_{\min}}{2\sqrt{j(2j+1)(j+1)}}$$

with ρ^* a state with eigenvalues (5.37). □

Let us first consider positive values of $W_{\min}$. The inner radius (5.33) vanishes for $W_{\min} = 1/(2j+1)$, corresponding to the fact that only the MMS state has a Wigner function with this minimal (and constant) value. The radius then increases as $W_{\min}$ decreases. At $W_{\min} = 0$, it reduces to the radius of the largest ball of AWP states,

$$r_{\text{in}}^{\text{AWP}} = \frac{1}{2\sqrt{j(2j+1)(j+1)}}. \tag{5.38}$$

Expressed as a function of dimension $N = 2j+1$ and re-scaled to generalized Bloch length, this result was also recently found in the context of SU(N)-covariant Wigner functions (i.e. as the phase space manifold changes dramatically with each Hilbert space dimension, rather than always being the sphere) [208]. While our bound is tight for all j in the SU(2)

setting (i.e. there always exist orbits infinitesimally further away that contain Wigner-negative states), it is unknown if this bound remains tight for such SU(N)-covariant Wigner functions for $N > 2$.

As a side comment of possible interest I would like to point out that, at least in the case of integer spin, the denominator of Eq. (5.38) happens to be proportional to the sum-of-squares formula:

$$\sum_{k=1}^{n} k^2 = \frac{n(2n+1)(n+1)}{6}. \tag{5.39}$$

This, perhaps, is a reflection of a deeper relationship to geometry and/or number theory[1].

At the critical value[2]

$$W_{\min} = \frac{\Delta_{j,j} - (2j+1)}{\Delta_{j,j}(2j+1) - 1} < 0, \tag{5.40}$$

the spectrum (5.37) acquires a first zero eigenvalue, $\lambda^*_{2j} = 0$. This corresponds to the situation where $\boldsymbol{\lambda}^*$ is simultaneously on the surface of the ball, on a face of the polytope and on an edge of the simplex as seen in Fig. 5.4. For more negative values of $W_{\min}$, Eq. (5.37) no longer represents a physical state because λ^*_{2j} becomes negative. In this situation, in order to determine the radius of larger balls containing only AWB states, additional constraints must be imposed in the optimisation procedure reflecting the fact that some elements of the spectrum of ρ are zero. Since the possible number of zero eigenvalues depends on j, we will not go further in this development. Nevertheless, in the end, when there is only one non-zero eigenvalue left (equal to 1, in which case the states are pure), the most negative $W_{\min}$ corresponds to the smallest kernel eigenvalue $\Delta_{j,j-1}$ (according to the conjecture (5.12)), and the radius is the distance $r = \sqrt{2j/(2j+1)}$ from pure states to the MMS.

Finally, it should be noted that any state resulting from the permutation of the elements of $\boldsymbol{\lambda}^*$ is also on the surface of the AWB inner ball and verify a similar equality as (5.24) for any permutation π. Thus by considering all permutations of the elements of $\boldsymbol{\lambda}^*$ we can find all states located where the AWB polytope is tangent to the AWB inner ball, as shown in Fig. 5.1 for $j = 1$ and $W_{\min} = 0$.

[1] ...or not.

[2] In the limit $j \to \infty$, as $\Delta_{j,j} \to 2$ [92], Eq. (5.40) tends to $-1/2$.

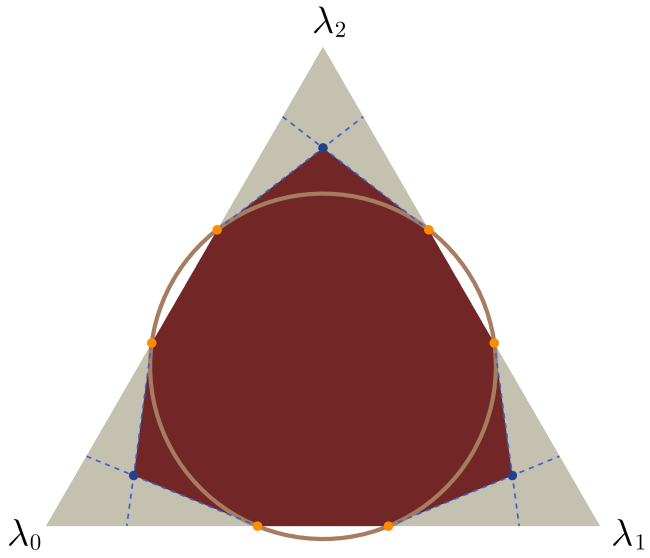

Figure 5.4: AWB polytope in the barycentric coordinate system for $j = 1$ and $W_{\min} = \frac{1}{3} + \frac{2}{3}\sqrt{2}\left(\sqrt{5} - 3\right) \approx -0.387$ as given by Eq. (5.40). The structure is similar to Fig. 5.1 but the polytope occupies a larger portion of the state space. We omit the part of the polytope that is outside the simplex.

5.4.2 Smallest outer ball of the AWB polytope

We now formulate a conjecture for the radius $r_{\text{out}}^{W_{\min}}$ of the smallest outer ball of the polytope containing all AWB states. With the set of AWB states forming a convex polytope, $r_{\text{out}}^{W_{\min}}$ must be the radius associated with the outermost vertex. Hence the problem is equivalent to finding this furthest vertex of the minimal polytope. As mentioned above, as $W_{\min}$ gets smaller and the polytopes get bigger, both the polytopes and their the inner and outer Hilbert Schmidt balls will eventually encompass unphysical states. We therefore acknowledge that intermediate calculations may take us outside of the state simplex, but final results must of course be restricted to the intersection of these objects with the simplex. When a vertex lies inside the simplex it may be referred to as a *vertex state*.

In principle, this can always be determined on a case-by-case basis via the following procedure. Recall from Sec. 5.3.2 that an AWB state with ordered spectrum $\boldsymbol{\lambda}^{\downarrow}$ located on a vertex is specified by $2j + 1$ linear eigenvalue constraints. The first is normalization,

the second is the AWB vertex criterion (i.e. Eq. (5.25) with a $W_{\min}$), and the remaining $2j-1$ come from a $(2j-1)$-sized sample from the $(2j)$-sized set of nearest-neighbour constraints (5.27). Thus the $2j$ states sitting on the $2j$ distinct vertices match up with the $\binom{2j}{2j-1} = 2j$ choices of bi-partitioning the ordered eigenvalues into a "left" set, $\boldsymbol{\omega}_n$, of size n and a "right" set, $\boldsymbol{\sigma}_n$, of size $2j+1-n$, each of which contain eigenvalues of equal value ω_n and σ_n respectively such that $\omega_n > \sigma_n$. The full eigenspectrum is the concatenation $\boldsymbol{\lambda}^{\downarrow}_{\mathrm{v}_n} = \boldsymbol{\omega}_n \circ \boldsymbol{\sigma}_n$, and normalization becomes

$$n\omega_n + (2j+1-n)\sigma_n = 1, \quad n \in \{1, ..., 2j\}. \tag{5.41}$$

As we are temporarily allowing the ordered spectrum $\boldsymbol{\lambda}^{\downarrow}$ to have negative components, Eq. (5.41) should be interpreted only as requiring the vertices to lie in the hyperplane generated by the state simplex (i.e. not necessarily within the simplex). Inserting $\boldsymbol{\lambda}^{\downarrow}_{\mathrm{v}_n}$ and (5.41) into the AWB vertex criterion the weights ω_n can be solved as a function of the kernel eigenvalues and $W_{\min}$:

$$\begin{aligned}\omega_n &= \frac{\sum_{i=n}^{2j} \Delta_i^{\uparrow} - (2j+1-n)W_{\min}}{n\sum_{i=n}^{2j} \Delta_i^{\uparrow} - (2j+1-n)\sum_{i=0}^{n-1} \Delta_i^{\uparrow}} \\ &= \frac{\tau_n - (2j+1-n)W_{\min}}{(2j+1)\tau_n - (2j+1-n)}\end{aligned} \tag{5.42}$$

where in the second line we used the unit-trace property (5.10) of the kernel and

$$\tau_n = \sum_{i=n}^{2j} \Delta_i^{\uparrow} = \sum_{i=0}^{2j-n} \Delta_i^{\downarrow} \tag{5.43}$$

is the sum over the largest $2j+1-n$ kernel eigenvalues. The purity γ_{v_n} and distance r_{v_n} of the n-th vertex is then given by

$$\gamma_{\mathrm{v}_n} = n\omega_n^2 + (2j+1-n)\sigma_n^2 \tag{5.44}$$

$$r_{\mathrm{v}_n} = \sqrt{\gamma_{\mathrm{v}_n} - \frac{1}{2j+1}}, \tag{5.45}$$

which are functions of only the kernel eigenvalues and $W_{\min}$. Note that purity, being defined as the sum of squares of the eigenvalues, remains a faithful notion of distance to the MMS even when such spectra are allowed to go negative. After computing each of these numbers, $r_{\mathrm{out}}^{W_{\min}}$ would correspond to the largest one, and the set of states satisfying

this condition would be the intersection of the associated ball with the state simplex. In Sec. 5.5.2 we present details of this procedure for $j = 1$ and $W_{\min} = 0$.

Despite this somewhat involved procedure, we numerically find it is always the case that the first vertex, v_1, remains within the state simplex for all $W_{\min} \in [\Delta_0^{\uparrow}, \frac{1}{2j+1}]$ and, relatedly, that

$$r_{\text{out}}^{W_{\min}} = r_{\mathrm{v}_1}. \tag{5.46}$$

We conjecture this to be true in all finite dimensions. Part of the difficulty in proving this in general comes from the non-trivial nature of the kernel eigenvalues (5.8) and from further numerical evidence suggesting that no vertex state ever majorizes any other vertex state.

Furthermore, with the most negative kernel eigenvalue (5.12) being $\Delta_0^{\uparrow} = \Delta_{j,j-1}$, the vertex state ρ_{v_1} takes the special form

$$\omega_1 |j, j-1\rangle\langle j, j-1| + \frac{1-\omega_1}{2j} \sum_{m \neq j-1} |j, m\rangle\langle j, m| \tag{5.47}$$

where

$$\begin{aligned} \omega_1 &= \frac{\sum_{m \neq j-1} \Delta_{j,m} - 2jW_{\min}}{\sum_{m \neq j-1} \Delta_{j,m} - 2j\Delta_{j,j-1}} \\ &= \frac{1 - \Delta_{j,j-1} - 2jW_{\min}}{1 - (2j+1)\Delta_{j,j-1}}. \end{aligned} \tag{5.48}$$

The minimal outer radius $r_{\text{out}}^{W_{\min}}$ is then conjectured to be

$$\begin{aligned} r_{\text{out}}^{W_{\min}} &= \sqrt{\gamma_{\mathrm{v}_1} - \frac{1}{2j+1}} \\ &= \sqrt{\omega_1^2 + 2j\left(\frac{1-\omega_1}{2j}\right)^2 - \frac{1}{2j+1}}. \end{aligned} \tag{5.49}$$

An operational interpretation of this radius is available by noting that the multiqubit realization of the $|j, j-1\rangle$ state, which has the most pointwise-negative Wigner function allowable (occurring at the North pole), is in fact the W state introduced in the context of LOCC entanglement classification [133]. And since the maximally mixed state has uniform eigenvalues, Eq. (5.47) may be interpreted as the end result of mixing the W state with the

maximally mixed state until the Wigner function at the North pole hits $W_{\min}$. The distance between the resulting state and the maximally mixed state is exactly our conjectured $r_{\text{out}}^{W_{\min}}$. In particular, when the Wigner function vanishes at the North pole, the radius reduces to a tight, purity-based AWP necessity condition.

Finally, when the lower bound is set to $W_{\min} = \Delta_{j,j-1}$, Eq. (5.48) becomes unity and the outer radius becomes the Hilbert-Schmidt distance to pure states, which reflects the fact that now the entire simplex is contained within the AWB polytope.

5.5 Relationship with entanglement and absolute Glauber-Sudarshan positivity

Another common quasi-probability distribution studied in the context of single spins is the Glauber-Sudarshan P function, defined through the equality

$$\rho = \frac{2j+1}{4\pi} \int P_\rho(\Omega) \, |\Omega\rangle\langle\Omega| \, d\Omega, \tag{5.50}$$

Compared to the Wigner function, the P function is not unique. Negative values of all P functions representing the same state can be interpreted as the presence of entanglement within the multi-qubit realization of the system [209]. In other words, a general state ρ of a single spin-j system admits a positive P function if and only if the many-body realization is separable (necessarily over symmetric states). This follows from the definition (5.50) of the P function as the expansion coefficients of a state ρ in the spin coherent state projector basis, and the fact that spin coherent states are the only pure product states available when the qubits are indistinguishable.

States that admit a positive P function after any global unitary transformation are called *absolutely classical* spin states [210] or *symmetric absolutely separable (SAS)* states [204]. In this section we focus entirely on the case of $W_{\min} = 0$ because negative values of the Wigner function are generally used as a witness of non-classicality and compare the AWP polytopes to the known results on SAS states. In the context of single spins, the set of SAS states is only completely characterized for spin-1/2 and spin-1. We also show that the Wigner negativity (5.6) of a positive-valued P-function state is upper-bounded by the Wigner negativity of a coherent state.

5.5.1 Spin-1/2

In the familiar case of a single qubit state ρ, the spectrum $(\lambda, 1-\lambda)$ is characterized by one number λ. The kernel eigenvalues, Eq. (5.8), are

$$\Delta_0 = \frac{1}{2}(1-\sqrt{3}), \quad \Delta_1 = \frac{1}{2}(1+\sqrt{3}) = 1-\Delta_0. \tag{5.51}$$

Letting $\lambda \geq \frac{1}{2}$ denote the larger of the two eigenvalues, the strong ordered form (5.22) becomes

$$\begin{aligned} \lambda_0\Delta_0 + \lambda_1\Delta_1 &= \lambda\Delta_0 + (1-\lambda)(1-\Delta_0) \\ &= \lambda(2\Delta_0 - 1) + 1 - \Delta_0. \end{aligned} \tag{5.52}$$

Thus the AWP polytope is described, in the 1-dimensional projection to the λ axis, as

$$\frac{1}{2} \leq \lambda \leq \frac{1-\Delta_0}{1-2\Delta_0} = \frac{1}{2} + \frac{1}{2\sqrt{3}}. \tag{5.53}$$

This may be equivalently expressed either in terms of purity γ or Bloch length $|\mathbf{n}| = \sqrt{2\gamma - 1}$,

$$\frac{1}{2} \leq \gamma \leq \frac{2}{3} \qquad \text{and} \qquad |\mathbf{n}| \leq \frac{1}{\sqrt{3}}. \tag{5.54}$$

Additionally, the distance to the maximally mixed state via Eq. (5.32) is $r \leq 1/\sqrt{6}$, which matches with the smallest ball of AWP states derived earlier, Eq. (5.33). In the case of spin-1/2 this radius coincides with the largest ball containing nothing but AWP states.

Regarding absolute P-positivity, all qubit states are SAS. This is a consequence of the Bloch ball being the convex hull of the spin-$\frac{1}{2}$ coherent states and global unitaries corresponding only to rigid rotations. Thus AWP qubit states are a strict subset of SAS qubit states.

Furthermore, due to the invariance of negativity under rigid rotation, for a single qubit there is no distinction between a state being positive (in either the Wigner or P sense) and being absolutely positive. This means that any state with Bloch radius $|\mathbf{n}| \in (1/\sqrt{3}, 1]$ has a positive P function but a negative Wigner function. This is perhaps the simplest example of the fact that, unlike the planar phase space associated with optical systems, in spin systems Glauber-Sudarshan positivity does not imply Wigner positivity.

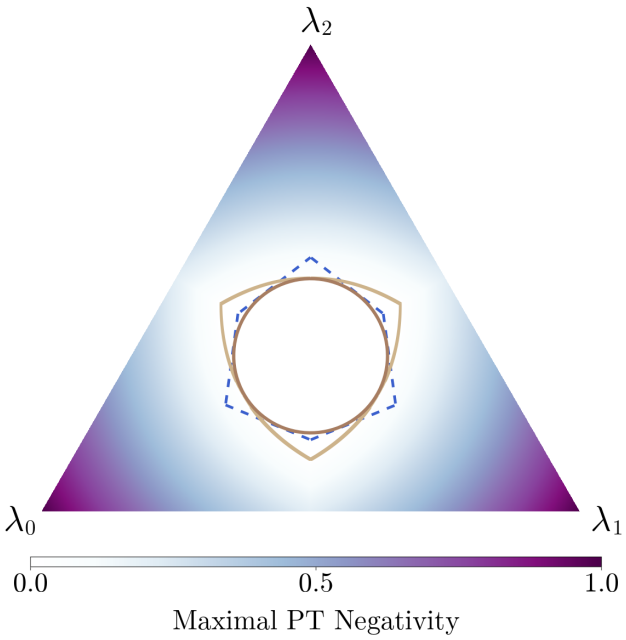

Figure 5.5: Maximal PT negativity over each unitary orbit in the $j = 1$ simplex of state spectra. The dashed blue line and red circle are respectively the AWP polytope and ball. The camel curve shows the boundary at which the negativity along the unitary orbit becomes non-zero.

5.5.2 Spin-1

For qutrits the set of AWP states and the set of SAS states are both more complicated, with neither being a strict subset of the other. For SAS states we need the following result in [204]: *the maximal value of the negativity, in the sense of the PPT criterion, in the unitary orbit of a two-qubit symmetric (or equivalently a spin-1) state ρ with spectrum $\lambda_0 \geq \lambda_1 \geq \lambda_2$ is*

$$\max\left[0, \sqrt{\lambda_0^2 + (\lambda_1 - \lambda_2)^2} - \lambda_1 - \lambda_2\right]. \tag{5.55}$$

In Fig. 5.5, we plot the resulting maximal negativity in the $j = 1$ simplex with the AWP polytope. There are clearly regions of spectra that satisfy either, both, or neither of the AWP and SAS conditions. Thus already for spin-1 there exist states with a positive P function and a negative W function and vice-versa. For $j = 1$ specifically, it was also shown in [204] that the *largest* ball of SAS states has a radius $r_{\text{in}}^P = 1/(2\sqrt{6}) \approx 0.20412$,

which is the same value as the radius $r_{\text{in}}^{\text{AWP}} = 1/(2\sqrt{6})$. Hence, for $j = 1$, the largest ball of AWP states coincides with the largest ball of SAS states as we can see in Fig. 5.5.

We now illustrate the procedure described in Sec. 5.4.2 and compute the vertex states and their radii for the case of spin-1. The two diagonal states associated to the vertices of the minimal polytope for $j = 1$ (see Fig. 5.3) are

$$\begin{aligned}\rho_{\text{v}_1} &= \omega_1 |1,-1\rangle\langle 1,-1| \\ &\quad + \frac{1-\omega_1}{2}(|1,0\rangle\langle 1,0| + |1,1\rangle\langle 1,1|), \qquad (5.56)\\ \rho_{\text{v}_2} &= \omega_2(|1,-1\rangle\langle 1,-1| + |1,0\rangle\langle 1,0|) \\ &\quad + (1-2\omega_2)|1,1\rangle\langle 1,1| \qquad (5.57)\end{aligned}$$

where the parameters ω_1 and ω_2 are found by solving the AWP criterion (5.25):

$$\begin{aligned}\omega_1 &= \frac{\Delta_{1,-1}+\Delta_{1,1}}{\Delta_{1,-1}+\Delta_{1,1}-2\Delta_{1,0}} = \frac{1}{15}(5+\sqrt{10}),\\ \omega_2 &= \frac{\Delta_{1,1}}{2\Delta_{1,1}-\Delta_{1,0}-\Delta_{1,-1}} = \frac{1}{6}\left(2+\sqrt{7-3\sqrt{5}}\right).\end{aligned} \qquad (5.58)$$

The two Hilbert-Schmidt radii (5.32) of the vertex states are then

$$\begin{aligned}r_{\text{v}_1} &= r_{\text{out}}^{\text{AWP}} = \frac{1}{\sqrt{15}} \approx 0.2582,\\ r_{\text{v}_2} &= \sqrt{\frac{1}{6}\left(7-3\sqrt{5}\right)} \approx 0.2205.\end{aligned} \qquad (5.59)$$

As conjectured, we see that $r_{\text{v}_1} = r_{\text{out}}^{W}$ for spin-1.

5.5.3 Spin-3/2

For spin-3/2, a numerical optimization (see Ref. [204] for more information) yielded the maximum negativity (in the sense of the negativity of the partial transpose of the state) in the unitary orbit of the states located on a face of the polytope. The results are displayed in Fig. 5.6 where, similar to the spin-1 case, we observe both SAS and entangled states on the face of the minimal AWP polytope. A notable difference is that, for $j = 3/2$, the largest ball containing only SAS states has a radius $r_{\text{in}}^{P} = 1/(2\sqrt{19})$ [204] which is strictly smaller than $r_{\text{in}}^{\text{AWP}} = 1/(2\sqrt{15})$. Therefore, the SAS states on the face of the polytope are necessarily outside this ball.

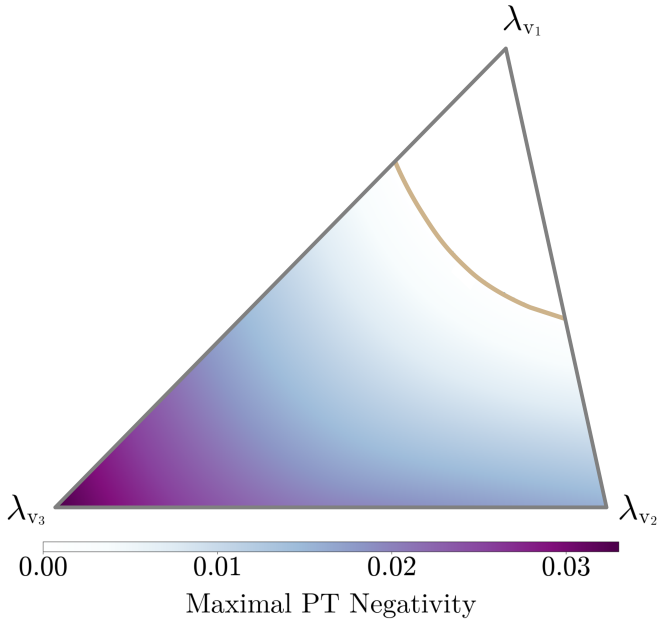

Figure 5.6: Maximal PT negativity over each unitary orbit on the face of the minimal $j = 3/2$ AWP polytope. The camel curve shows the boundary at which the negativity along the unitary orbit becomes non-zero. The notation of the vertices corresponds to the eigenspectra given in Table 5.1.

5.5.4 Spin-$j > 3/2$

In Fig. 5.7, we compare the radius of the AWP ball (5.33) with the lower bound on the radius of the ball of SAS states [210]

$$r^P \equiv \frac{\left[(4j+1)\binom{4j}{2j} - (j+1)\right]^{-1/2}}{\sqrt{4j+2}} \leq r^P_{\text{in}}. \tag{5.60}$$

This plot suggests that the balls of AWP states can be much larger than the balls of SAS states. This is confirmed by our numerical observations that sampling the hypersurface of the polytope for $j = 2, 5/2$ and 3 always yields states that have negative partial transpose in their unitary orbit. We also plot in Fig. 5.7 the conjectured radius $r^{\text{AWP}}_{\text{out}}$ of the minimal ball containing all AWP states. Notably, the scalings of $r^{\text{AWP}}_{\text{out}}$ and $r^{\text{AWP}}_{\text{in}}$ with j are different. The scaling $r^{\text{AWP}}_{\text{in}} \propto j^{-3/2}$ follows directly from Eq. (5.33). The scaling $r^{\text{AWP}}_{\text{out}} \propto j^{-1}$

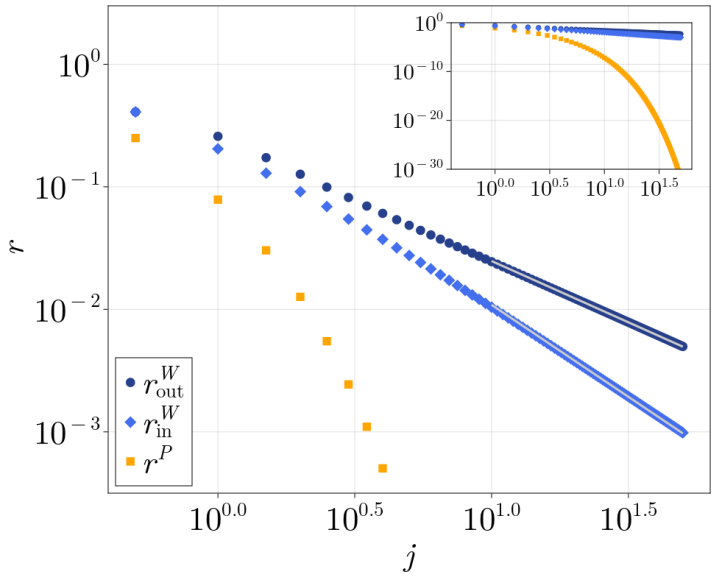

Figure 5.7: Comparison of the radii of the outer AWP ball (dark blue) and the inner AWP ball (blue) and the lower bound on the SAS ball radius (orange). For $j \geq 10$, we found excellent fits with $r^{\text{AWP}}_{\text{out,fit}} = 0.25 \times j^{-1}$ and $r^{\text{AWP}}_{\text{in,fit}} = 0.336 \times j^{-1.5}$. These are explained in the text.

can be explained by noting that the infinite-spin limit of the SU(2) Wigner kernel is the Heisenberg-Weyl Wigner kernel, which only has the two eigenvalues ± 2 [92]. Hence for sufficiently large j we may approximate $\Delta_{j,j-1} \approx -2$, which yields $\omega_1 \approx 3/(3+4j)$ from (5.48). The Laurent series of Eq. (5.49) with this approximation has leading term $1/(4j)$, exactly matching the results shown in Fig. 5.7.

5.5.5 Bound on Wigner negativity

The spin-1 case showed us that there are SAS states outside the AWP polytope, i.e. with a Wigner function admitting negative values. Here, we show very generally that the Wigner negativity (5.6) of states with an everywhere positive P function (in particular SAS states), denoted hereafter by $\rho_{P\geqslant 0}$, is upper bounded by the Wigner negativity of coherent states. Indeed, such states can always be represented as a mixture of coherent states

$$\rho_{P\geqslant 0} = \sum_i w_i \left|\alpha_i\right\rangle \left\langle\alpha_i\right| \tag{5.61}$$

with $w_i \geqslant 0$ and $\sum_i w_i = 1$. Their Wigner negativity can then be upper bounded as follows

$$\begin{aligned}
\delta(\rho_{P\geqslant 0}) &= \frac{1}{2}\int_\Gamma \left|W_{\rho_{P\geqslant 0}}(\Omega)\right| d\mu(\Omega) - \frac{1}{2} \\
&= \frac{1}{2}\int_\Gamma \left|\sum_i w_i W_{|\alpha_i\rangle}(\Omega)\right| d\mu(\Omega) - \frac{1}{2} \\
&\leqslant \underbrace{\sum_i w_i}_{=1} \underbrace{\left(\frac{1}{2}\int_\Gamma \left|W_{|\alpha_i\rangle}(\Omega)\right| d\mu(\Omega)\right)}_{=\delta(|\alpha\rangle)+\frac{1}{2}} - \frac{1}{2} \\
&= \delta\left(|\alpha\rangle\right)
\end{aligned} \tag{5.62}$$

where $\delta\left(|\alpha\rangle\right)$ is the Wigner negativity of a coherent state. Since it has been observed that the negativity of a coherent state decreases with j [1], the same is true for positive P function states.

5.6 Conclusion

We have investigated the non-classicality of unitary orbits of mixed spin-j states. Our first result is Proposition 1, which gives a complete characterization for any spin quantum number j of the set of absolutely Wigner bounded (AWB) states in the form of a polytope centred on the maximally mixed state in the simplex of mixed spin states. This amounts to an extension and alternative derivation of results from [207, 206] in the setting of quantum spin. We have studied the properties of the vertices of this polytope for different spin quantum numbers, as well as of its largest/smallest inner/outer Hilbert-Schmidt balls. In particular, we have shown that the radii of the inner and outer balls scale differently as a function of j (see Eqs. (5.33) and (5.49) as well as Fig. 5.7). We have provided an equivalent condition for a state to be AWB based on majorization theory (Proposition 2). We have also compared our results on the positivity of the Wigner function with those on the positivity of the spherical Glauber-Sudarshan function, which can be equivalently used as a classicality criterion for spin states or a separability criterion for symmetric multiqubit states. The spin-1 and spin-3/2 cases, for which analytical results are known, were closely examined and important differences were highlighted, such as the existence of Wigner-negative absolutely separable states, and, conversely, the existence of entangled absolutely Wigner-positive states. See Chapter 6 for a discussion on future work.

Acknowledgements
We would like to thank Yves-Eric Corbisier for his help in creating Fig. 5.2 with Blender [211]. The other figures were created by Jérôme Denis, mostly using the package Makie [212]. We would also like to thank V. Abgaryan and his colleagues for their correspondence regarding Refs. [206, 207, 208].

5.7 Appendices

5.7.1 Proof of relation (5.11)

We show here that the eigenvalues $\Delta_m \equiv \Delta_{j,m}$ of the Wigner kernel (5.1) verify

$$\sum_{m=-j}^{j} \Delta_m^2 = 2j+1. \tag{5.63}$$

Using the expression (5.8) we get

$$\sum_{m=-j}^{j} \Delta_m^2 = \sum_{m=-j}^{j} \sum_{L,L'=0}^{2j} \frac{(2L+1)(2L'+1)}{(2j+1)^2} \times C^{j,m}_{j,m;L,0} C^{j,m}_{j,m;L',0} \tag{5.64}$$

The Clebsh-Gordan coefficients satisfy the following relations [116]

$$C^{c,\gamma}_{a,\alpha;b,\beta} = (-1)^{a-\alpha} \sqrt{\frac{2c+1}{2b+1}} C^{b,-\beta}_{a,\alpha;c,-\gamma} \tag{5.65}$$

$$\sum_{\alpha,\beta=-j}^{j} C^{c,\gamma}_{a,\alpha;b,\beta} C^{c',\gamma'}_{a,\alpha;b,\beta} = \delta_{cc'}\delta_{\gamma\gamma'}. \tag{5.66}$$

Hence, by splitting the sum over m in two

$$\sum_{m} C^{j,m}_{j,m;L,0} C^{j,m}_{j,m;L',0} = \sum_{m_1,m_2} C^{j,m_2}_{j,m_1;L,0} C^{j,m_2}_{j,m_1;L',0} \tag{5.67}$$

and using (5.65) and (5.66), we get from (5.64)

$$\begin{aligned}\sum_{m=-j}^{j}\Delta_m^2 &= \frac{1}{2j+1}\underbrace{\sum_{L=0}^{2j}2L+1}_{=(2j+1)^2}\\ &= 2j+1\end{aligned} \tag{5.68}$$

We also include an alternative proof for interest. Consider the Dicke transition operators $|j,r\rangle\langle j,s|$ and $|j,t\rangle\langle j,u|$. These operators are orthonormal,

$$\mathrm{tr}\left(|j,r\rangle\langle j,s|^\dagger \circ |j,t\rangle\langle j,u|\right) = \delta_{ru}\delta_{st}, \tag{5.69}$$

so traciality of their Wigner functions,

$$W_{rs}(\Omega) = \langle j,s|\Delta(\Omega)|j,r\rangle \qquad \text{and} \qquad W_{tu}(\Omega) = \langle j,u|\Delta(\Omega)|j,t\rangle, \tag{5.70}$$

gives

$$\begin{aligned}\frac{2j+1}{4\pi}\int W_{rs}(\Omega)W_{tu}(\Omega)d\Omega &= \delta_{ru}\delta_{st}\\ \frac{2j+1}{4\pi}\int W_{rs}(\Omega)W_{sr}(\Omega)d\Omega &= 1\\ \frac{2j+1}{4\pi}\int \langle j,s|\Delta(\Omega)|j,r\rangle\langle j,r|\Delta(\Omega)|j,s\rangle d\Omega &= 1.\end{aligned} \tag{5.71}$$

Sum over r on both sides and use a resolution of the identity to get

$$\begin{aligned}\frac{2j+1}{4\pi}\int \langle j,s|\Delta^2(\Omega)|j,s\rangle d\Omega &= 2j+1\\ \frac{1}{4\pi}\int \langle j,s|\Delta^2(\Omega)|j,s\rangle d\Omega &= 1.\end{aligned} \tag{5.72}$$

Now sum over s and use the Ω-independence of the kernel eigenvalues to get

$$\begin{aligned}\frac{1}{4\pi}\int \mathrm{tr}[\Delta^2(\Omega)]d\Omega &= 2j+1\\ \mathrm{tr}[\Delta^2(\Omega)] &= 2j+1.\end{aligned} \tag{5.73}$$

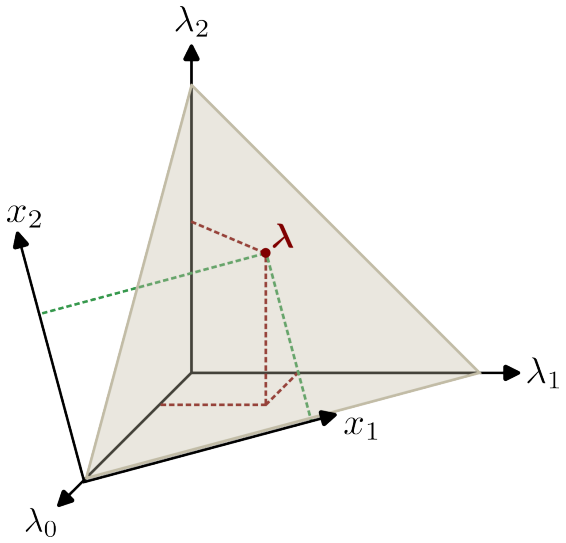

Figure 5.8: Barycentric and cartesian coordinate systems of spin state spectra for $j = 1$. The simplex in this case is an equilateral triangle, shown here in gray. The red dot corresponds to a given spectrum and its projections onto the barycentric and Cartesian coordinate system are indicated by the red and green dashed lines respectively.

5.7.2 Barycentric coordinates

A mixed spin-j state necessarily has eigenvalues λ_i that are positive and add up to one:

$$\lambda_i \geq 0, \qquad \sum_{i=0}^{2j} \lambda_i = 1. \tag{5.74}$$

This means that every state ρ has its eigenvalue spectrum in the probability simplex of dimension $2j$. For example, for $j = 1$, this simplex is a triangle shown in grey in Fig. 5.8. In geometric terms, the spectrum $(\lambda_0, \lambda_1, \lambda_2)$ defines the barycentric coordinates of a point $\boldsymbol{\lambda}$ in the simplex, as it can be considered as the centre of mass of a system of $2j$ masses placed on the vertices of the triangle.

Let's explain how to go from the barycentric coordinate system to the Cartesian coordinate system spanning the simplex. If we denote by $\{\mathbf{r}^{(i)} : i = 0, \ldots, 2j\}$ the set of $2j + 1$ vertices of the simplex, the Cartesian coordinates of a point $\boldsymbol{\lambda}$ are given by

$$x_k = \sum_{i=0}^{2j} \lambda_i \, r_k^{(i)} \tag{5.75}$$

where $r_k^{(i)}$ is the k-th Cartesian coordinate of the i-th vertex of the simplex. For $j = 1$, the simplex is an equilateral triangle with vertices having Cartesian coordinates $\mathbf{r}_1 = (0, 0)$, $\mathbf{r}_2 = (1, 0)$ and $\mathbf{r}_3 = (1/2, \sqrt{3}/2)$. For $j = 3/2$, it is a regular tetrahedron with vertices having Cartesian coordinates $\mathbf{r}_1 = (0, 0, 0)$, $\mathbf{r}_2 = (1, 0, 0)$, $\mathbf{r}_3 = (1/2, \sqrt{3}/2, 0)$ and $\mathbf{r}_4 = (1/2, (2\sqrt{3})^{-1}, \sqrt{2/3})$.

5.7.3 AWP polytope vertices for $j \leq 2$

We give in Table 5.1 for $j \leq 2$ the spin state spectra associated with the vertices of the minimal AWP polytope as they can be determined as explained in Sec. 5.3.2.

j	Vertices in barycentric coordinates
1/2	$\boldsymbol{\lambda}_{\mathrm{v}_1} \approx (0.789, 0.211)$
1	$\boldsymbol{\lambda}_{\mathrm{v}_1} \approx (0.423, 0.423, 0.153)$ $\boldsymbol{\lambda}_{\mathrm{v}_2} \approx (0.544, 0.228, 0.228)$
3/2	$\boldsymbol{\lambda}_{\mathrm{v}_1} \approx (0.294, 0.294, 0.294, 0.119)$ $\boldsymbol{\lambda}_{\mathrm{v}_2} \approx (0.33, 0.33, 0.170, 0.170)$ $\boldsymbol{\lambda}_{\mathrm{v}_3} \approx (0.4, 0.2, 0.2, 0.2)$
2	$\boldsymbol{\lambda}_{\mathrm{v}_1} \approx (0.313, 0.172, 0.172, 0.172, 0.172)$ $\boldsymbol{\lambda}_{\mathrm{v}_2} \approx (0.266, 0.266, 0.156, 0.156, 0.156)$ $\boldsymbol{\lambda}_{\mathrm{v}_3} \approx (0.24, 0.24, 0.24, 0.14, 0.14)$ $\boldsymbol{\lambda}_{\mathrm{v}_4} \approx (0.226, 0.226, 0.226, 0.226, 0.097)$

Table 5.1: Barycentric coordinates (corresponding to the spectrum of a mixed spin state) of the vertices of the minimal polytope of AWP states.

Chapter 6

Conclusions and Outlook

Inspired by previous and ongoing work in quantum information science and quantum foundations, this thesis aimed to present the first collection of results on the properties of Wigner negativity as manifest on a spherical phase space while treating it as a nonclassical physical resource. This was done using the canonical spin Wigner function, applicable to any physical system equivalent to a spin-j system, including indistinguishable sets of two-level atoms (qubits) and two-mode fixed-photon subspaces. The key takeaway is perhaps that the structure of spherical Wigner negativity is unexpectedly rich, with subtle and interesting relationships to symmetric state entanglement and state purity. Given these relationships, this work complements the growing body of research on general spin state nonclassicality and will likely be of relevance for information processing tasks involving permutationally-invariant states, transformations, and/or measurements.

It was found that unlike several measures of pure state entanglement, the ranking of the Dicke basis (generalized W states) based on Wigner negativity is highly spin-dependent, with the balanced state in general not being seen as the most nonclassical Dicke state. An approximation formula for the Wigner negativity of the generalized Greenberger–Horne–Zeilinger states was obtained, and these states were found to generically have a low amount of negativity relative to the Dicke basis and Hilbert space as a whole. Spin coherent states were proved to never be Wigner-positive but were numerically found to have minimal negativity for all spins considered. Pure states that maximize negativity were found to be generically quite different than those that maximize other phase-space notions of nonclassicality. Apart from the notable exception of the tetrahedron state in five dimensions, such maximally Wigner-negative spin states were only found to be partially

symmetric as quantified by the relatively small point-groups associated to their Majorana constellations. It was conjectured that the maximality of negativity must therefore not be based solely on either a symmetry or delocalization principle. This was especially present in the cases of the octahedron state and the icosahedron state, which were both found to have a surprisingly low amount of negativity. A similarity to entanglement was found in random states, which also appear to contain a high amount of nonclassicality on average. The relationship to state mixedness was investigated, and the existence of polytopes of absolutely Wigner bounded states was established in all dimensions and explicitly characterized. Geometric properties of these polytopes were analyzed with emphasis on the case of absolute positivity, culminating in tight, purity-based sufficiency and necessity (conjectured) criteria. It was consequently shown there must exist Wigner-negative absolutely separable states and, conversely, entangled absolutely Wigner-positive states.

There are many directions for future work. One immediate task could be to prove that spin coherent states minimize Wigner negativity over pure states. This, in addition to the present result that such states are never Wigner positive, would close the door on the possibility that SU(2) systems posses a positive subtheory. Given that spin coherent states minimize the spin uncertainty relation, together with the rapid decay of the negativity of spin coherent states to its guaranteed Wigner-positive coherent state in the infinite spin-limit, it is reasonable to believe that the lack of a positive subtheory is highly likely[1]. To prove this however appears to be a difficult problem, though a possibly fruitful approach may be to investigate any relationships with the Lieb conjecture [213] and its subsequent proof [214]. This theorem states that spin coherent states minimize the pure state Wehrl entropy [215], i.e. the continuous Shannon entropy of the spherical Husimi Q function.

Another task would be to determine the maximally Wigner-negative spin states for higher spins. This would entail a more targeted approach to evaluating the Wigner negativity integral (or equivalently the L^1 norm), either by exploiting some further structure or by using more computational power. It is conceivable that the use of spherical designs [216] may provide some computational relief, though the work of [93] on discrete sub-representations of the spherical s-ordered class suggests otherwise[2]. If such maximally Wigner-negative states could be found then perhaps a clearer pattern in the sequence of maximal constellations may arise, allowing further analysis on what, if any, geometric principle underlies such constellations.

[1] This is indeed the case, at least numerically, for the low dimensional spins considered here.

[2] Understanding this further is a research direction in of itself.

One may also study non-symmetric composite spin systems and any possible relationship to the entanglement structure therein. Some work has been done on the spin-boson coupling [192] which showed that Wigner negativity can act as an entanglement witness under certain circumstances. A perhaps even simpler next step could be to consider just two spins using the framework used in this thesis. The phase space would be more complicated, though it would be worthwhile to see how the entanglement-negativity relationship manifests in the case of distinguishable subsystems. It would also be interesting to compare different negativities; for example, is the largest possible amount of Wigner negativity of a $\frac{1}{2} \otimes \frac{1}{2}$ system the same as the case of spin-$\frac{3}{2}$? Both live in the same Hilbert space $\mathbb{C}^4$ but with different physical interpretations (i.e. different phase spaces); see also [217]. More generally, one could explore the structure of the Clebsch-Gordan decomposition through the lens of the Wigner negativity of the constituent spins.

Regarding the results on mixed states, one notable observation drawn from the numerics is that the set of symmetric absolutely separable (SAS) states appears to shrink relative to the set of absolutely Wigner positive (AWP) states as j increases, which in turn occupies a progressively smaller volume of the simplex of state spectra. As a direct comparison between Wigner negativity and entanglement, further research is needed to explore this behaviour. A related direction for future work could be to explore the ratio of the volume of the absolutely Wigner bounded (AWB) polytopes to the volume of the full simplex; this would essentially be the *global indicator of classicality* introduced and studied in Refs. [205, 207, 208] but particularised to spin systems.

More generally, and as briefly mentioned in Chapter 5, the techniques used for the Wigner function may be easily applied to other distinguished quasiprobability distributions. For example, preliminary results suggest that the absolutely Husimi bounded (AHB) polytopes have the same geometry as the simplex, but are simply reduced in size by a factor depending on $Q_{\min} \in [0, \frac{1}{2j+1}]$. Future work could explore this further and investigate its consequences for the geometric measure of entanglement of multiqubit symmetric states (which as discussed in Chapter 4 is related to the flatness of the Husimi function). Another interesting idea is to study how these polytopes change with respect to the spherical s-ordering parameter.

Moving to a more abstract and speculative discussion, let us return to the fact that spin coherent states are always slightly Wigner-negative. As mentioned in Chapter 4 this property appears to be unique to the spin Wigner function in comparison to the Gaussian subtheory of continuous Heisenberg-Weyl symmetry and the stabilizer subtheory of discrete Heisenberg-Weyl symmetry. And while it is understandable that one may view the (likely)

lack of a positive subtheory for spin as a reason to doubt the future of Wigner negativity on the sphere, I believe, mainly due to the canonicality of the spin Wigner function and its strong mathematical relationship to the original Wigner function, that we should instead view this as a meaningful clue to be investigated further. This seems especially pertinent to the case of the qubit. Indeed the spin Wigner function is perfectly well-defined for the single qubit while the Gross-Wigner function is not, at least not in the same sense as in odd dimensions. And since the qubit is so fundamental to quantum information science, it seems reasonable to speculate that studying the relationship between these two Wigner functions will provide insight to both. Perhaps relatedly, it is worth explicitly pointing out that the spin Wigner function and the Gross-Wigner function may be thought to come from two different generalizations of the Pauli matrices: the former views them as Hermitian matrices (i.e. algebra elements, observables) while the latter views them as unitary matrices (i.e. group elements, translations). See also this quote from the seminal 1989 paper by Joseph C. Várilly and José M. Gracia-Bondía:

> Some people have thought of a *discrete* formulation of spin variables. In this context, the interesting papers by Wootters [24] and by Cohendet *et at.* [26] must be mentioned. Here, phase space is taken to be the direct product of two copies of the cyclic group $\mathbb{Z}_n$. A correspondence between operators on $\mathbb{C}^n$ and functions on $\mathbb{Z}_n \times \mathbb{Z}_n$, incorporating the covariance and traciality properties, can be constructed without much trouble for n odd.... The symmetry group can be taken to be the finite Heisenberg group based on $\mathbb{Z}_n$. This and the fact that in a discrete representation all the points are essentially equivalent...suggest that this "Quantum Mechanics with finitely many degrees of freedom" is a discrete version of ordinary Moyal theory rather than a theory for spin. [89]

A few years later one of the authors says further:

> From the physical point of view, the prevalence of the Heisenberg groups in quantization is an artifact...Schemes based on other groups may look anomalous to the Heisenberg-trained mind. [85]

This train of thought has led me to consider a possible relationship between phase space topology/geometry and the nonclassicality of its associated Moyal theory. Are some phase space manifolds (i.e. types of physical systems) somehow intrinsically more nonclassical

than others? Some heuristic credence can be given, at least in the presence of symmetry where the phase space is (a quotient of) the underlying dynamical group [83, 84]. In this setting it is reasonable to suspect that the amount of Wigner negativity present (perhaps in some aggregate sense) is a reflection of the degree of non-commutativity of the underlying group, *via* the shape of the associated phase space. And since some groups may be thought of as being "more" non-commutative than others[3], perhaps therefore some phase spaces are "more" quantum than others. This idea is in line with the observation that the Heisenberg-Weyl Moyal theories possess a positive subtheory while the SU(2) Moyal theory (almost certainly) does not. This could be because the Heisenberg-Weyl group is *nilpotent* and so can be mathematically interpreted as being "barely" non-commutative[4]. The group SU(2) on the other hand is not nilpotent and so is "more" non-commutative than Heisenberg-Weyl. Perhaps this is the reason why the coherent state is positive but the spin coherent state is not. Perhaps a consistent way to compare phase spaces is to study the Perelomov G-coherent state associated to the underlying group G [81]. What about SU(3)? What about other non-nilpotent groups? Is it reasonable to conjecture that any Moyal theory based on a nilpotent group will possess a positive subtheory? What about the converse? Given that the significance of Wigner negativity in Heisenberg-Weyl systems is (in my view) hard to overstate, these ideas and related ones I believe could be the subject matter for interesting, foundational, and possibly practical future work.

Finally and relatedly, of course another important line of inquiry would be to connect spherical Wigner negativity and beyond to quantum contextuality (either in the Kochen-Specker [54, 55], Spekkens [218], or perhaps some other sense [219]) as has been done in Heisenberg-Weyl systems. Such a connection would significantly broaden the understanding of both topics. I believe, at least for the Kochen-Specker approach, that the mathematical field of *integral geometry* may be relevant [220]. Among other topics, this field discusses the reconstruction of a function from its integrals over sets of strata (i.e. line integrals over various sets of parallel lines). In the case of bosonic systems such line integrals are the Gaussian quadratures, viewed as probability distribution *marginals*, which of course are proper probability distributions that can then be used to reconstruct the Wigner function via the (inverse) Radon transform. See [62] and related work for this idea in the context of connecting Wigner negativity to Kochen-Specker contextuality. Hence

[3]Perhaps measured, for example, by some relative volume of the commutator subgroup and/or the associated abelianization of the group.

[4]This can be seen by the fact that nested commutators of the algebra elements $\{a, a^\dagger, I\}$ terminate after a finite number of nests.

this generalized picture from integral geometry may be thought of as a vast expansion of the Radon transform to more general phase space manifolds [220], which in my view retains the underlying spirit of Kochen-Specker contextuality: composing locally consistent data to yield a globally inconsistent datum [221, 222]. Phase spaces with more complicated topology may have more complicated strata, which in turn may affect the marginals' incompatibility as it relates to Wigner function reconstruction. This in turn may affect the Wigner negativity structure, which, intuitively speaking, reflects this incompatibility. This idea is furthermore, at least naively, in line with the spherical system not having a positive subtheory because the sphere does not have a proper set of parallel lines due to the hairy ball theorem [223], which perhaps implies a more frustrated reconstruction process and therefore "more" Wigner negativity present in its associated Moyal theory.

References

[1] J Davis, M Kumari, R B Mann, and S Ghose. Wigner negativity in spin-j systems. *Phys. Rev. Res.*, 3:033134, Aug 2021. iv, 30, 47, 53, 78, 80, 101

[2] J Davis, R A Hennigar, R B Mann, and S Ghose. Stellar representation of extremal Wigner-negative spin states. *Journal of Physics A: Mathematical and Theoretical*, 56(26):265302, Jun 2023. iv, 30, 47, 75

[3] J Denis, J Davis, R B Mann, and J Martin. Polytopes of absolutely Wigner bounded spin states, 2023. iv, 74

[4] E Wigner. On the quantum correction for thermodynamic equilibrium. *Phys. Rev.*, 40:749–759, Jun 1932. 1

[5] H Weyl. Quantenmechanik und gruppentheorie. *Zeitschrift für Physik*, 46(1-2):1–46, 1927. 1

[6] J E Moyal. Quantum mechanics as a statistical theory. *Mathematical Proceedings of the Cambridge Philosophical Society*, 45(1):99–124, 1949. 1

[7] H J Groenewold. On the principles of elementary quantum mechanics. *Physica*, 12(7):405–460, Oct 1946. 1

[8] W Heisenberg. Über quantentheoretische umdeutung kinematischer und mechanischer beziehungen. *Zeitschrift für Physik*, 33(1):879–893, 1925. 1

[9] R P Rundle and M J Everitt. Overview of the phase space formulation of quantum mechanics with application to quantum technologies. *Advanced Quantum Technologies*, 4(6):2100016, 2021. 2, 78

[10] K Husimi. Some formal properties of the density matrix. *Proceedings of the Physico-Mathematical Society of Japan. 3rd Series*, 22(4):264–314, 1940. 2

[11] E C G Sudarshan. Equivalence of semiclassical and quantum mechanical descriptions of statistical light beams. *Phys. Rev. Lett.*, 10:277–279, Apr 1963. 2

[12] R J Glauber. Coherent and incoherent states of the radiation field. *Phys. Rev.*, 131:2766–2788, Sep 1963. 2

[13] Y Kano. A new phase-space distribution function in the statistical theory of the electromagnetic field. *Journal of Mathematical Physics*, 6(12):1913–1915, Dec 1965. 2

[14] K E Cahill and R J Glauber. Ordered expansions in boson amplitude operators. *Phys. Rev.*, 177:1857–1881, Jan 1969. 2, 13

[15] K E Cahill and R J Glauber. Density operators and quasiprobability distributions. *Phys. Rev.*, 177:1882–1902, Jan 1969. 2

[16] G S Agarwal and E Wolf. Calculus for functions of noncommuting operators and general phase-space methods in quantum mechanics. I. mapping theorems and ordering of functions of noncommuting operators. *Phys. Rev. D*, 2:2161–2186, Nov 1970. 2

[17] M Hillery, R F O'Connell, M O Scully, and E Wigner. Distribution functions in physics: Fundamentals. *Physics Reports*, 106(3):121–167, Apr 1984. 2

[18] N Lütkenhaus and S M Barnett. Nonclassical effects in phase space. *Phys. Rev. A*, 51:3340–3342, Apr 1995. 2

[19] A Grossmann. Parity operator and quantization of delta-functions. *Communications in Mathematical Physics*, 48(3):191–194, 1976. 2, 25, 77

[20] A Royer. Wigner function as the expectation value of a parity operator. *Phys. Rev. A*, 15:449–450, Feb 1977. 2, 25, 77, 80

[21] R F Bishop and A Vourdas. Displaced and squeezed parity operator: Its role in classical mappings of quantum theories. *Phys. Rev. A*, 50:4488–4501, Dec 1994. 2

[22] J H Hannay and M V Berry. Quantization of linear maps on a torus-fresnel diffraction by a periodic grating. *Physica D: Nonlinear Phenomena*, 1(3):267–290, Sep 1980. 2

[23] J Schwinger. Unitary operator bases. *Proceedings of the National Academy of Sciences*, 46(4):570–579, Apr 1960. 2

[24] W K Wootters. A Wigner-function formulation of finite-state quantum mechanics. *Annals of Physics*, 176(1):1–21, May 1987. 2, 109

[25] K S Gibbons, M J Hoffman, and W K Wootters. Discrete phase space based on finite fields. *Phys. Rev. A*, 70:062101, Dec 2004. 2

[26] O Cohendet, P Combe, M Sirugue, and M Sirugue-Collin. A stochastic treatment of the dynamics of an integer spin. *Journal of Physics A: Mathematical and General*, 21(13):2875, Jul 1988. 2, 109

[27] U Leonhardt. Quantum-state tomography and discrete Wigner function. *Phys. Rev. Lett.*, 74:4101–4105, May 1995. 2

[28] U Leonhardt. Discrete Wigner function and quantum-state tomography. *Phys. Rev. A*, 53:2998–3013, May 1996. 2

[29] A B Klimov and C Muñoz. Discrete Wigner function dynamics. *Journal of Optics B: Quantum and Semiclassical Optics*, 7(12):S588–S600, Dec 2005. 2

[30] A B Klimov, C Muñoz, and J L Romero. Geometrical approach to the discrete Wigner function in prime power dimensions. *Journal of Physics A: Mathematical and General*, 39(46):14471–14497, Nov 2006. 2

[31] A Vourdas. Quantum systems with finite Hilbert space. *Reports on Progress in Physics*, 67(3):267–320, Mar 2004. 2

[32] D Gross. Hudson's theorem for finite-dimensional quantum systems. *Journal of Mathematical Physics*, 47(12):122107, Dec 2006. 2, 3, 75

[33] R Jagannathan, T S Santhanam, and R Vasudevan. Finite-dimensional quantum mechanics of a particle. *International Journal of Theoretical Physics*, 20(10):755–773, Oct 1981. 2

[34] A Singh and S M Carroll. Modeling position and momentum in finite-dimensional Hilbert spaces via generalized Pauli operators, 2020. 2

[35] S L Braunstein and P van Loock. Quantum information with continuous variables. *Rev. Mod. Phys.*, 77:513–577, Jun 2005. 3

[36] C Weedbrook, S Pirandola, R García-Patrón, N J Cerf, T C Ralph, J H Shapiro, and S Lloyd. Gaussian quantum information. *Rev. Mod. Phys.*, 84:621–669, May 2012. 3

[37] M Walschaers. Non-Gaussian quantum states and where to find them. *PRX Quantum*, 2:030204, Sep 2021. 3

[38] M A Nielsen and I L Chuang. *Quantum Computation and Quantum Information: 10th Anniversary Edition*. Cambridge University Press, Cambridge, 2010. 3

[39] J Watrous. *The Theory of Quantum Information*. Cambridge University Press, Cambridge, 2018. 3

[40] R L Hudson. When is the wigner quasi-probability density non-negative? *Reports on Mathematical Physics*, 6(2):249–252, Oct 1974. 3, 33, 75

[41] F Soto and P Claverie. When is the Wigner function of multidimensional systems nonnegative? *Journal of Mathematical Physics*, 24(1):97–100, Jan 1983. 3, 33

[42] D Gottesman. Stabilizer codes and quantum error correction, 1997. 3

[43] S D Bartlett, B C Sanders, S L Braunstein, and K Nemoto. Efficient classical simulation of continuous variable quantum information processes. *Phys. Rev. Lett.*, 88:097904, Feb 2002. 3

[44] S D Bartlett and B C Sanders. Efficient classical simulation of optical quantum information circuits. *Phys. Rev. Lett.*, 89:207903, Oct 2002. 3

[45] A Mari and J Eisert. Positive Wigner functions render classical simulation of quantum computation efficient. *Phys. Rev. Lett.*, 109:230503, Dec 2012. 3, 74

[46] V Veitch, N Wiebe, C Ferrie, and J Emerson. Efficient simulation scheme for a class of quantum optics experiments with non-negative Wigner representation. *New Journal of Physics*, 15(1):013037, Jan 2013. 3

[47] S Rahimi-Keshari, T C Ralph, and C M Caves. Sufficient conditions for efficient classical simulation of quantum optics. *Phys. Rev. X*, 6:021039, Jun 2016. 3

[48] E F Galvão. Discrete Wigner functions and quantum computational speedup. *Phys. Rev. A*, 71:042302, Apr 2005. 3

[49] C Cormick, E F Galvão, D Gottesman, J P Paz, and A O Pittenger. Classicality in discrete Wigner functions. *Phys. Rev. A*, 73:012301, Jan 2006. 3

[50] W van Dam and M Howard. Noise thresholds for higher-dimensional systems using the discrete Wigner function. *Phys. Rev. A*, 83:032310, Mar 2011. 3

[51] V Veitch, C Ferrie, D Gross, and J Emerson. Negative quasi-probability as a resource for quantum computation. *New Journal of Physics*, 14(11):113011, Nov 2012. 3, 33, 74

[52] L Kocia, Y Huang, and P Love. Discrete Wigner function derivation of the Aaronson–Gottesman tableau algorithm. *Entropy*, 19(7), 2017. 3

[53] S Aaronson and D Gottesman. Improved simulation of stabilizer circuits. *Phys. Rev. A*, 70:052328, Nov 2004. 3

[54] S Kochen and E P Specker. The problem of hidden variables in quantum mechanics. *Journal of Mathematics and Mechanics*, 17(1):59–87, 1967. 3, 110

[55] C Budroni, A Cabello, O Gühne, M Kleinmann, and J-Å Larsson. Kochen-Specker contextuality. *Rev. Mod. Phys.*, 94:045007, Dec 2022. 3, 110

[56] S Bravyi and A Kitaev. Universal quantum computation with ideal Clifford gates and noisy ancillas. *Phys. Rev. A*, 71:022316, Feb 2005. 3

[57] R Raussendorf. Contextuality in measurement-based quantum computation. *Phys. Rev. A*, 88:022322, Aug 2013. 3

[58] M Howard, J Wallman, V Veitch, and J Emerson. Contextuality supplies the 'magic' for quantum computation. *Nature*, 510(7505):351–355, Jun 2014. 3, 74

[59] J Bermejo-Vega, N Delfosse, D E Browne, C Okay, and R Raussendorf. Contextuality as a resource for models of quantum computation with qubits. *Phys. Rev. Lett.*, 119:120505, Sep 2017. 3

[60] R W Spekkens. Negativity and contextuality are equivalent notions of nonclassicality. *Phys. Rev. Lett.*, 101:020401, Jul 2008. 3

[61] N Delfosse, C Okay, J Bermejo-Vega, D E Browne, and R Raussendorf. Equivalence between contextuality and negativity of the Wigner function for qudits. *New Journal of Physics*, 19(12):123024, Dec 2017. 3, 74

[62] R I Booth, U Chabaud, and P-E Emeriau. Contextuality and Wigner negativity are equivalent for continuous-variable quantum measurements. *Phys. Rev. Lett.*, 129:230401, Nov 2022. 3, 74, 110

[63] P-E Emeriau. The interplay between quantum contextuality and Wigner negativity, 2022. 3

[64] D Schmid, H Du, J H Selby, and M F Pusey. Uniqueness of noncontextual models for stabilizer subtheories. *Phys. Rev. Lett.*, 129:120403, Sep 2022. 3

[65] V Veitch, S A Hamed Mousavian, D Gottesman, and J Emerson. The resource theory of stabilizer quantum computation. *New Journal of Physics*, 16(1):013009, Jan 2014. 3, 74

[66] R Takagi and Q Zhuang. Convex resource theory of non-Gaussianity. *Phys. Rev. A*, 97:062337, Jun 2018. 3

[67] F Albarelli, M G Genoni, M G A Paris, and A Ferraro. Resource theory of quantum non-Gaussianity and Wigner negativity. *Phys. Rev. A*, 98:052350, Nov 2018. 3, 74

[68] X Wang, M M Wilde, and Y Su. Quantifying the magic of quantum channels. *New Journal of Physics*, 21(10):103002, Oct 2019. 3, 74

[69] J A Vaccaro and D T Pegg. Wigner function for number and phase. *Phys. Rev. A*, 41:5156–5163, May 1990. 3

[70] M V Berry. Semi-classical mechanics in phase space: A study of Wigner's function. *Philosophical Transactions of the Royal Society of London. Series A, Mathematical and Physical Sciences*, 287(1343):237–271, Oct 1977. 3

[71] N Mukunda. Wigner distribution for angle coordinates in quantum mechanics. *American Journal of Physics*, 47(2):182–187, Feb 1979. 3

[72] J P Bizarro. Weyl-Wigner formalism for rotation-angle and angular-momentum variables in quantum mechanics. *Phys. Rev. A*, 49:3255–3276, May 1994. 3

[73] O Arratia and M A del Olmo. Moyal quantization on the cylinder. *Reports on Mathematical Physics*, 40(2):149–157, Oct 1997. 3

[74] I Rigas, L L Sánchez-Soto, A B Klimov, J Řeháček, and Z Hradil. Full quantum reconstruction of vortex states. *Phys. Rev. A*, 78:060101, Dec 2008. 3

[75] H A Kastrup. Wigner functions for the pair angle and orbital angular momentum. *Phys. Rev. A*, 94:062113, Dec 2016. 3

[76] J-P Gazeau and R Murenzi. Integral quantization for the discrete cylinder. *Quantum Reports*, 4(4):362–379, Sep 2022. 3

[77] F A Berezin. Quantization. *Mathematics of the USSR-Izvestiya*, 8(5):1109, Oct 1974. 4

[78] F A Berezin. General concept of quantization. *Communications in Mathematical Physics*, 40(2):153–174, Jun 1975. 4

[79] F Bayen, M Flato, C Fronsdal, A Lichnerowicz, and D Sternheimer. Deformation theory and quantization. I. Deformations of symplectic structures. *Annals of Physics*, 111(1):61–110, Mar 1978. 4

[80] F Bayen, M Flato, C Fronsdal, A Lichnerowicz, and D Sternheimer. Deformation theory and quantization. II. Physical applications. *Annals of Physics*, 111(1):111–151, Mar 1978. 4

[81] A Perelomov. *Generalized Coherent States and Their Applications*. Springer Berlin Heidelberg, Berlin, Heidelberg, 1986. 4, 12, 22, 110

[82] J-P Gazeau. *Coherent States in Quantum Physics*. Wiley, 1 edition, Sep 2009. 4

[83] C Brif and A Mann. A general theory of phase-space quasiprobability distributions. *Journal of Physics A: Mathematical and General*, 31(1):L9–L17, Jan 1998. 4, 5, 12, 83, 110

[84] C Brif and A Mann. Phase-space formulation of quantum mechanics and quantum-state reconstruction for physical systems with Lie-group symmetries. *Phys. Rev. A*, 59:971–987, Feb 1999. 4, 5, 12, 22, 24, 27, 77, 110

[85] J M Gracia-Bondía. *Generalized Moyal quantization on homogeneous symplectic spaces*. Contemporary Mathematics. American Mathematical Society, Providence, R.I, 1992. 4, 12, 109

[86] J M Radcliffe. Some properties of coherent spin states. *Journal of Physics A: General Physics*, 4(3):313–323, May 1971. 4, 12, 15

[87] F T Arecchi, E Courtens, R Gilmore, and H Thomas. Atomic coherent states in quantum optics. *Phys. Rev. A*, 6:2211–2237, Dec 1972. 4, 11, 12, 13, 14, 15, 27, 42, 52, 137

[88] R L Stratonovich. On distributions in representation space. *Journal of Experimental and Theoretical Physics*, 4(31):1012–1020, 1956. 4, 75, 77

[89] J M Gracia-Bondía and J C Várilly. The Moyal representation for spin. *Annals of Physics*, 190(1):107–148, Feb 1989. 4, 5, 22, 26, 27, 35, 75, 76, 77, 83, 109, 135

[90] Y S Kim and W W Zachary. *The Physics of Phase Space Nonlinear Dynamics and Chaos, Geometric Quantization, and Wigner Function*. Springer Berlin, Berlin, softcover reprint of the original 1st ed. 1987 edition, 2014. 4, 22

[91] J P Dowling, G S Agarwal, and W P Schleich. Wigner distribution of a general angular-momentum state: Applications to a collection of two-level atoms. *Phys. Rev. A*, 49:4101–4109, May 1994. 4, 22, 75, 77

[92] J-P Amiet and S Weigert. Contracting the Wigner kernel of a spin to the Wigner kernel of a particle. *Phys. Rev. A*, 63:012102, Dec 2000. 4, 5, 22, 25, 28, 31, 42, 76, 91, 100

[93] S Heiss and S Weigert. Discrete Moyal-type representations for a spin. *Phys. Rev. A*, 63:012105, Dec 2000. 4, 22, 26, 79, 107

[94] A B Klimov. Exact evolution equations for SU(2) quasidistribution functions. *Journal of Mathematical Physics*, 43(5):2202–2213, 2002. 4, 22

[95] P de M Rios and E Straume. *Symbol Correspondences for Spin Systems*. Springer International Publishing, 2014. 4, 12, 26

[96] T Tilma, M J Everitt, J H Samson, W J Munro, and K Nemoto. Wigner functions for arbitrary quantum systems. *Phys. Rev. Lett.*, 117:180401, Oct 2016. 4, 22

[97] B Koczor, R Zeier, and S J Glaser. Continuous phase-space representations for finite-dimensional quantum states and their tomography. *Phys. Rev. A*, 101:022318, Feb 2020. 4, 5, 22, 25, 27, 28, 31, 42, 59, 61, 75, 77, 80

[98] A B Klimov, J L Romero, and H de Guise. Generalized SU(2) covariant Wigner functions and some of their applications. *Journal of Physics A: Mathematical and Theoretical*, 50(32):323001, August 2017. 4, 8, 12, 22, 75, 77

[99] G S Agarwal. Relation between atomic coherent-state representation, state multipoles, and generalized phase-space distributions. *Phys. Rev. A*, 24:2889–2896, Dec 1981. 4, 22, 27, 78, 83

[100] B Friedrich and D Herschbach. Stern and Gerlach: How a bad cigar helped reorient atomic physics. *Physics Today*, 56(12):53–59, Dec 2003. 5

[101] L C Biedenharn and J D Louck. *Angular momentum in quantum physics: theory and application*. Encyclopedia of mathematics and its applications; Section, Mathematics of physics. Cambridge University Press, Cambridge; New York, NY, USA, 1984. 5, 8, 17, 21

[102] O Giraud, P Braun, and D Braun. Classicality of spin states. *Phys. Rev. A*, 78:042112, Oct 2008. 5, 52, 53, 76

[103] T Bastin, S Krins, P Mathonet, M Godefroid, L Lamata, and E Solano. Operational families of entanglement classes for symmetric n-qubit states. *Phys. Rev. Lett.*, 103:070503, Aug 2009. 5, 19

[104] P Mathonet, S Krins, M Godefroid, L Lamata, E Solano, and T Bastin. Entanglement equivalence of n-qubit symmetric states. *Phys. Rev. A*, 81:052315, May 2010. 5, 19

[105] M Aulbach, D Markham, and M Murao. The maximally entangled symmetric state in terms of the geometric measure. *New Journal of Physics*, 12(7):073025, jul 2010. 5, 46, 57, 60, 61, 64, 73

[106] Z Wang and D Markham. Nonlocality of symmetric states. *Phys. Rev. Lett.*, 108:210407, May 2012. 5, 19

[107] D Baguette, T Bastin, and J Martin. Multiqubit symmetric states with maximally mixed one-qubit reductions. *Phys. Rev. A*, 90:032314, Sep 2014. 5, 49, 50

[108] O Giraud, D Braun, D Baguette, T Bastin, and J Martin. Tensor representation of spin states. *Phys. Rev. Lett.*, 114:080401, Feb 2015. 5, 49

[109] A Z Goldberg, A B Klimov, M Grassl, G Leuchs, and L L Sánchez-Soto. Extremal quantum states. *AVS Quantum Science*, 2(4):044701, 2020. 5, 70

[110] E Serrano-Ensástiga and D Braun. Majorana representation for mixed states. *Phys. Rev. A*, 101:022332, Feb 2020. 5, 22, 50

[111] A Z Goldberg, M Grassl, G Leuchs, and L L Sánchez-Soto. Quantumness beyond entanglement: The case of symmetric states. *Phys. Rev. A*, 105:022433, Feb 2022. 5

[112] J Denis and J Martin. Extreme depolarization for any spin. *Phys. Rev. Res.*, 4:013178, Mar 2022. 5, 22

[113] E Majorana. Atomi orientati in campo magnetico variabile. *Il Nuovo Cimento*, 9(2):43–50, Feb 1932. 5, 18, 21

[114] Luisa C, editor. *Scientific Papers of Ettore Majorana: A New Expanded Edition*. Springer International Publishing, Cham, 2020. 5, 18, 21

[115] A W Harrow. The church of the symmetric subspace, 2013. 5, 16, 75

[116] D A Varshalovich, A N Moskalev, and V K Khersonskii. *Quantum Theory of Angular Momentum*. World Scientific, 1988. 8, 78, 102

[117] N Jeevanjee. *An Introduction to Tensors and Group Theory for Physicists*. Birkhauser Boston, Boston, 2011. 8

[118] J J Sakurai and J Napolitano. *Modern quantum mechanics*. Cambridge University Press, Cambridge, third edition edition, 2021. 8

[119] U Fano. Geometrical characterization of nuclear states and the theory of angular correlations. *Phys. Rev.*, 90:577–579, May 1953. 10

[120] H Bacry. Physical significance of minimum uncertainty states of an angular momentum system. *Phys. Rev. A*, 18:617–619, Aug 1978. 11, 37, 38, 50

[121] D A Trifonov. The uncertainty way of generalization of coherent states. In *Proceedings of the International Conference on Geometry, Integrability and Quantization*, volume 1, pages 257–283. Bulgarian Academy of Sciences, Institute for Nuclear Research and Nuclear Energy, 2000. 11

[122] N B e Sá. Uncertainty for spin systems. *Journal of Mathematical Physics*, 42(3):981–990, Mar 2001. 11

[123] H Bacry. Orbits of the rotation group on spin states. *Journal of Mathematical Physics*, 15(10):1686–1688, 1974. 12

[124] H Bacry. *Group theory and constellations*. Publibook, Paris, 2004. 12

[125] R P Feynman. An operator calculus having applications in quantum electrodynamics. *Phys. Rev.*, 84:108–128, Oct 1951. 13

[126] R Gilmore. *Lie Groups, Physics, and Geometry: An Introduction for Physicists, Engineers and Chemists*. Cambridge University Press, 2008. 13, 27

[127] R Gilmore. Baker-Campbell-Hausdorff formulas. *Journal of Mathematical Physics*, 15(12):2090–2092, Dec 1974. 13

[128] C Chryssomalakos, E Guzmán-González, and E Serrano-Ensástiga. Geometry of spin coherent states. *Journal of Physics A: Mathematical and Theoretical*, 51(16):165202, Apr 2018. 15, 19

[129] A Vourdas. Analytic representations in quantum mechanics. *Journal of Physics A: Mathematical and General*, 39(7):R65–R141, Feb 2006. 15, 20

[130] D Gottesman, A Kitaev, and J Preskill. Encoding a qubit in an oscillator. *Phys. Rev. A*, 64:012310, Jun 2001. 15

[131] J Conrad, J Eisert, and F Arzani. Gottesman-Kitaev-Preskill codes: A lattice perspective. *Quantum*, 6:648, February 2022. 15

[132] J A Gross. Designing codes around interactions: The case of a spin. *Phys. Rev. Lett.*, 127:010504, Jul 2021. 15

[133] W Dür, G Vidal, and J I Cirac. Three qubits can be entangled in two inequivalent ways. *Phys. Rev. A*, 62:062314, Nov 2000. 16, 41, 57, 94

[134] P Jordan. Der zusammenhang der symmetrischen und linearen gruppen und das mehrkorperproblem. *Zeitschrift fur Physik*, 94(7–8):531–535, Jul 1935. 17

[135] B C Sanders and C C Gerry. Connection between the NOON state and a superposition of SU(2) coherent states. *Phys. Rev. A*, 90:045804, Oct 2014. 18, 36

[136] J P Dowling. Quantum optical metrology – the lowdown on high-N00N states. *Contemporary physics*, 49(2):125–143, 2008. 18, 36, 38, 57

[137] B Yurke, S L McCall, and J R Klauder. SU(2) and SU(1,1) interferometers. *Phys. Rev. A*, 33:4033–4054, Jun 1986. 18

[138] E Knill, R Laflamme, and G J Milburn. A scheme for efficient quantum computation with linear optics. *Nature*, 409(6816):46–52, Jan 2001. 18

[139] P Kok, W J Munro, K Nemoto, T C Ralph, J P Dowling, and G J Milburn. Linear optical quantum computing with photonic qubits. *Rev. Mod. Phys.*, 79:135–174, Jan 2007. 18

[140] J Schwinger. The Majorana formula. *Transactions of the New York Academy of Sciences*, 38(1 Series II):170–184, Nov 1977. 18

[141] J H Hannay. The Berry phase for spin in the Majorana representation. *Journal of Physics A: Mathematical and General*, 31(2):L53–L59, Jan 1998. 18

[142] P Bruno. Quantum geometric phase in Majorana's stellar representation: Mapping onto a many-body aharonov-bohm phase. *Phys. Rev. Lett.*, 108:240402, Jun 2012. 18

[143] A R Usha Devi, Sudha, and A K Rajagopal. Majorana representation of symmetric multiqubit states. *Quantum Inf Process*, 11(3):685–710, Jun 2012. 19

[144] U Chabaud, D Markham, and F Grosshans. Stellar representation of non-gaussian quantum states. *Phys. Rev. Lett.*, 124:063605, Feb 2020. 20, 22

[145] G Ramachandran and V Ravishankar. On polarised spin-j assemblies. *Journal of Physics G: Nuclear Physics*, 12(6):L143–L145, Jun 1986. 22

[146] C Chryssomalakos, E Guzmán-González, L Hanotel, and E Serrano-Ensástiga. Stellar representation of multipartite antisymmetric states. *Communications in Mathematical Physics*, 381(2):735–764, Jan 2021. 22

[147] C Chryssomalakos, L Hanotel, E Guzmán-González, D Braun, E Serrano-Ensástiga, and K Życzkowski. Symmetric multiqudit states: Stars, entanglement, and rotosensors. *Phys. Rev. A*, 104:012407, Jul 2021. 22

[148] U Chabaud and S Mehraban. Holomorphic representation of quantum computations. *Quantum*, 6:831, October 2022. 22

[149] U Chabaud and M Walschaers. Resources for bosonic quantum computational advantage. *Phys. Rev. Lett.*, 130:090602, Mar 2023. 22

[150] M A de Gosson. *Quantum Harmonic Analysis: An Introduction*. De Gruyter, Jun 2021. 25

[151] J R Driscoll and D M Healy. Computing Fourier transforms and convolutions on the 2-sphere. *Advances in Applied Mathematics*, 15(2):202–250, Jun 1994. 26, 135

[152] R Gilmore. Q and P representatives for spherical tensors. *Journal of Physics A: Mathematical and General*, 9(7):L65–L66, Jul 1976. 26

[153] J M Gracia-Bondía and J C Várilly. Nonnegative mixed states in Weyl-Wigner-Moyal theory. *Physics Letters A*, 128(1–2):20–24, Mar 1988. 33

[154] A Mandilara, E Karpov, and N J Cerf. Extending Hudson's theorem to mixed quantum states. *Phys. Rev. A*, 79:062302, Jun 2009. 33

[155] A Mandilara, E Karpov, and N J Cerf. Gaussianity bounds for quantum mixed states with a positive Wigner function. *Journal of Physics: Conference Series*, 254:012011, Nov 2010. 33

[156] I Rigas, L L Sánchez-Soto, A B Klimov, J Řeháček, and Z Hradil. Non-negative Wigner functions for orbital angular momentum states. *Phys. Rev. A*, 81:012101, Jan 2010. 33

[157] D M Greenberger, M A Horne, and A Zeilinger. Going beyond Bell's theorem, 1989. 36

[158] D M Greenberger, M A Horne, A Shimony, and A Zeilinger. Bell's theorem without inequalities. *American Journal of Physics*, 58(12):1131–1143, Dec 1990. 36

[159] N D Mermin. Quantum mysteries revisited. *American Journal of Physics*, 58(8):731–734, 08 1990. 36

[160] B C Sanders. Quantum dynamics of the nonlinear rotator and the effects of continual spin measurement. *Phys. Rev. A*, 40:2417–2427, Sep 1989. 36

[161] J J Bollinger, W M Itano, D J Wineland, and D J Heinzen. Optimal frequency measurements with maximally correlated states. *Phys. Rev. A*, 54:R4649–R4652, Dec 1996. 36

[162] M Hillery, V Bužek, and A Berthiaume. Quantum secret sharing. *Physical Review A*, 59(3):1829, 1999. 36

[163] D Bouwmeester, J-W Pan, M Daniell, H Weinfurter, and A Zeilinger. Observation of three-photon Greenberger-Horne-Zeilinger entanglement. *Phys. Rev. Lett.*, 82:1345–1349, Feb 1999. 36

[164] L Pezzè, A Smerzi, M K Oberthaler, R Schmied, and P Treutlein. Quantum metrology with nonclassical states of atomic ensembles. *Rev. Mod. Phys.*, 90:035005, Sep 2018. 36, 39

[165] A B Klimov and S M Chumakov. On the SU(2) Wigner function dynamics. *Revista mexicana de física*, 48(4):317–324, 2002. 38

[166] N Akhtar, B C Sanders, and C Navarrete-Benlloch. Sub-Planck structures: Analogies between the Heisenberg-Weyl and SU(2) groups. *Phys. Rev. A*, 103:053711, May 2021. 39

[167] M G M Moreno and F Parisio. All bipartitions of arbitrary Dicke states, 2018. 46

[168] J K Stockton, J M Geremia, A C Doherty, and H Mabuchi. Characterizing the entanglement of symmetric many-particle spin-1/2 systems. *Physical Review A*, 67(2):022112, February 2003. 46

[169] E Chitambar and G Gour. Quantum resource theories. *Rev. Mod. Phys.*, 91:025001, Apr 2019. 48

[170] N Gisin and H Bechmann-Pasquinucci. Bell inequality, Bell states and maximally entangled states for n qubits. *Physics Letters A*, 246(1):1–6, 1998. 48

[171] A Higuchi and A Sudbery. How entangled can two couples get? *Physics Letters A*, 273(4):213–217, 2000. 48

[172] A J Scott. Multipartite entanglement, quantum-error-correcting codes, and entangling power of quantum evolutions. *Phys. Rev. A*, 69:052330, May 2004. 48

[173] F Verstraete, J Dehaene, and B De Moor. Normal forms and entanglement measures for multipartite quantum states. *Phys. Rev. A*, 68:012103, Jul 2003. 48

[174] P Facchi, G Florio, G Parisi, and S Pascazio. Maximally multipartite entangled states. *Phys. Rev. A*, 77:060304, Jun 2008. 48

[175] J Zimba. Anticoherent spin states via the Majorana representation. *Electronic Journal of Theoretical Physics*, 3(10):143–156, 2006. 48

[176] D Baguette and J Martin. Anticoherence measures for pure spin states. *Phys. Rev. A*, 96:032304, Sep 2017. 49

[177] G Björk, A B Klimov, P de la Hoz, M Grassl, G Leuchs, and L L Sánchez-Soto. Extremal quantum states and their Majorana constellations. *Phys. Rev. A*, 92:031801, Sep 2015. 49, 64

[178] M Grassl. Extremal polarization states. http://polarization.markus-grassl.de/. 49

[179] F Bouchard, P de la Hoz, G Björk, R W Boyd, M Grassl, Z Hradil, E Karimi, A B Klimov, G Leuchs, J Řeháček, and L L Sánchez-Soto. Quantum metrology at the limit with extremal Majorana constellations. *Optica*, 4(11):1429–1432, Nov 2017. 49

[180] P Kolenderski and R Demkowicz-Dobrzanski. Optimal state for keeping reference frames aligned and the Platonic solids. *Phys. Rev. A*, 78:052333, Nov 2008. 49

[181] A Z Goldberg and D F V James. Quantum-limited Euler angle measurements using anticoherent states. *Phys. Rev. A*, 98:032113, Sep 2018. 49, 50

[182] J Martin, S Weigert, and O Giraud. Optimal detection of rotations about unknown axes by coherent and anticoherent states. *Quantum*, 4:285, Jun 2020. 49

[183] A Z Goldberg, A B Klimov, G Leuchs, and L L Sánchez-Soto. Rotation sensing at the ultimate limit. *J. Phys. Photonics*, 3(2):022008, Apr 2021. 49

[184] A Z Goldberg, P de la Hoz, G Björk, A B Klimov, M Grassl, G Leuchs, and L L Sánchez-Soto. Quantum concepts in optical polarization. *Adv. Opt. Photon.*, 13(1):1–73, Mar 2021. 50

[185] D Baguette, F Damanet, O Giraud, and J Martin. Anticoherence of spin states with point-group symmetries. *Phys. Rev. A*, 92:052333, Nov 2015. 50, 70

[186] W Ganczarek, M Kuś, and K Życzkowski. Barycentric measure of quantum entanglement. *Phys. Rev. A*, 85:032314, Mar 2012. 50

[187] A Shimony. Degree of entanglement. *Annals of the New York Academy of Sciences*, 755(1):675–679, 1995. 51

[188] R Hübener, M Kleinmann, T-C Wei, C González-Guillén, and O Gühne. Geometric measure of entanglement for symmetric states. *Phys. Rev. A*, 80:032324, Sep 2009. 51

[189] V V Dodonov, O V Man'ko, V I Man'ko, and A Wünsche. Hilbert-Schmidt distance and non-classicality of states in quantum optics. *Journal of Modern Optics*, 47(4):633–654, Mar 2000. 51

[190] O Giraud, P Braun, and D Braun. Quantifying quantumness and the quest for Queens of Quantum. *New Journal of Physics*, 12(6):063005, jun 2010. 52, 53, 64

[191] J Martin, O Giraud, P Braun, D Braun, and T Bastin. Multiqubit symmetric states with high geometric entanglement. *Phys. Rev. A*, 81:062347, Jun 2010. 53

[192] I I Arkhipov, A Barasiński, and J Svozilík. Negativity volume of the generalized Wigner function as an entanglement witness for hybrid bipartite states. *Scientific Reports*, 8(1):16955, Dec 2018. 53, 108

[193] J J Bollinger, W M Itano, D J Wineland, and D J Heinzen. Optimal frequency measurements with maximally correlated states. *Phys. Rev. A*, 54:R4649–R4652, Dec 1996. 57

[194] B Koczor, R Zeier, and S J Glaser. Fast computation of spherical phase-space functions of quantum many-body states. *Phys. Rev. A*, 102:062421, Dec 2020. 59, 61

[195] A Z Goldberg, J L Romero, ´Á S Sanz, A B Klimov, G Leuchs, and L L Sánchez-Soto. Random majorana constellations, 2021. 67

[196] L L Whyte. Unique arrangements of points on a sphere. *The American Mathematical Monthly*, 59(9):606–611, Nov 1952. 72

[197] E B Saff and A B J Kuijlaars. Distributing many points on a sphere. *The mathematical intelligencer*, 19(1):5–11, 1997. 72

[198] R H Hardin, N J A Sloane, and W D Smith. Minimal energy arrangements of points on a sphere, 1997. 72

[199] D J Wales and S Ulker. Structure and dynamics of spherical crystals characterized for the Thomson problem. *Phys. Rev. B*, 74:212101, Dec 2006. 72

[200] J M Gracia-Bondá and J C Várilly. Non-negative mixed states in Weyl-Wigner-Moyal theory. *Physics Letters A*, 128(1–2):20–24, Mar 1988. 75

[201] T Bröcker and R F Werner. Mixed states with positive Wigner functions. *Journal of Mathematical Physics*, 36(1):62–75, Jan 1995. 75

[202] A Mandilara, E Karpov, and N J Cerf. Gaussianity bounds for quantum mixed states with a positive Wigner function. *Journal of Physics: Conference Series*, 254(1):012011, nov 2010. 75

[203] F Verstraete, K Audenaert, and B De Moor. Maximally entangled mixed states of two qubits. *Phys. Rev. A*, 64:012316, Jun 2001. 75

[204] E Serrano-Ensástiga and J Martin. Maximum entanglement of mixed symmetric states under unitary transformations, 2021. 75, 95, 97, 98

[205] N Abbasli, V Abgaryan, M Bures, A Khvedelidze, I Rogojin, and A Torosyan. On measures of classicality/quantumness in quasiprobability representations of finite-dimensional quantum systems. *Physics of Particles and Nuclei*, 51(4):443–447, July 2020. 75, 108

[206] V Abgaryan and A Khvedelidze. On families of Wigner functions for n-level quantum systems. *Symmetry*, 13(6):1013, June 2021. 75, 79, 80, 81, 83, 101, 102

[207] V Abgaryan, A Khvedelidze, and A Torosyan. The global indicator of classicality of an arbitrary n-level quantum system. *Journal of Mathematical Sciences*, 251(3):301–314, October 2020. 75, 76, 80, 81, 83, 101, 102, 108

[208] V Abgaryan, A Khvedelidze, and A Torosyan. Kenfack – Życzkowski indicator of nonclassicality for two non-equivalent representations of Wigner function of qutrit. *Physics Letters A*, 412:127591, October 2021. 75, 90, 102, 108

[209] F Bohnet-Waldraff, D Braun, and O Giraud. Partial transpose criteria for symmetric states. *Phys. Rev. A*, 94:042343, Oct 2016. 76, 95

[210] F Bohnet-Waldraff, O Giraud, and D Braun. Absolutely classical spin states. *Phys. Rev. A*, 95:012318, Jan 2017. 76, 95, 99

[211] Blender Online Community. *Blender - a 3D modelling and rendering package*. Blender Foundation, Stichting Blender Foundation, Amsterdam, 2018. 102

[212] S Danisch and J Krumbiegel. Makie.jl: Flexible high-performance data visualization for Julia. *Journal of Open Source Software*, 6(65):3349, September 2021. 102

[213] E H Lieb. Proof of an entropy conjecture of Wehrl. *Communications in Mathematical Physics*, 62(1):35–41, 1978. 107

[214] E H Lieb and J P Solovej. Proof of an entropy conjecture for Bloch coherent spin states and its generalizations. *Acta Mathematica*, 212(2):379–398, 2014. 107

[215] A Wehrl. On the relation between classical and quantum-mechanical entropy. *Reports on Mathematical Physics*, 16(3):353–358, 1979. 107

[216] P Delsarte, J M Goethals, and J J Seidel. Spherical codes and designs. *Geometriae Dedicata*, 6(3):363–388, 1977. 107

[217] P Zanardi. Virtual quantum subsystems. *Phys. Rev. Lett.*, 87:077901, Jul 2001. 108

[218] R W Spekkens. Contextuality for preparations, transformations, and unsharp measurements. *Phys. Rev. A*, 71:052108, May 2005. 110

[219] S Mansfield and E Kashefi. Quantum advantage from sequential-transformation contextuality. *Phys. Rev. Lett.*, 121:230401, Dec 2018. 110

[220] S Helgason. *Integral Geometry and Radon Transforms*. Springer New York, New York, NY, 2010. 110, 111

[221] S Abramsky and A Brandenburger. The sheaf-theoretic structure of non-locality and contextuality. *New Journal of Physics*, 13(11):113036, 2011. 111

[222] R S Barbosa, T Douce, P-E Emeriau, E Kashefi, and S Mansfield. Continuous-variable nonlocality and contextuality. *Communications in Mathematical Physics*, 391(3):1047–1089, May 2022. 111

[223] H Poincaré. Sur les courbes définies par les équations différentielles. *Journal de mathématiques pures et appliquées*, 1:167–244, 1885. 111

[224] R Gilmore. Geometry of symmetrized states. *Annals of Physics*, 74(2):391–463, Dec 1972. 135

APPENDICES

Appendix A

Derivation of the spherical Wigner function

Fix a spin j throughout and denote $\{|j, m_{\boldsymbol{n}}\rangle\}_{m_{\boldsymbol{n}}=-j}^{j}$ for the Dicke basis quantized along the axis $\boldsymbol{n} \in \mathbb{R}^3$ (2.21). Note that each such axis points to a unique $(\theta, \phi) \equiv \Omega \in S^2$. When $\boldsymbol{n} = \boldsymbol{z}$ in the standard coordinates we follow convention and drop the subscript as in $|j, m\rangle \equiv |j, m_{\boldsymbol{z}}\rangle$.

First consider the covariance axiom (2.47d). This will end up being the most powerful axiom in the sense that it alone dictates most of the Wigner function structure. Begin by expanding each phase-point operator in the operator basis associated to the standard Dicke basis,

$$\Delta(\Omega) = \sum_{m,m'=-j}^{j} \Delta_{mm'}(\Omega)|j, m\rangle\langle j, m'|, \tag{A.1}$$

where

$$\Delta_{mm'}(\Omega) = [\Delta(\Omega)]_{mm'} = \langle j, m|\Delta(\Omega)|j, m'\rangle \tag{A.2}$$

are the matrix elements. Covariance under the action of an arbitrary $g \in \mathrm{SU}(2)$ has it that

$$\Delta(g \cdot \Omega) = U_g \Delta(\Omega) U_g^\dagger. \tag{A.3}$$

Here the action on phase space, $g \cdot \Omega = R_g \Omega \equiv R_g \boldsymbol{n}$, is given by the three-dimensional rotation matrices $R_g \in \mathrm{SO}(3)$, while the action on Hilbert space is given by the spin-j

unitary representation U_g such that $U_g|j, m_{\boldsymbol{n}}\rangle = |j, m_{R_g\boldsymbol{n}}\rangle$. In the standard Dicke basis the covariance axiom becomes

$$\langle j, m|\Delta(g\cdot\Omega)|j, m'\rangle = \langle j, m|U_g\,\Delta(\Omega)\,U_g^\dagger|j, m'\rangle \tag{A.4}$$

$$\Delta_{mm'}(g\cdot\Omega) = \sum_{p,q=-j}^{j}\langle j, m|U_g|j, p\rangle\Delta_{pq}(\Omega)\langle j, q|U_g^\dagger|j, m'\rangle \tag{A.5}$$

$$= \sum_{p,q=-j}^{j} D^{(j)}_{mp}(g)D^{*(j)}_{m'q}(g)\Delta_{pq}(\Omega) \tag{A.6}$$

where $D^{(j)}_{mn}(g)$ are Wigner D-matrices (2.6). Using the product relation Eq. (2.8) covariance becomes

$$\begin{aligned}&\Delta_{mm'}(g\cdot\Omega)\\ &= \sum_{p,q=-j}^{j}\left[\sum_{\ell=0}^{2j}\frac{2\ell+1}{2j+1}\left\langle\begin{matrix} j & \ell \\ m & m'-m\end{matrix}\middle|\begin{matrix} j \\ m'\end{matrix}\right\rangle\left\langle\begin{matrix} j & \ell \\ p & q-p\end{matrix}\middle|\begin{matrix} j \\ q\end{matrix}\right\rangle D^{*(\ell)}_{m'-m,q-p}(g)\right]\Delta_{pq}(\Omega) \qquad \text{(A.7)}\\ &= \sum_{\ell=0}^{2j}(-1)^{j-m}\left\langle\begin{matrix} j & j \\ m & -m'\end{matrix}\middle|\begin{matrix} \ell \\ m-m'\end{matrix}\right\rangle\sum_{p,q=-j}^{j}(-1)^{j-p}\left\langle\begin{matrix} j & j \\ p & -q\end{matrix}\middle|\begin{matrix} \ell \\ p-q\end{matrix}\right\rangle D^{*(\ell)}_{m'-m,q-p}(g)\Delta_{pq}(\Omega), \qquad \text{(A.8)}\end{aligned}$$

where the Clebsch-Gordan symmetry property

$$\left\langle\begin{matrix} j_1 & j_2 \\ m_1 & m_2\end{matrix}\middle|\begin{matrix} J \\ M\end{matrix}\right\rangle = (-1)^{j_1-m_1}\sqrt{\frac{2J+1}{2j_2+1}}\left\langle\begin{matrix} j_1 & J \\ m_1 & -M\end{matrix}\middle|\begin{matrix} j_2 \\ -m_2\end{matrix}\right\rangle \tag{A.9}$$

was used twice. The coefficient occurring in the last two sums happens to be the matrix element of the multipole operator $T^{(j)\dagger}_{\ell\mu}$ (2.12):

$$\langle j, p|T^{(j)\dagger}_{\ell,\mu}|j, q\rangle = (-1)^{j-p}\left\langle\begin{matrix} j & j \\ p & -q\end{matrix}\middle|\begin{matrix} \ell \\ -\mu\end{matrix}\right\rangle. \tag{A.10}$$

With this in mind, re-write Eq. (A.8) as

$$\Delta_{mm'}(g\cdot\Omega) = \sum_{\ell=0}^{2j}(-1)^{j-m}\left\langle\begin{matrix} j & j \\ m & -m'\end{matrix}\middle|\begin{matrix} \ell \\ m-m'\end{matrix}\right\rangle\sum_{\mu=-\ell}^{\ell}D^{*(\ell)}_{m'-m,\mu}(g)$$

$$\times \sum_{p=-j}^{j} (-1)^{j-p} \left\langle \begin{matrix} j & j \\ p & -p-\mu \end{matrix} \middle| \begin{matrix} \ell \\ -\mu \end{matrix} \right\rangle \Delta_{p,p+\mu}(\Omega), \tag{A.11}$$

where the sum over the difference $\mu = q - p$ may be split from the p sum and restricted to $-\ell, ..., \ell$ because those are the only allowed magnetic quantum numbers for the total spin being decomposed in the Clebsch-Gordan coefficient[1].

Now consider the spherical functions in Eq. (A.11):

$$\tilde{Y}_{\ell,\mu}(\Omega) = \sum_{p=-j}^{j} (-1)^{j-p} \left\langle \begin{matrix} j & j \\ p & -p-\mu \end{matrix} \middle| \begin{matrix} \ell \\ -\mu \end{matrix} \right\rangle \Delta_{p,\mu+p}(\Omega). \tag{A.12}$$

These functions in fact transform exactly like the spherical harmonics under rotation. This can be seen by computing $\tilde{Y}_{\ell,\mu}(g \cdot \Omega)$ via a recursive application of the covariance axiom:

$$\tilde{Y}_{\ell,\mu}(g \cdot \Omega) = \sum_{p=-j}^{j} (-1)^{j-p} \left\langle \begin{matrix} j & j \\ p & -p-\mu \end{matrix} \middle| \begin{matrix} \ell \\ -\mu \end{matrix} \right\rangle \Delta_{p,\mu+p}(g \cdot \Omega) \tag{A.13}$$

$$= \sum_{p=-j}^{j} (-1)^{j-p} \left\langle \begin{matrix} j & j \\ p & -p-\mu \end{matrix} \middle| \begin{matrix} \ell \\ -\mu \end{matrix} \right\rangle \times \sum_{k=0}^{2j} (-1)^{j-p} \left\langle \begin{matrix} j & j \\ p & -p-\mu \end{matrix} \middle| \begin{matrix} k \\ -\mu \end{matrix} \right\rangle \sum_{s=-k}^{k} D^{*(k)}_{\mu,s}(g) \times \sum_{a=-j}^{j} (-1)^{j-a} \left\langle \begin{matrix} j & j \\ a & -a-s \end{matrix} \middle| \begin{matrix} k \\ -s \end{matrix} \right\rangle \Delta_{a,a+s}(\Omega) \tag{A.14}$$

$$= \sum_{k=0}^{2j} \underbrace{\sum_{p=-j}^{j} \left\langle \begin{matrix} j & j \\ p & -p-\mu \end{matrix} \middle| \begin{matrix} \ell \\ -\mu \end{matrix} \right\rangle \left\langle \begin{matrix} j & j \\ p & -p-\mu \end{matrix} \middle| \begin{matrix} k \\ -\mu \end{matrix} \right\rangle}_{\delta_{\ell,k}} \sum_{s=-k}^{k} D^{*(k)}_{\mu,s}(g) \tilde{Y}_{k,s}(\Omega) \tag{A.15}$$

[1] A possible source of confusion here is the mere presence of Clebsch-Gordan coefficients – which have to do with the possible transitions/decays within a many-spin system – despite only ever considering one abstract spin-j particle. As implicitly discussed in Sec. 2.1.1, the resolution is the isomorphism $L(\mathcal{H}) \simeq \mathcal{H}^* \otimes \mathcal{H}$ in finite dimensions, meaning that the SU(2) action on operators is essentially a tensor product representation, which is reducible into simple *multipoles*. Hence the Clebsch-Gordon coefficients occurring in all of these calculations are still in the context of two "different" spins systems: the Hilbert space of column vectors and the Hilbert space of row vectors.

$$= \sum_{s=-\ell}^{\ell} D^{*(\ell)}_{\mu,s}(g)\tilde{Y}_{\ell,s}(\Omega) \tag{A.16}$$

where the Clebsch-Gordon orthogonality relations were used in the second last line. Thus for each $\ell \in \{0, ..., 2j\}$, we have a set of functions $\tilde{Y}_{\ell,\mu}$ with $\mu \in \{-\ell, ..., \ell\}$ that transform exactly like the spherical harmonics $Y_{\ell,\mu}$ under rotation. In representation-theoretic terms, this means that the Hilbert space generated by the first $2j$ multipole sectors of spherical harmonics, $\{Y_{\ell,\mu}\}$ where $\ell = 0, ..., 2j$ and $\mu = -\ell, \ell$, is *equivalent* to the space of functions $\{\tilde{Y}_{\ell,\mu}\}$ just established. Therefore by Schur's lemma, the two sets of functions are sector-wise identical up to a complex scalar; see [89, 224]. Hence they are related via

$$\tilde{Y}_{\ell,\mu} = \lambda^{(j)}_{\ell} Y_{\ell,\mu} \tag{A.17}$$

for some $2j+1$ constants $\lambda^{(j)}_{\ell} \in \mathbb{C}$. Using the fact that the Wigner D-matrix of the identity element $e \in \mathrm{SU}(2)$ is the identity matrix, Eq. (A.11) for $g = e$ becomes

$$\Delta_{mm'}(\Omega) = \sum_{\ell=0}^{2j} (-1)^{j-m} \left\langle \begin{matrix} j & j \\ m & -m' \end{matrix} \middle| \begin{matrix} \ell \\ m-m' \end{matrix} \right\rangle \sum_{\mu=-\ell}^{\ell} \delta_{m'-m,\mu} \tilde{Y}_{\ell,\mu}(\Omega) \tag{A.18}$$

$$= \sum_{\ell=0}^{2j} \lambda^{(j)}_{\ell} (-1)^{j-m} \left\langle \begin{matrix} j & j \\ m & -m' \end{matrix} \middle| \begin{matrix} \ell \\ m-m' \end{matrix} \right\rangle Y_{\ell,m'-m}(\Omega). \tag{A.19}$$

And given the connection to the multipole operators in Eq. (A.10), Eq. (A.18) can be re-written in terms of μ to obtain a compact form for the kernel:

$$\Delta(\Omega) = \sum_{\ell=0}^{2j} \lambda^{(j)}_{\ell} \sum_{\mu-=-j}^{j} T^{(j)\dagger}_{\ell\mu} Y_{\ell\mu}(\Omega). \tag{A.20}$$

It is worthwhile to stop and appreciate (A.20). From it we see that the kernel (and therefore also the Wigner function) is naturally constructed in terms of multipole sectors, each of which show a nice pairing between the spherical harmonics and the spherical tensor operators – which are just the operator versions of the spherical harmonics (2.11). We can also say that any Wigner function of a spin-j state lives in the Hilbert subspace of $L^2(S^2)$ generated by spherical harmonics of degree no larger than $\ell = 2j$. And as spherical harmonics are eigenfunctions of the spherical Laplace operator this therefore places an upper bound on the scale of angular resolution of the Wigner function[2]. Finally we can

[2]From the perspective of Fourier theory this means that the spherical Wigner function is *band-limited* [151]. Intuitively, the maximum "wiggliness" of the Wigner function depends on j.

say that the orthogonality of the spherical tensor operators implies through the Weyl rule (2.46) that the Wigner function of the spherical tensor operator is proportional to the spherical harmonic of the same parameters with proportionality factor $\lambda_\ell^{(j)}$:

$$W_{T^{(j)}_{\ell,m}}(\theta,\phi) = \lambda_\ell^{(j)} Y_{\ell,m}(\theta,\phi). \tag{A.21}$$

While one could stop here – and for practical calculations one usually does – there is more conceptual ground to be gained from the covariance axiom. So far the derivation has taken place almost entirely in the Dicke basis quantized along the z-axis. Now, simultaneously expand each phase-point operator $\Delta(\Omega)$ in the Dicke basis associated to the axis $\boldsymbol{n}$ pointing to Ω:

$$\Delta(\Omega) = \sum_{m_{\boldsymbol{n}},m'_{\boldsymbol{n}}=-j}^{j} \Delta_{m_{\boldsymbol{n}}m'_{\boldsymbol{n}}}(\Omega)|j,m_{\boldsymbol{n}}\rangle\langle j,m'_{\boldsymbol{n}}|, \tag{A.22}$$

where

$$\Delta_{m_{\boldsymbol{n}}m'_{\boldsymbol{n}}}(\Omega) = [\Delta(\Omega)]_{m_{\boldsymbol{n}}m'_{\boldsymbol{n}}} = \langle j,m_{\boldsymbol{n}}|\Delta(\Omega)|j,m'_{\boldsymbol{n}}\rangle \tag{A.23}$$

are the matrix elements of $\Delta(\Omega)$ in the $\{|m_{\boldsymbol{n}}\rangle\}$ basis. In this setting, the covariance axiom becomes

$$\sum_{m_{\boldsymbol{n}},m'_{\boldsymbol{n}}=-j}^{j} \Delta_{m_{\boldsymbol{n}}m'_{\boldsymbol{n}}}(R_g\Omega)|j,m_{R_g\boldsymbol{n}}\rangle\langle j,m'_{R_g\boldsymbol{n}}| = \sum_{m_{\boldsymbol{n}},m'_{\boldsymbol{n}}=-j}^{j} \Delta_{m_{\boldsymbol{n}}m'_{\boldsymbol{n}}}(\Omega)|j,m_{R_g\boldsymbol{n}}\rangle\langle j,m'_{R_g\boldsymbol{n}}|. \tag{A.24}$$

For (A.24) to hold it must be that

$$\Delta_{m_{\boldsymbol{n}}m'_{\boldsymbol{n}}}(R_g\Omega) = \Delta_{m_{\boldsymbol{n}}m'_{\boldsymbol{n}}}(\Omega) \qquad \forall g \in \mathrm{SU}(2). \tag{A.25}$$

Thus the expansion coefficients $\Delta_{m_{\boldsymbol{n}}m'_{\boldsymbol{n}}}(\Omega)$ do not depend on Ω and the argument is dropped in the notation. Now consider covariance of the phase-point operator $\Delta(\Omega)$ under the specific action of a rotation ϕ about $\boldsymbol{n}$, denoted $g_{\boldsymbol{n},\phi}$. This action on S^2 leaves the axis $\boldsymbol{n}$ invariant, $R_{g_{\boldsymbol{n},\phi}}\boldsymbol{n} = \boldsymbol{n}$, but the Dicke states $|j,m_{\boldsymbol{n}}\rangle$ pick up a phase because they are eigenstates[3] of $U_{g_{\boldsymbol{n},\phi}} = e^{i\phi\boldsymbol{n}\cdot\boldsymbol{J}}$ with eigenvalue $e^{im\phi}$. Covariance implies

$$\Delta(g_{\boldsymbol{n},\phi}\cdot\Omega) = U_{g_{\boldsymbol{n},\phi}}\Delta(\Omega)U^\dagger_{g_{\boldsymbol{n},\phi}} \tag{A.26}$$

[3]When $j = 1/2$, $\boldsymbol{n} = \boldsymbol{z}$, and $\phi = \pi$ this is similar to the Pauli Z measurement in the computational basis of a qubit.

$$\sum_{m_{\boldsymbol{n}},m'_{\boldsymbol{n}}=-j}^{j} \Delta_{m_{\boldsymbol{n}}m'_{\boldsymbol{n}}} |j,m_{\boldsymbol{n}}\rangle\langle j,m'_{\boldsymbol{n}}| = \sum_{m_{\boldsymbol{n}},m'_{\boldsymbol{n}}=-j}^{j} \Delta_{m_{\boldsymbol{n}}m'_{\boldsymbol{n}}} e^{i(m_{\boldsymbol{n}}-m'_{\boldsymbol{n}})\phi} |j,m_{\boldsymbol{n}}\rangle\langle j,m'_{\boldsymbol{n}}|. \tag{A.27}$$

The above can only hold for arbitrary ϕ if

$$e^{i(m_{\boldsymbol{n}}-m'_{\boldsymbol{n}})\phi} = 1 \qquad \Longrightarrow \qquad m_{\boldsymbol{n}} = m'_{\boldsymbol{n}} \qquad \Longrightarrow \qquad \Delta_{m_{\boldsymbol{n}}m'_{\boldsymbol{n}}} \equiv \Delta(m)\delta_{m_{\boldsymbol{n}}m'_{\boldsymbol{n}}} \tag{A.28}$$

Thus each phase-point operator $\Delta(\Omega)$ is diagonal in the Dicke basis associated to Ω, and all phase-point operators have the same spectrum:

$$\Delta(\Omega) = \sum_{m_{\boldsymbol{n}}=-j}^{j} \Delta(m) |j,m_{\boldsymbol{n}}\rangle\langle j,m_{\boldsymbol{n}}|. \tag{A.29}$$

Given the result of Eq. (A.29), which was obtained by a simultaneous operator expansion in many different bases, we may now use the previous part of the derivation that took place in specifically the z basis to act as a representative for all phase-point operators. Specifically, set Ω to the North Pole ($\theta = 0, \phi = 0$) and $m = m'$ in Eq. (A.19), together with the property of the spherical harmonic $Y_{\ell,0}(0,0) = \sqrt{\frac{2\ell+1}{4\pi}}$ to find the spectrum along the z axis:

$$\Delta(m) = \Delta_{mm}(0,0) = \sqrt{\frac{2\ell+1}{4\pi}} \sum_{\ell=0}^{2j} \lambda_\ell^{(j)} (-1)^{j-m} \left\langle \begin{matrix} j & j \\ m & -m \end{matrix} \middle| \begin{matrix} \ell \\ 0 \end{matrix} \right\rangle. \tag{A.30}$$

Let us summarize everything so far: the kernel is built from data categorized by multipole sectors (A.20), each phase-point operator is diagonal along the quantization axis pointing to it, and they all share the same spectrum given by (A.30). In other words the covariance axiom alone has completely characterized the SU(2) Wigner function up to $2j+1$ complex numbers $\lambda_\ell^{(j)}$, one for each multipole.

Now consider the realness axiom (2.47a), which requires each phase point operator to be Hermitian. Given Eq. (A.30) and the rotational invariance of the spectrum it must be that the numbers $\lambda_\ell^{(j)} \in \mathbb{R}$.

Now consider the traciality axiom (2.47c). This asks the function $\frac{2j+1}{4\pi}\operatorname{tr}[\Delta(\Omega)\Delta(\Omega')]$ to behave like the delta function on the sphere. But we already know from (A.20) that the Wigner function lives in the band-limited ($0 \le \ell \le 2j$) subspace of $L^2(S^2)$. The delta function for this subspace is well-known [87] and is given by

$$\frac{2j+1}{4\pi}\operatorname{tr}[\Delta(\Omega)\Delta(\Omega')] = \sum_{\ell=0}^{2j} \sum_{m=-\ell}^{\ell} Y_{\ell,m}(\Omega) Y^*_{\ell,m}(\Omega'). \tag{A.31}$$

After taking the trace in the Dicke basis and inserting (A.19) into the left hand side, the following relation may be found after another Clebsch-Gordan orthogonality relation:

$$\frac{2j+1}{4\pi}\sum_{\ell=0}^{2j}(\lambda_\ell^{(j)})^2\sum_{m=-\ell}^{\ell}Y_{\ell,m}(\Omega)Y_{\ell,m}^*(\Omega')=\sum_{\ell=0}^{2j}\sum_{m=-\ell}^{\ell}Y_{\ell,m}(\Omega)Y_{\ell,m}^*(\Omega'). \tag{A.32}$$

For this to hold it must be the case that $\lambda_\ell^{(j)}=\epsilon_i^{(j)}\sqrt{\frac{4\pi}{2j+1}}$ where $\epsilon_\ell^{(j)}=\pm1$ for all $\ell=0,...,2j$.

And now finally consider standardization (2.47b). As mentioned earlier the standardization implies (indirectly, but still necessarily) that the kernel must have unit trace. And since the spherical tensor operators all have vanishing trace except for $\mathrm{tr}[T_{00}^{(j)}]=1$, Eq. (A.20) and $Y_{0,0}=\frac{1}{\sqrt{4\pi}}$ together imply that $\epsilon_0^{(j)}=1$.

Thus the 2^{2j}-sized set of spherical Wigner kernels obeying the Stratonovich axioms is

$$\Delta(\Omega)=\sqrt{\frac{4\pi}{2j+1}}\sum_{\ell=0}^{2j}\epsilon_\ell\sum_{\mu-=-\ell}^{\ell}T_{\ell\mu}^{(j)\dagger}Y_{\ell\mu}(\Omega). \tag{A.33}$$

where $\epsilon_\ell=\pm1$ for all non-trivial multipoles.